ISSN NO. 0737-5352-8

INTERACTION OF SHALLOW COLD SURGES WITH TOPOGRAPHY ON SCALES OF 100-1000 KILOMETERS

James J. Toth

CIRA Cooperative Institute for Research in the Atmosphere

Colorado State University

INTERACTION OF SHALLOW COLD SURGES

WITH TOPOGRAPHY ON SCALES

OF 100-1000 KILOMETERS

by

James J. Toth

Department of Atmospheric Science
Colorado State University
Fort Collins, CO 80523

This research was supported by NOAA
under Grant No. NE 85 RAH 05045 through CIRA

December 1987

ABSTRACT

A shallow cold air mass is defined as one not extending to the top of the mountain ridge with which it interacts. The structure of such an airmass is examined using both observational data and a hydrostatic version of the Colorado State University Regional Atmospheric Modeling System. The prime constraint on a shallow cold surge is that the flow must ultimately be parallel to the mountain ridge. It is found that the effects of this constraint are altered significantly by surface sensible heat flux. Cold surges are slowed during the daylight hours, a result consistent with previous observational studies in Colorado east of the Continental Divide.

Two case studies are described in detail, and several other events are cited. Since observations alone do not provide a complete description of diversion of the cold air by the mountain range, numerical model simulations provide additional insight into important mechanisms.

A case study on 14 June 1985 is described using observational and model data. The model development of a deep boundary layer within the frontal baroclinic zone is consistent with the observations for this and other cases. This development is due to strong surface heating. Turning off the model shortwave radiation is seen to produce a rapid southward acceleration of the surface front, with very shallow cold air behind the front.

Model simulations with specified surface temperature differences confirm the importance of upward heat flux from the surface in slowing the southward movement of the cold surge. It is concluded that the slowing is not due simply to the thermal wind developing in response to the heating of higher terrain to the west. Since surface heating is distributed

over a deeper layer on the warm side of the temperature discontinuity, there is frontolysis at the surface. But this modification would develop even over flat terrain. Sloping terrain introduces additional effects. Heating at the western, upslope side of the cold surge inhibits the development of pressure gradients favorable to northerly flow. A second contribution comes from westerly winds at ridgetop level. These winds are heated over the higher terrain and flow downslope, further retarding the progression of the cold air at the surface.

ACKNOWLEDGEMENTS

I appreciate the patience, guidance, prodding, and encouragement of my adviser, R.H. Johnson, and of all the committee members, R.E. Carbone, W.R. Cotton, T.B. McKee, R.A. Pielke, and R.S. Robinson. I also appreciate the encouragement and support from T.H. VonderHaar through the Cooperative Institute for Research in the Atmosphere (CIRA) during my entire stay at Colorado State University (CSU).

Interactions with various research groups have been valuable. Without listing all of the individuals, thanks go to everyone who helped me gather, process, and analyze data and discuss the results. Special thanks to Craig Tremback who taught me to use his version of the CSU Regional Atmospheric Modeling System (RAMS), which allowed this study to go beyond mere speculation. Thanks also to Gail Cordova and Judy Sorbie for skillfully preparing the manuscript and drafting some of the figures.

This research was supported by the National Oceanic and Atmospheric Administration through CIRA under grant NE 85 RAH 05045. The National Center for Atmospheric Research, sponsored by the National Science Foundation, made available computer time for the RAMS numerical model.

TABLE OF CONTENTS

1 INTRODUCTION 1

2 BACKGROUND 4

2.1 General considerations 4

2.1.1 Geostrophic adjustment, Kelvin waves, and rotating gravity currents 4

2.1.2 Shelf waves and conservation of potential vorticity 9

2.1.3 Flow over and around mountains 10

2.2 Observed phenomena 11

2.2.1 Coastal phenomena 11

2.2.2 Continental phenomena 13

2.3 Behavior of cold surges in northeast Colorado 14

3 A SYNOPTIC-SCALE COLD FRONT–14 JUNE 1985 20

3.1 Synoptic situation 20

3.2 Regional upper-air analyses 21

3.3 Development of mesoscale convective systems 31

3.4 Regional surface analyses 34

3.5 Details of the thermal structure 36

3.6 Discussion 51

4 OUTFLOW FROM A CONVECTIVE SYSTEM–1 AUGUST 1986 52

4.1 Synoptic situation 52

4.2 Importance of the convective system 57

4.3 The outflow boundary over northeast Colorado 61

4.4 Discussion 63

5 MODEL SIMULATIONS OF THE 14 JUNE 1985 CASE 65

5.1 The hydrostatic version of the RAMS model 65

5.1.1 Model treatment of surface fluxes 66

5.1.2 Vertical coordinate 68

5.1.3 Sensitivity and adequacy of the model 70

5.2 Simulation of the 14 June 1985 cold front 70

5.2.1 Coarse model analyses 71

5.2.2 Nested grid model analyses 76

5.2.3 Impact of short-wave radiative heating on cold surge evolution 82

5.3 Comparison of the impact of idealized surface fluxes 85

5.3.1 Analyses 86

5.3.2 Trajectories 87

5.3.3 Frontogenetical processes 91

5.4 Summary 100

6 IDEALIZED MODEL SIMULATIONS **101**
6.1 Role of surface heat flux 102
6.2 Impact of terrain blocking 107

7 CONCEPTUAL MODELS OF THE INTERACTION OF COLD SURGES WITH TOPOGRAPHY **118**
7.1 Impact of the geostrophic wind above the cold air 120
7.2 The impact of surface heating 121

8 SUMMARY AND CONCLUSIONS **127**
8.1 Conclusions 127
8.2 Suggestions for future research 128

LIST OF FIGURES

2.1 Summary of two-dimensional geostrophic adjustment 5
2.2 As in Fig. 2.1.d, but for flow confined between two channel walls. 7
2.3 Geographical and political features in and around Colorado 15
2.4 Total cold frontal passages for each hour at Denver, Colorado 17

3.1 Surface trough and frontal positions on 14–15 June 1985 22
3.2 Locations of radiosonde stations 24
3.3 Subjective regional upper–air analyses for 1200 UTC 14 June 1985. 25
3.3 continued 26
3.4 Same as Fig. 3.3, but for 0000 UTC 15 June 1985. 27
3.4 continued 28
3.5 Same as Fig. 3.3, but for 1200 UTC 15 June 1985. 29
3.5 continued 30
3.6 Visible satellite images on 14–15 June 1985 32
3.7 Composite digitized radar on 15 June 1985 33
3.8 Surface analyses on 14–15 June 1985. 35
3.9 Objective analyses of surface pressure changes 37
3.10 Radiosonde soundings at 0000 UTC 15 June 1985 38
3.11 An isentropic cross-section parallel to the Continental Divide 40
3.12 North-south cross-sections for 0000 UTC 15 June 1985 41
3.13 East-west cross-sections for 0000 UTC 15 June 1985 42
3.14 Time series from the Liberal, KS, wind profiler for 14-15 June 1985 43
3.15 Analyses of the PRE-STORM sounding network data for 85 kPa 44
3.15 continued 45
3.16 Same as Fig. 3.15, but for 70 kPa 47
3.16 continued 48
3.17 PRE-STORM soundings for PTT and IAB at 0000 UTC 15 June 1985 49
3.18 Thickness changes 50

4.1 Full resolution visible satellite images on 1 August 1986 53
4.2 Upper air analyses at 1200 UTC 1 August 1986 54
4.3 Temperature and dewpoint soundings for DEN and LBF 55
4.4 Surface plots with subjective analyses of the surface isentropes 56
4.5 Subjective analyses of the adjusted pressure 58
4.6 Surface pressure changes (contour interval 100 Pa) on 1–2 August 1986 60
4.7 Surface plots on 1 August 1986 for the PROFS mesonet region 62

5.1 Drag coefficients for heat and momentum as a function of the bulk Richardson number 67
5.2 The 26 vertical levels used in all model simulations 69

5.3 Smoothed topography used in the model for the 14 June 1985 case. 72
5.4 Isentropes (2 K interval) and wind vectors at 1.8 km 73
5.5 Soundings as in Fig. 3.10 but for the model output 75
5.6 Constant height analyses as in Fig. 5.4 but for 3.0 km 77
5.7 As in Fig. 5.4d, but for the nested, fine-grid simulation. 78
5.8 Same as Fig. 5.7, but for 3.0 km. 79
5.9 North-south cross-sections near the middle of the PRE-STORM network 81
5.10 Constant height analyses as in Fig. 5.4 but for the simulated night case 83
5.11 Isobars of the perturbation pressure for the simulated night case and for the actual daytime case at 1.8 km 84
5.12 Temperature analyses at 1.8 km as in previous figures but for specified surface temperature differences of –5°C 86
5.13 Trajectories for the day case (–5°C). 88
5.14 Same as Fig. 5.13, but for the night case (2°C). 89
5.15 Additional trajectories for the day case 90
5.16 North-south cross-sections through eastern Colorado 93
5.17 The convergence term, at the end of the simulation, contributing to changes in the north-south component of the temperature gradient 94
5.18 Same as Fig. 5.12, but after only 2 h of the simulation. 95
5.19 Same as Fig. 5.16, but after only 2 h of the simulation. 96
5.20 Adiabatic terms, near the surface baroclinic zone, after 2h, contributing to changes in the vertical component of the potential temperature gradient. . 98
5.21 Eastward advection of vertical stability 99

6.1 Idealized topography used for the simulations in this chapter (thick line) and smoothed topography for an actual cross-section through Colorado (thin line). 101
6.2 Initial temperature structure used for heating experiment. Isentropes are at 2 K intervals. 102
6.3 Surface flow after 12 h with surface heating alone. Isentrope interval 2 K. . . . 104
6.4 North-south isentropic cross-sections after 4 h (top panel) and after 12 h (bottom panel). Contour interval 2 K. 105
6.5 Contours (50 Pa interval) of pressure perturbation after 12 h. The thick dashed line indicates the axis of maximum perturbation. 106
6.6 Mountain-parallel component of the wind (1 m s^{-1} interval) after 4 h (top panel) and after 12 h (bottom panel). 108
6.7 Surface outflow 1 h after the initial conditions described in the text 110
6.8 North south cross-section with isentropic analysis (2 K interval) after 1 h. Location of the section is shown in the previous Figure. 111
6.9 Surface isentropes, same as the top panel of Fig. 6.7, but after 9 h for the no-heating case (top) and heating case (bottom). Location of east-west cross section is indicated. 112
6.10 Same as 6.9, but for pressure perturbation (interval 50 Pa). 113
6.11 East-west cross section (location indicated in the previous two Figures) with isentropic analyses (1 K interval) for the no heating case (top panel) and for the heating case (bottom panel). 115
6.12 Same as Fig. 6.11, but with pressure perturbation analyzed (50 Pa interval). . 116

6.13 Same as Fig. 6.11, but with the wind component perpendicular to the cross section analyzed (1 m s^{-1} interval). Southerly flow is positive. 117

7.1 Idealized relationship of cold air, pressure gradient, and wind for damming situations 119
7.2 Effect of uniform surface heating on a sloping frontal zone (a) distribution of surface heat flux convergence (b) the initial surface temperature discontinuity becomes diffuse. 122
7.3 Cold advection, intensity proportional to the length of the arrows, without heating (left) and with surface heating (right). 123
7.4 Interaction of mechanisms contributing to a daytime retardation of cold surges east of the Continental Divide. 125

Chapter 1

INTRODUCTION

Forecasting the weather in and around mountainous terrain is a challenging problem. Mountains introduce, directly or indirectly, atmospheric gradients and circulations ranging in spatial scale from the size of the smallest peak or valley to the size of the entire planet. The lifetimes of the various features span a wide temporal range. Large and small features, those induced by the mountains as well as those the atmosphere develops without mountains, interact to make understanding appear impossible. The only approach must be to break the problem down into manageable pieces (Smith, 1986).

The piece isolated for this study is the interaction of a synoptic-scale, or a large mesoscale front or boundary with a mountain range. Atmospheric features of this large a horizontal extent ($\sim$1000 km) have lifetimes of 12 h or greater. This means that, away from the equator, the Coriolis force is important. The problem is further limited to fronts or boundaries having mostly shallow cold air behind them. Shallow is defined as less than, or on the order of, the height of the mountain ridge. A moving cold air mass, either of synoptic or mesoscale origin, will be referred to as a cold surge. The significance of a shallow cold surge is that surface cooling must occur only with temperature advection parallel to the mountain. There is no cold air advection over the mountain ridgetop and, in fact, warm advection at ridgetop level may inhibit surface cooling on the downslope side.

Cold surges interact with topography in many parts of the world and there are some common features. The Alpine Experiment (ALPEX), conducted in Europe in 1981-82, was designed to explore some of these problems. However, the motivation for this study is the behavior of shallow cold surges along the Colorado Front Range and over the gently-sloping plains to the east. In this area, upslope stratus and precipitation may form in the cool air if sufficient moisture is present. During the cold season, arctic fronts or other boundaries imbedded within developing cyclones often determine the location of intense snowfall (Schlatter *et al.*, 1983; Schultz, 1985). During the summer months, Wilson and Schreiber (1986) have identified shallow boundaries of synoptic-scale origin, along with thunderstorm outflows (Sinclair and Purdom, 1983; Droegmeier and Wilhelmson, 1985) and other boundaries of uncertain origin, as strongly contributing to the initiation of convective storms in northeast Colorado.

The purpose of this study then is to shed light on the important physical processes operating in connection with shallow cold surges in eastern Colorado and adjoining areas. The impact of the mountains on surges like these can be considered in two categories: terrain blocking and terrain heating/cooling. The first category, terrain blocking, is a direct constraint on the movement of the cold air. This alone is a problem which has received much attention recently, and several studies will be reviewed in chapter 2. The second category enters when considering radiative surface heating/cooling. The mountains become elevated heat sources/sinks and, by modifying the horizontal temperature gradients and, thus, the horizontal pressure gradients, they alter the dynamical forces driving the movement of the cold air. This second category, terrain heating/cooling, generates diurnally varying surface flow over northeast Colorado during relatively undisturbed conditions (Johnson and Toth, 1982; Smith and McKee, 1983; Reiter and Tang, 1984; Toth and Johnson, 1985; Abbs and Pielke, 1986).

One of the major results of the numerical modeling portion of the study in this paper is a confirmation of Wiesmueller's (1982) observation that there is also a diurnal variation in the movement of shallow surface cold fronts near the Front Range. Thus both categories of mountain impact occur. Observed fronts propagate more rapidly southward at night, especially during the summer. Various physical processes operate in conjunction with this effect (moisture distribution, surface characteristics), but diurnal boundary layer changes appear to be critical, and these are investigated numerically.

In Chapters 3 and 4, observational studies of two cases of shallow cold surges moving through eastern Colorado are presented. The first case is a weak synoptic-scale cold front on 14 June 1985. This occurred during the Oklahoma–Kansas Preliminary Regional Experiment for STORM–Central (OK PRE–STORM). Along with the behavior near the mountains, the behavior of the front as it moved through the PRE-STORM dense observational network to the east is also of interest. The second case is the movement of an outflow boundary through the Program for Regional Observing and Forecasting Services (PROFS) surface mesonetwork in northeast Colorado on the morning of 1 August 1986. This boundary originated the previous night with a large mesoscale convective system in the Nebraska panhandle, yet it too behaved much like a shallow, spatially large-scale cold front. The boundary moved rapidly during the early morning hours as it approached and intersected the Front Range, but then slowed during the time of maximum heating.

These case studies, combined with previous studies by other investigators, provide some insight into the propagation of cold surges and their evolution over 12-24 h. But the available data do not have the spatial or temporal resolution to provide as much insight as desired. As a result, three-dimensional numerical modeling investigations were conducted. It is shown in Chapter 5 that the Colorado State University Regional Atmospheric Modeling System (CSU RAMS) model is capable of simulating the essential features of the 14 June 1985 case, particularly the behavior of the front near the mountains. In order to provide insight into the relative importance of the various physical processes, model simulations for idealized situations are presented in Chapter 6. In Chapter 7, there is a discussion of conceptual models based on the earlier observational and numerical results. Chapter 8 is a summary along with conclusions and suggestions for future research.

Chapter 2

BACKGROUND

This study focuses on cold surges approaching and moving along the eastern slopes of a mountain barrier. There are some common features related to the interaction of cold fronts and stable layers with topography in all parts of the world. In this chapter, the impact of mountains, or in their highly idealized form, side boundaries, is first reviewed for general situations. Secondly, actual phenomena around the world and on various horizontal scales are briefly described. Finally, the unique behavior of cold surges around the topographic features in the vicinity of Colorado is summarized.

2.1 General considerations

2.1.1 Geostrophic adjustment, Kelvin waves, and rotating gravity currents

The actual flows described later can not be expected to reach a state of equilibrium in geostrophic balance by the end of the short period studied. But, the evolution with time is closely related to the geostrophic adjustment problem, first explored in detail by Rossby (1937), and described in several meteorology and geophysical fluid dynamics textbooks. A brief summary from Gill (1982; also in Gill, 1976) is illustrated in Figs. 2.1 and 2.2 and described below. The coordinates have been chosen to suggest analogies with an actual situation where there is a shallow inversion throughout a region, with deeper cold air to the north.

For the idealized situation, it is assumed that the linearized shallow water equations apply to a single layer of fluid, of constant and uniform density, with infinite horizontal extent. The equations are:

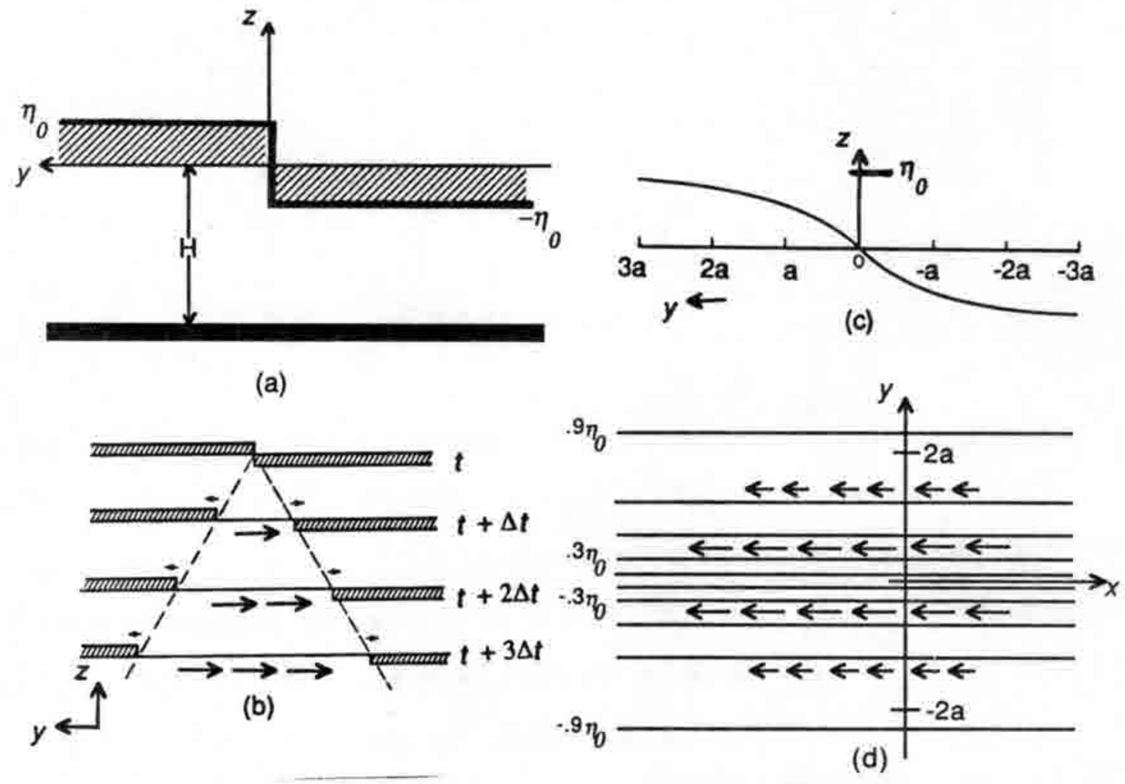

Figure 2.1: Summary of two-dimensional geostrophic adjustment as presented by Gill (1982). (a) The initial step function perturbation to the fluid height splits into two wave fronts, shown spreading apart at successively later times (b) for the case of no rotation. (c) Final geostrophically adjusted fluid height for the same initial conditions, but with rotation. (d) Plan view of (c).

$$\partial u/\partial t - fv = -g\partial\eta/\partial x \ ,$$

$$\partial v/\partial t + fu = -g\partial\eta/\partial y \ ,$$

and

$$\partial\eta/\partial t = -H(\partial u/\partial x + \partial v/\partial y) \ ,$$

where η is a small perturbation on the mean depth, H. Initially (Fig. 2.1a) the perturbation is a step function:

$$\eta = \eta_o \ , y > 0 \ ,$$

$$\eta = -\eta_o \ , y < 0 \ .$$

For the case of no rotation ($f = 0$, Fig. 2.1b, illustrating flow at four different times), the perturbation splits into two wave fronts propagating at the gravity wave speed, $c = \sqrt{gH}$, in opposite directions. As the wave fronts move apart, the fluid between them is left moving southward at a speed $(1/2)c^{-1}g\eta_o$.

With rotation (f assumed constant) there are initially transient gravity wave effects. But the final geostrophically balanced solution (Fig. 2.1c) keeps most of the kinetic energy confined near the initial perturbation. The distance $a = c/f$ is the Rossby radius of deformation. The significance of the length a is that by the time the initial perturbation has propagated this distance, traveling at a speed c, the Coriolis force has had time (f^{-1}) to cause the moving fluid to be deflected westward and to approach a geostrophic balance. At north or south distances much greater than a, the fluid remains near its initial state. An alternative view of the final geostrophically balanced easterly flow can be seen in Fig. 2.1d, a horizontal contour map of η. Hydrostatically, gradients of η correspond to pressure gradients, and so this map of η is roughly equivalent to the isobars presented in later chapters.

Gill (1982, section 10.7) investigated the geostrophic adjustment effects introduced by the presence of side boundaries. The previous situation with an initial step function is the same except that the fluid is confined within a north-south channel. Gill developed an analytic solution for this case. After a long time (Fig. 2.2), there is a geostrophically balanced northeasterly flow near the center of the channel. With a wider channel, the flow at the center would be more easterly, approximately the same as in Fig. 2.1d. But at the channel walls, there can be no east-west flow. Upstream there is northerly flow along the east wall (not shown), while downstream the northerly flow is along the west wall. This flow is also geostrophically balanced. Both the speed of the along-wall flow and the disturbance height ($\eta - \eta_o$) decay exponentially away from the wall, with length scale a, the Rossby radius of deformation. The effect is the same as if the solution in Fig. 2.1d had been "bent" to fit the walls. On the other hand, the along-wall flow is analogous to the no-rotation case in Fig. 2.1b. This is because the leading edges of the northerlies propagate upstream along the east wall, corresponding to the left wave front in Fig. 2.1b,

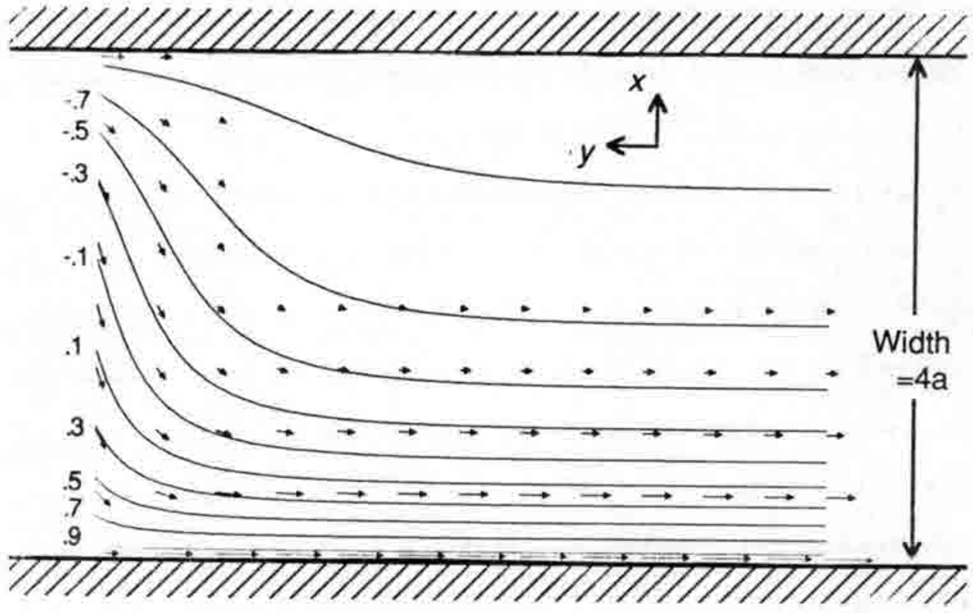

Figure 2.2: As in Fig. 2.1.d, but for flow confined between two channel walls.

and downstream along the west wall, corresponding to the right wave front in Fig. 2.1b. As in the non-rotating case, there is a continual conversion of potential to kinetic energy since the flow is moving from higher to lower heights. Furthermore, there is no limit on how far along the wall the impact of the initial disturbance can propagate. Chen (1984) suggests that the release of potential energy contributes to lee cyclogenesis.

This idealized channel example can be modified and adapted to apply to actual atmospheric flows. The northerly flow along the west wall is characteristic of advancing cold air, particularly along the Colorado Front Range. Since the flow along the west wall is of most interest, the east wall should be considered to be absent or, alternatively, the channel could be assumed to be very wide.

A complication arises when describing the leading edge of the northerly flow. Sinusoidal gravity waves, propagating parallel to a wall, with amplitude decaying exponentially away from the wall, behaving in the along-wall direction as if there was no rotation, yet maintaining a geostrophic balance with the pressure gradient perpendicular to the wall, are known as Kelvin waves. In the northern hemisphere, Kelvin waves can propagate only with the boundary on the right. Thus, although they are not sinusoidal, the wave fronts propagating up- and downstream along the walls in the idealized example (far beyond the left and right sides of Fig. 2.2) are appropriately referred to by Gill (1982) as "Kelvin wave fronts". But the linear, inviscid, idealized situations are strictly analogous only to cold surges propagating into a pre-existing, more shallow, cold inversion ahead. When this is not the case, and there is no vertical density discontinuity in the air ahead of the cold surge, it is more appropriate to refer to the flow at the leading edge as a gravity current or, perhaps, as a trapped or rotating (Griffiths, 1986) gravity current. Nevertheless, as noted by Chen (1984), the rotating gravity current and the Kelvin wave have these features in common: one-way propagation, phase speed approximately the gravity wave speed, and the along-boundary flow is in geostrophic balance. In other words, it would be appropriate to refer to a "rotating gravity current" as a "Kelvin gravity current" since it is related to a non–rotating gravity current in the same way that a Kelvin wave is related to a non–rotating gravity wave.

Behind the leading edge, a number of terms have been applied to the northerly flow along the mountain range (wall). The most popular term seems to be "cold air damming" (Richwein, 1980). Cold air damming is often described as resulting from the inability to maintain geostrophic balance near the mountain. This statement is somewhat misleading, since it suggests that the northerly flow is an antitriptic wind moving directly from high to low pressure. The statement may be appropriate for the flow at the southern, leading edge. Also, as a pre-existing easterly flow suddenly impinges on the mountain range (e.g., near the middle left of Fig. 2.2), the flow there might be highly ageostrophic. But with time ($\sim f^{-1}$), to the extent that the flow moving south along the mountain becomes a "free" gravity current (Griffiths, 1986), it should be expected to "bank" the cold air against the mountain. In fact, rather than antitriptic flow, Griffiths describes the rotating gravity currents as being semigeostrophic. Even with friction, the along-mountain flow can be approximately in geostrophic balance with the mountain-perpendicular pressure gradient. Chen (1984), in rotating tank experiments, obtained this banking effect.

If in fact there is a pre-existing stable layer ahead of the cold surge, then for the idealized example the impact of the neglected nonlinearities must still be considered. The leading edge may develop into a bore, effectively a propagating hydraulic jump. The same situation is also favorable for the development of solitary waves (Christie et al., 1979; Doviak and Ge, 1984; Haase and Smith, 1984). As noted by Griffiths (1986), even without a pre-existing stable layer, solitary waves may develop along the gravity current itself, and these are closely related to the solitary Kelvin waves described by Maxworthy (1983). In this study, neither the observational data nor the model data provided a clear determination of whether these wave effects were present.

Even with the simple assumption of a vertical wall as an approximation to the mountain range, the introduction of friction and nonlinearities complicates the problem. A further complication is the fact that the cold air approaches the Front Range over sloping plains. This introduces the possibility of shelf waves.

2.1.2 Shelf waves and conservation of potential vorticity

As an approximation, the cold air over the plains might be considered to have a flat top. As the air mass advances westward over the upward sloping ground, and if the top remains at a constant elevation above sea level, columns of air must shrink vertically and stretch horizontally. If the top is not high enough, the cold air might never be able to reach the Front Range. This vertical shrinking, combined with conservation of potential vorticity, requires that large negative relative vorticity (anticyclonic shear) develop along the western edge of the cold air. Strong southerly flow is often observed along the extreme western edge of a quasi-stationary but very shallow cold air mass along the Front Range. Although the southerly flow is not present for the two observed cases discussed in the next chapter, it does appear in the idealized model simulations shown in Chapter 6.

Wave motions are also possible along the western edge of the cold air. The restoring force for these waves is due to the sloping bottom topography. Vertical shrinking causes a decrease in relative vorticity as the air moves west, and vertical stretching causes an increase in relative vorticity as the air moves east. This is analogous to the free atmosphere situation that is responsible for Rossby waves, where an increase of planetary vorticity causes northward moving parcels to develop negative relative vorticity, and the opposite holds for southward moving parcels. Analogous to the Rossby waves, which, relative to the mean flow, propagate with higher planetary vorticity on the right, the shelf waves propagate with higher bottom topography on the right (Gill, 1982). It is interesting that these continental shelf waves, named for the oceanographic situation in which they are usually found, propagate in the same direction as the rotating gravity current and the Kelvin wave. On the planetary scale, northern hemisphere observations show that the cold air near the surface splits away from the main planetary propagating disturbance east of mountain ranges and moves farther south than would be expected without mountains (Hsu and Wallace, 1985). Hsu and Wallace have suggested that shelf waves are largely responsible for this behavior. But it is not clear how important the shelf waves are for the synoptic and mesoscale systems of ~1000 km scale studied here.

2.1.3 Flow over and around mountains

Smith (1982) and others have developed analytic solutions for the specific situation of a front approaching and moving over and around mountains. These solutions provide some insight, but most of them are based on assumptions that do not seem to be appropriate for the problem studied here. For example, although Smith allowed for both x and y variations, he needed to assume isolated mountains rather than an infinite barrier. His solutions also implied that disturbances created by the mountains were primarily ageostrophic. As noted above, when cold air flows for several hours parallel to a mountain barrier, it is possible to develop a geostrophic, or at least semigeostrophic, flow. Although Smith's model developed the basic distortion of the front (e. g., a tendency for cold air damming), he did feel that certain omitted phenomena, including nonlinearities and boundary layer effects, could be crucial.

Fronts approaching an infinite mountain range have been considered analytically (Bannon, 1984; Davies, 1984), but it has been necessary to assume no variation in the along-mountain direction. This also requires that the approaching front be parallel to the range. Davies found that for a simple one-layer model, which assumed semigeostrophic balance between the along-front motion of the cold air and the cross-front pressure gradient, the evolution of the front depended on two parameters. One is the ratio of the mountain height to the depth of the cold air. Deeper cold air is better able to cross the mountain relatively unmodified. The other parameter is a ratio of the mountain width to the Rossby radius of deformation. With a wide mountain (gentle slope), a shallow but only slightly colder air mass (small c and small Rossby radius) may eventually cross the mountain. Bannon (1984) considers a similar situation. He emphasizes the impact of the mountain in modifying the circulations found in semigeostrophic studies of fronts over flat terrain. Bannon (1986) further treats shallow and deep flows over a mountain. For the purpose of this study, Bannon's "shallow" flow would be considered a deep cold surge.

With or without rotation, a critical parameter in all studies that allow for continuous atmospheric stability is the quantity u/Nh, traditionally referred to as the Froude number. N is the Brunt–Vaisala frequency, a measure of the atmospheric stability, h is the mountain height, and u is the windspeed in the cold air. If the air is very stable, the mountain is high, and the wind speed is low, this number will be small, implying that the cold air cannot cross the mountain. But if this number is large, the inertia of the cold air will be enough to overcome the buoyancy forces. Baines (1987) argues that the term "Froude number" for u/Nh is inappropriate since, historically, the term has been used for the ratio of the fluid speed to the wave drag or wave speed, and it is unnecessarily confusing to have a variety of Froude numbers. He suggests that this quantity be referred to simply as "Nhu". Typically N, and therefore "Nhu" varies greatly from day to night in the boundary layer. This can be expected to contribute to differing behavior of the cold surges.

Other analytical and numerical studies have been done in connection with phenomena observed in specific locations around the world. These are discussed in the next section together with the observations.

2.2 Observed phenomena

2.2.1 Coastal phenomena

In contrast to the situation in Colorado, many of the observed cases involve an atmospheric front over the ocean, approaching a continent and interacting with the coastal mountain range. Frequently there is a pre-existing stable marine layer. This means the discussion in section 2.1a of idealized, linear waves may apply. The coastal lows of southern

Africa have been interpreted by Gill (1977) and by Bannon (1981) as forced Kelvin waves. In this view, migrating synoptic systems do not themselves interact with the mountain range, but instead produce disturbances in the marine layer. In Bannon's view, the subsidence associated with a migrating anticyclone depresses the marine inversion, creating a surface low which then propagates with the coast on the left (Southern Hemisphere). Actually, the linear analysis by Gill and Bannon provides only for sinusoidal Kelvin waves. According to the linear theory, coastal highs should be just as common as coastal lows. Either nonlinear effects (Gill), or Bannon's explanation could account for the prevalence of the lows.

Several investigators have looked at disturbances in and on the marine layer along the west coast of North America. Dorman (1985) performed a case study of a disturbance propagating northward along the California coast. He felt the disturbance was a solitary Kelvin wave of elevation, generated by the frictional effect of onshore winds above the marine layer. The frictional force causes the marine layer to pile up against the coastal mountains, thus raising the inversion. With time, the nonlinear behavior of the solitary Kelvin wave and the curvature of the coastline lead to the development of a mesoscale eddy within the marine layer. Mass *et al.* (1986) and Mass and Albright (1987) describe surges of marine air along the coast of Oregon and Washington as being more closely related to the gravity current description than to a Kelvin wave. The gravity current is generated as a synoptic-scale front approaches the coast. They suggest that the gravity current description may also be appropriate for the South Africa and the California disturbances. A final example of a coastal, poleward propagation of relatively cool marine air may be the surge from the Gulf of California (Hales, 1972) that often supplies moisture for the Arizona summer monsoon. The Gulf Surge in its initial stages is constrained on the east by the Sierra Madre Mountains of Mexico.

On the east coast of the United States, "back-door" cold fronts move from northeast to southwest. The Appalachian mountains block the cold air flow, an effect named "damming" by Richwein (1980). Bosart *et al.* (1973) studied many cases of back-door cold fronts. One of the interesting statistics they obtained was a slight preference for more rapid movement between 0000 and 0600 local time. They felt that this was purely coincidence. But it may be related to the observed nocturnal acceleration in eastern Colorado. A typical east coast damming event has recently been documented by Forbes *et al.* (1987) and simulated numerically by Stauffer and Warner (1987).

The orientation of the east coast of China is similar to the east coast of the United States, although the inland mountains are very different. Just off the China coast, cold fronts interacting with the north–south Yuh mountain range of Taiwan are observed to accelerate south at night (Johnson, personal communication). Diurnal variations in frontal movement are noted by Taiwan forecasters only during the spring and fall seasons.

Returning to the Southern Hemisphere, Baines (1980) developed a simple model for the interaction of a cold front with the southeast coast of Australia. Cold air there travels more rapidly along the coastal mountains and is known as the "southerly buster". Baines' model includes an exponential decay of the gravity current away from the coast, and it also accounts for the faster speed of the front next to the mountains, where the cold air is deepest. However, Coulman *et al.* (1985) found that, at least near the leading edge of the front, there was no decay in amplitude away from the coast. They also found evidence that the southerly buster was entraining warm air as it propagated northward. Nocturnal wind surges in northeastern Australia have been discussed by Smith *et al.* (1982 and 1986). An approaching front would seem to be the most likely generation mechanism for the southerly surges in this area. But, in fact, Smith *et al.* (1986) found that other mechanisms including boundary layer drainage winds and low-level jets interacting with the sea breeze are more important. In any case, the structure of the southerly surges is consistent with a gravity current description.

2.2.2 Continental phenomena

Smith (1986) discusses the variety of winds that develop as fronts interact with the Alps. These include the bora, the mistral, and the foehn. The bora is somewhat related to cold air damming, involving air moving anticyclonically around the eastern edge of the Alps. Chen (1984) and Smith discuss related cold air damming situations including, in addition to those already mentioned, the pampero wind in the area of Argentina east of the Andes. But the situation most closely related to the Front Range and sloping plains to the east seems to be the continental portion of Asia east of the Tibetan Plateau.

Nakamura and Doutani (1985) used a shallow water equation model to demonstrate that the Tibetan Plateau, modeled as a rectangular plateau with vertical walls, is capable of generating Kelvin waves. In a numerical model with more realistic topography, they found ageostrophic winds were confined mostly to the leading edge of cold surges. They concluded that the mountain slope "acts as a rather vertical wall to generate the Kelvin waves in the formation stage and that it acts as a rather smooth slope to produce the shelf waves in the propagating stage". Sumi (1985) concluded that high resolution in the lower troposphere is essential for modeling the cold surges. He found that the pressure gradient term was most important in the early development of the cold surge, but the nonlinear advection terms dominated in the later stages.

2.3 Behavior of cold surges in northeast Colorado

The Program for Regional Observing and Forecasting Services (PROFS) surface mesonetwork, covering a large portion of northeast Colorado, and the 300 m Boulder Atmospheric Observatory (BAO) tower have provided frequent and detailed looks at the surface and near-surface behavior of fronts. Shapiro (1984) and Young and Johnson (1984), using the BAO tower data, studied fronts that had become highly distorted on the mesoscale after encountering the terrain features of northeast Colorado (Fig. 2.3). They found that the leading edge of the cold air was nearly vertical and propagated as a gravity current. In each case the front was dry, supported by strong synoptic-scale cold advection, and not complicated by feedbacks from cloud microphysical processes. In another case, Shapiro *et al.* (1985) used Doppler radar wind profiler observations to further show that there was a large hydraulic head at the leading edge of the gravity current. They suggested that hydraulic heads, bores, and solitary waves may be a common but unrecognized or unresolved feature of fronts. Shapiro *et al.* (1984), using profiler winds, constructed detailed sections across a strong upper- level front and across a shallow surface front. In most cases, however, the Colorado wind profiler network has proven not able to obtain winds close enough to the ground to be useful for studying large, shallow cold surges.

Figure 2.3: Geographical and political features in and around Colorado discussed in this and later chapters.

The effects of shallow cold surges are significant at all times of the year. During the warmer months, Doswell (1980) has shown how the shallow easterly flow behind a weak cold front helps develop severe weather over the High Plains. There is increased moisture advection, and the slightly cooler air at the surface contributes to a capping inversion. Cotton *et al.* (1983) describe a weak cold front which moves into northeastern Colorado during the early morning hours. The front dissipates during the afternoon, but contributes to the upscale development of convection into a mesoscale convective complex (MCC).

Synoptic–scale or large mesoscale forcing of convection is sometimes obvious (e.g., Bluestein *et al.*, 1984), but at other times it is more subtle and difficult to identify. This is especially true when there are interactions with other convergence zones. These include the downslope–generated, eastward-propagating large-scale convergence zone discussed by Banta (1984) and by Toth and Johnson (1985), and the quasi-stationary convergence zone within the PROFS mesonet area, discussed by Szoke *et al.* (1984). This last feature appears to be caused by blocking of the synoptic-scale flow, but it may also be generated by surface heating/cooling (Abbs and Pielke, 1986). Schlatter (1984) studied two well–defined intersecting thunderstorm outflow boundaries. He also noted the presence of east–west oriented cloud bands south of the PROFS area, but did not speculate about their origin. Wilson and Schreiber (1986) identified some low–level boundaries as being of synoptic–scale origin, but many others were of uncertain origin. It's possible that some of the uncertain boundaries result from the interaction of synoptic–scale or large mesoscale systems with topography.

Even in deeper, winter cyclonic systems, shallow surges of cold air appear to modulate the intensity of precipitation. An example of this can be seen in the analysis of the Denver Christmas Eve blizzard by Schlatter *et al.* (1983). Schultz (1985) presents a schematic diagram of cold air damming along the Front Range during a snowstorm. Warm, moist, upslope, easterly flow overrides the cold northerly flow near the mountains. The northerly flow provides an additional lifting mechanism, enhancing the snowfall over the plains. Dunn (1987) further discusses the mesoscale details of cold air damming along the Front Range.

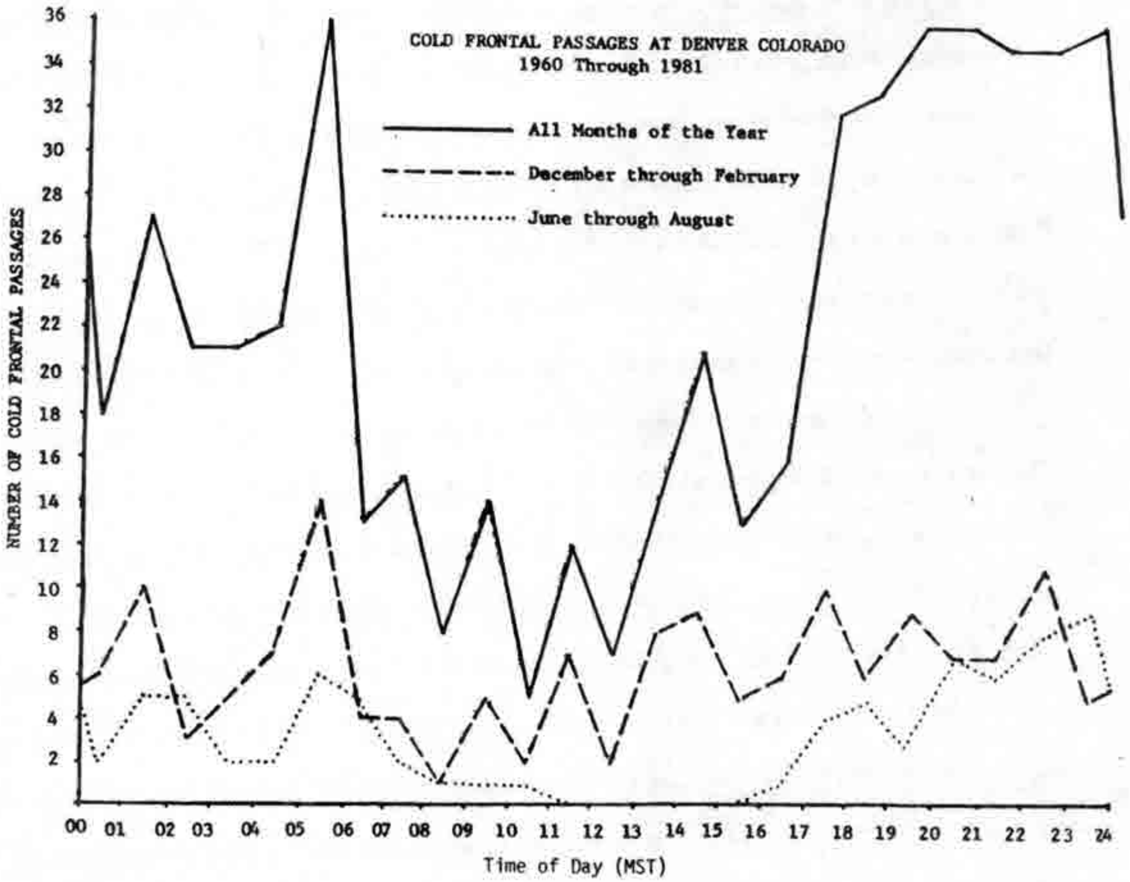

Figure 2.4: Total cold frontal passages for each hour at Denver, Colorado, during the years 1960–1981 (from Wiesmueller, 1983).

After reviewing the frequency of cold frontal passages at Denver, Colorado, by time-of-day (Fig. 2.4), Wiesmueller (1982) determined that there is, in fact, a greater tendency for fronts to pass during the nighttime hours. This tendency is mostly associated with weak, shallow fronts, and so it is most noticeable during the summer months. The stronger fronts of winter are less influenced by diurnal effects.

Obviously, one impact of strong surface heating is to "burn-off" a shallow cold air mass, and this influences the apparent movement of the front. Most studies of the impact of surface heating on mesoscale systems have been concerned with *differential* surface heating (e.g., Orlanski, 1986). But spatially *uniform* surface heating can affect the structure of a frontal zone. This was simulated numerically for an idealized front by Pinkerton (1978). The integrated effect of the turbulent heat flux is to create a layer of constant potential temperature extending some distance above the surface. The final result in Pinkerton's simulation is a frontal zone identified with closely-spaced vertical isentropes in the ~1.5 km deep boundary layer at the leading edge and by isentropes above the boundary layer tilted the same as for the initial front. There is also a reduction in the magnitude of the surface temperature gradient, partly because the surface heating is distributed over a deeper boundary layer ahead of the front. The variation in boundary layer depth also has an impact on horizontal and vertical wind shears, and the variation in horizontal temperature gradients affects the thermal wind shear. Garratt and Physick (1987) also found that the effect of surface heating on a gravity current was to produce a deeper and less intense baroclinic zone for daytime conditions when compared to night. Keyser and Anthes (1982), in their model that excluded surface heat flux, showed that the surface momentum flux as well as the turbulent redistribution of heat and momentum within the atmosphere have a significant effect on the structure of an idealized front. There is a narrow updraft above the boundary layer at the leading edge of the front, in agreement with many observations. The boundary layer air behind the front is slightly unstable, but the region above the frontal zone and also the boundary layer well ahead of the front are stable.

Wiesmueller (1982) feels that the primary mechanism retarding frontal movement over eastern Colorado during the day is the large-scale enhancement of southerly winds in the boundary layer. This is a geostrophic response to the heating of higher terrain to the west (northerly thermal wind). Although this effect is certainly present, the amplitude of the actual diurnal wind oscillation near the Front Range (Johnson and Toth, 1982; Smith and McKee, 1983; Reiter and Tang, 1984; Toth and Johnson, 1985; Abbs and Pielke, 1986), or even the oscillation of the geostrophic wind, cannot alone account for the increase in the frontal propagation speed by ~10–15 m s^{-1} from day to night.

Considering Wiesmueller's findings for Denver, the behavior of fronts farther east of the mountains is of interest. Brundidge (1965) commented on the complex structure of nocturnal fronts as they passed a 430 m tower near Dallas, Texas, during the fall and winter months of 1961–62. Ahead of the fronts, low-level nocturnal inversions, several hundred feet deep, made determination of the exact time of frontal passage difficult.

(This uncertainty also applies to other studies of diurnal behavior of fronts, including Wiesmueller's frequency distribution. A subjective estimate of frontal passage can be made based on wind shift, temperature drop, and pressure increase; but it is difficult to specify objective criteria for these parameters in a manner appropriate for all types of fronts and at all times of the day.) Brundidge also found that as the fronts progressed, warm air was being entrained into them. So, the frontal surfaces were not behaving as material surfaces, a conclusion also reached by Sanders (1955) using much coarser resolution data. Interestingly, it was purely by coincidence that all but one of the 11 frontal passages studied by Brundidge were nocturnal.

The interaction between cold surges and precipitating cloud systems is not one–way. Cloud microphysical processes can certainly feedback to affect the evolution of shallow cold surges. Boatman and Reinking (1984) discuss the interaction between mesoscale circulations and precipitation mechanisms in the shallow arctic air masses of winter. As shown by Carbone (1982), in a study of a frontal zone near Sacramento, California, precipitation cooling can act in a cooperative manner with synoptic–scale cold advection to maintain an intense surface frontal zone propagating as a gravity current. The relative importance of precipitation feedback will not be addressed in this study. Also, the impact of strong winds above the cold air will be neglected. Lilly (1981) suggested that turbulent mixing and detrainment at the top of a cold air mass is a mechanism for sustaining upslope flow within the cold air.

It is appropriate to ignore these last two effects for the shallow cold surges during the summer months. Winds aloft are light, and moist convection is usually absent for the period from late–night until early or late afternoon. In addition, the potential impact of surface heating/cooling is strongest during the summer. This is the main focus of this study. Two summer observational case studies are presented in the next two chapters.

Chapter 3

A SYNOPTIC-SCALE COLD FRONT–14 JUNE 1985

In this and the next chapter two case studies are presented which are representative of typical shallow cold surges east of the Colorado Front Range. Summer cases were selected since the synoptic–scale forcing is weaker at this time of year, and so the impact of the mountains and the surface heating on the movement of cold surges is more pronounced, an effect noted by Wiessmueller (1982). Additionally, during the warmer months, the boundaries associated with the cold surges to the east of the Continental Divide often play an important role in the evolution of deep, moist convection. Although these cases are specific to northeast Colorado, the findings of this study, along with Wiesmueller's conclusions regarding frontal movement, likely apply in many other areas. For example, diurnal variations in frontal passage at Taipei, Taiwan, (see Chap 2) are observed only during the transition seasons, not when synoptic–scale forcing is strong.

On 14 June 1985, the feature of interest is a weak synoptic–scale cold front. Special observational data for this event were available from the Oklahoma–Kansas Preliminary Regional Experiment for STORM–Central (OK PRE-STORM; Cunning, 1986). Although the experimental area was well east of the Continental Divide, the data provide, when combined with routinely available data from eastern Colorado, some insight into the east–west variability of the structure of the southward moving cold surge. The analyses of these data also provide a basis for evaluating the realism of the numerical model output presented in the next chapter.

3.1 Synoptic situation

On the morning of 14 June 1985, the 1200 Universal Coordinated Time (UTC; 0600 local time) National Meteorological Center (NMC) surface analysis indicated stationary frontogenesis extending east–west through northeast Colorado and across southern Nebraska (Fig. 3.1a). A north-south trough had been analyzed during the previous afternoon and night. Prior to 14/1800 UTC, the continuity of the NMC analyses was poor, reflecting the fact that the front/boundary was diffuse and difficult to analyze. After this time, although the surface temperature gradients remained relatively diffuse, the front was placed along a distinct windshift line. By the following afternoon, the front over Oklahoma had once again become very weak and diffuse, and it was dropped by NMC after the 15/1800 UTC analysis. Thus the surface front as analyzed by NMC had a total lifetime of only 30 h.

With the benefit of later analyses, and considering that the polar front jet stream extended northwest to southeast across central Nebraska and northeast Kansas, a more appropriate conceptual model for the surface features is indicated in Fig. 3.1b. The system can be thought of as a shallow, stable, baroclinic wave propagating southeast along the polar front. Across the eastern two–thirds of Kansas, even though there was a distinct windshift, the front resembled more a cold occlusion than a cold front.

There are many differences, but in some ways the system is similar to southern Australia summertime frontogenesis, as discussed by Reeder and Smith (1986). In their two–dimensional numerical model, which is a nonlinear extension of the analytic Eady model of baroclinic instability, a broad zone of large temperature gradient develops but is confined to a layer within 3 km of the surface. Reeder and Smith believe this evolution explains some of the observed features of summertime fronts approaching the southern Australia coast, particularly the shallowness of the cold air behind the front. The upper–air observations suggest that their description is an appropriate one for the vertical structure of the western portion of the 14 June 1985 disturbance; i.e., cold advection is confined to a layer within 3 km of the surface.

3.2 Regional upper–air analyses

The long wave pattern, a moderate amplitude ridge centered over the west coast of the United States and a trough in the east centered near 80°W longitude, evolved little

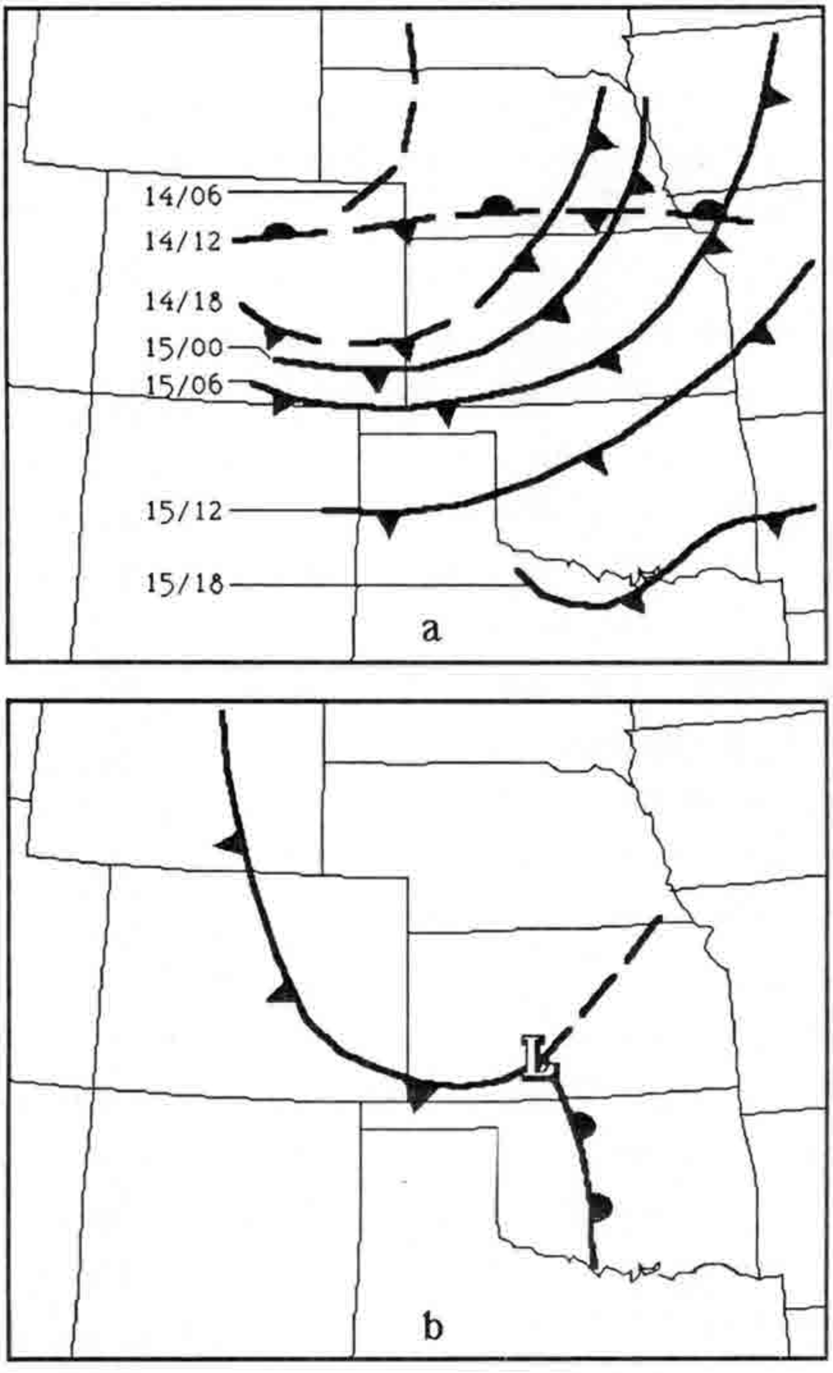

Figure 3.1: (a) Surface trough and frontal positions at 6 h intervals, labeled with the date and the UTC hour, as analyzed by the National Meteorological Center on 14–15 June 1985. (b) Reanalysis of surface features for 15/00 UTC. The actual warm front is very broad and diffuse over the Texas panhandle and western Oklahoma.

during the period, and so only the regional features will be shown. The locations and elevations of the radiosonde stations discussed are shown in Fig. 3.2. Over the PRE-STORM area, stations DDC, TOP, and OKC are National Weather Service (NWS) sites providing routine operational soundings at 12 h intervals. On this date, these NWS sites did not launch any special PRE–STORM soundings. Soundings were, however, taken by the special PRE–STORM network (RSL, FRI, PTT, IAB, CNU, END, HOY, FSB, HET, and SUL in Fig. 3.2) at three–hour intervals from 14/2100 to 15/0900 UTC. Data from an eleventh PRE–STORM network station (WWR, in northwest Oklahoma) were judged to be of questionable accuracy, unfortunately, and have not been included in the analyses.

Subjective regional analyses of the standard constant pressure surfaces at 14/1200, 15/0000, and 15/1200 UTC are presented in Figs. 3.3-3.5. In the middle and upper troposphere, northwesterly flow prevailed throughout the period. The 50 kPa temperatures warmed over most of the area, with 24 h increases (Fig. 3.3 to Fig. 3.5) ranging up to 4°C over Colorado. The 30 kPa polar jetstream extended from Wyoming through central Nebraska and into northeast Kansas at 14/1200 UTC (Fig. 3.3), dipped into central Kansas at 15/0000 UTC as a short wave trough passed (Fig. 3.4), and then redeveloped over northeast Nebraska by 15/1200 UTC (Fig. 3.5). Although the short wave trough is reflected at all levels in the troposphere, areas of strong temperature advection are confined to the levels below 50 kPa.

At the beginning of the period (Fig. 3.3), an 85 kPa thermal ridge extended from southeast Colorado into eastern Nebraska, with a height trough extending from eastern South Dakota to northeast Colorado. The 70 kPa height trough is much less pronounced and is nearly coincident with the one at 85 kPa. There is moderate geostrophic warm advection ahead of the trough and cold advection behind. By 15/0000 UTC (Fig. 3.4), the short wave trough is passing through the center of the Kansas PRE-STORM area. The soundings for FRI and TOP at this time were strongly affected by an an intense thunderstorm[1] . Although it is difficult to separate cause and effect around the mesoscale

[1]At Manhattan, KS, just to the east of FRI, the 2350 UTC surface observation was zero visibility in a heavy rainshower and hail with thunder.

Figure 3.2: Locations of radiosonde stations. The "L" in southwest Kansas marks the location of the Liberal wind profiler. Dashed lines indicate the location of the isentropic cross-sections in Figs 3.11–13.

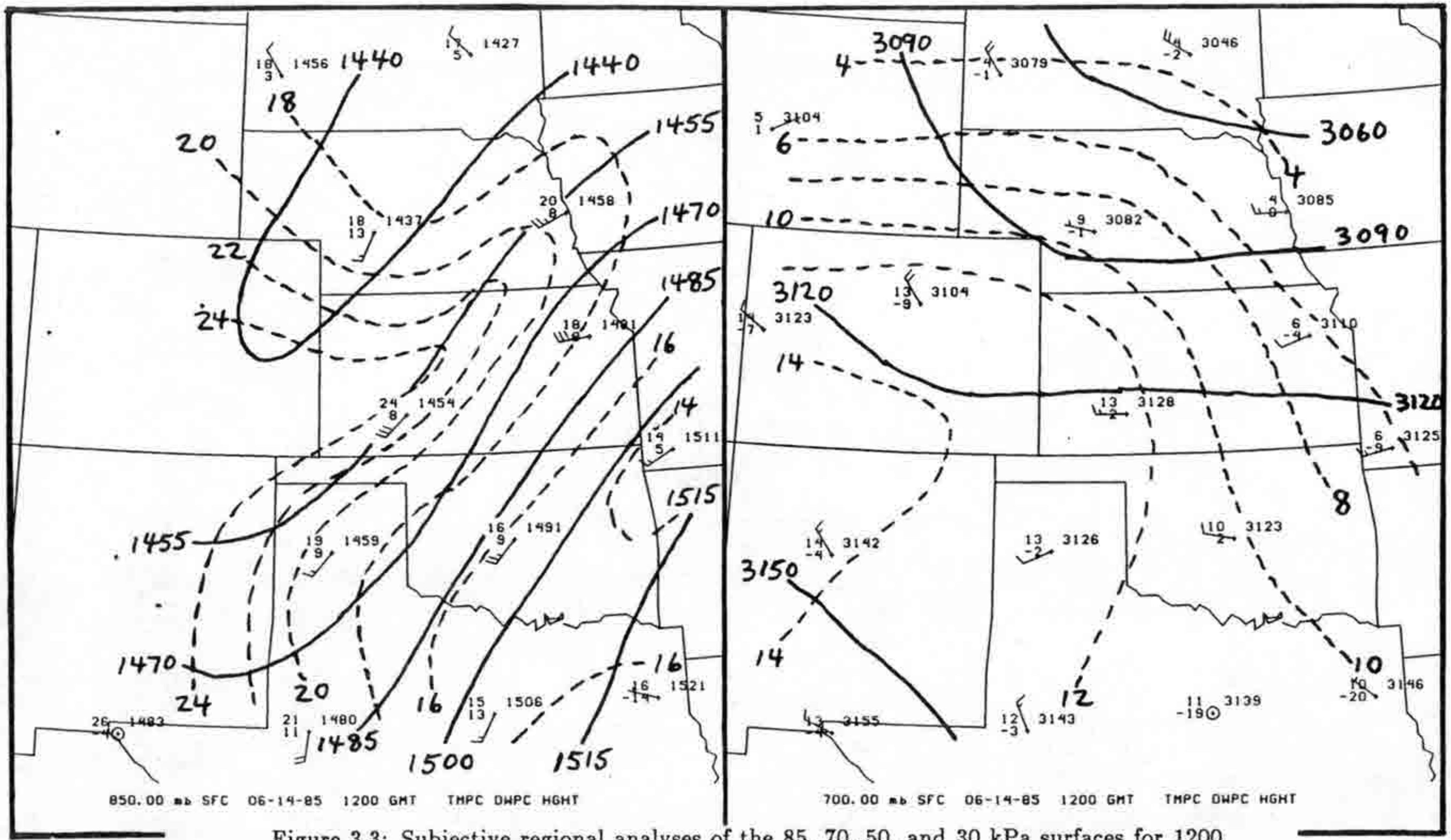

Figure 3.3: Subjective regional analyses of the 85, 70, 50, and 30 kPa surfaces for 1200 UTC 14 June 1985. The actual dewpoint temperature is plotted below the temperature [both °C]. One full barb = 5 m s^{-1}. Solid lines are height contours [m]; dashed lines are isotherms [°C], except at 30 kPa where the dashed lines are isotachs [m s^{-1}].

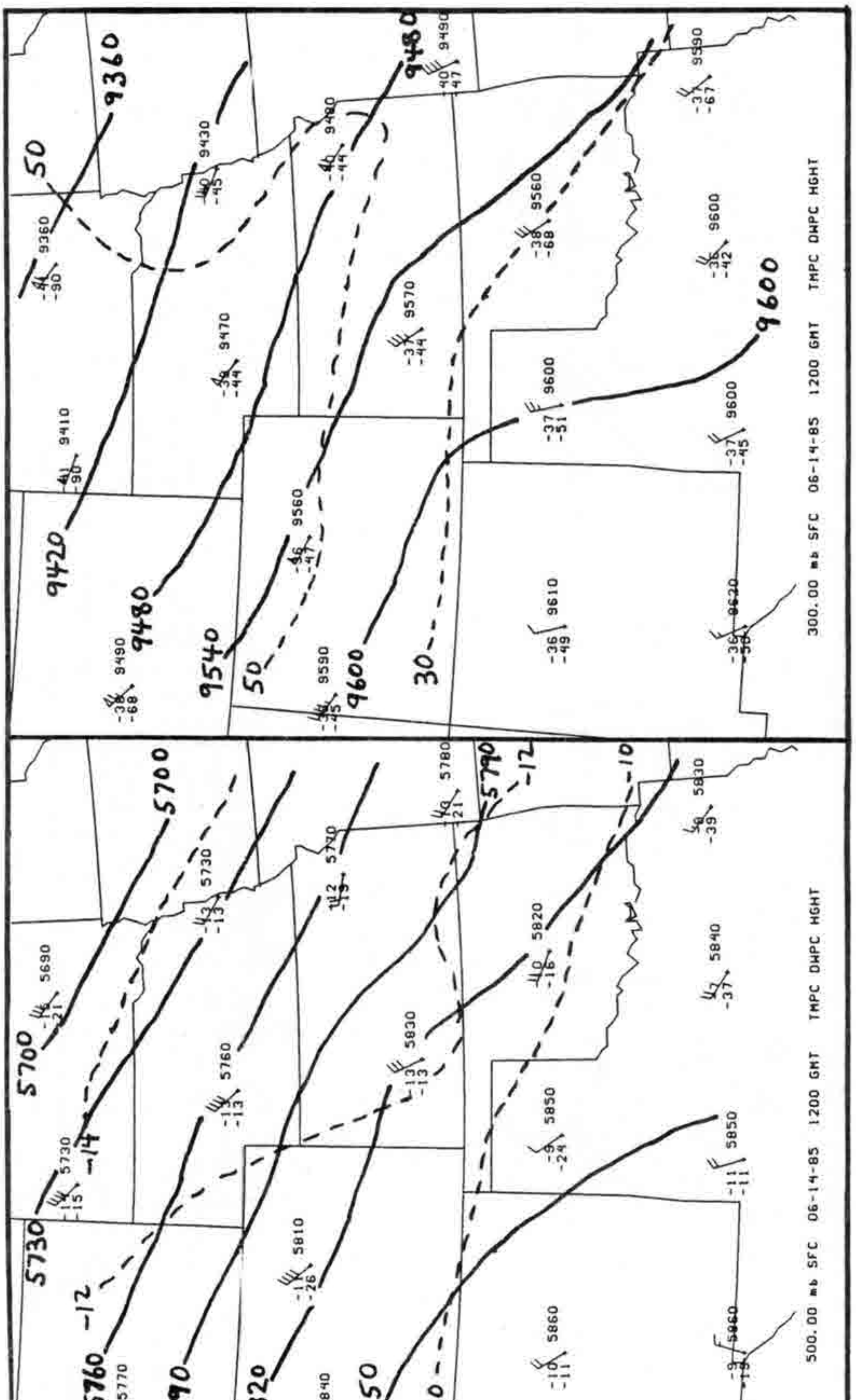

Figure 3.3: continued

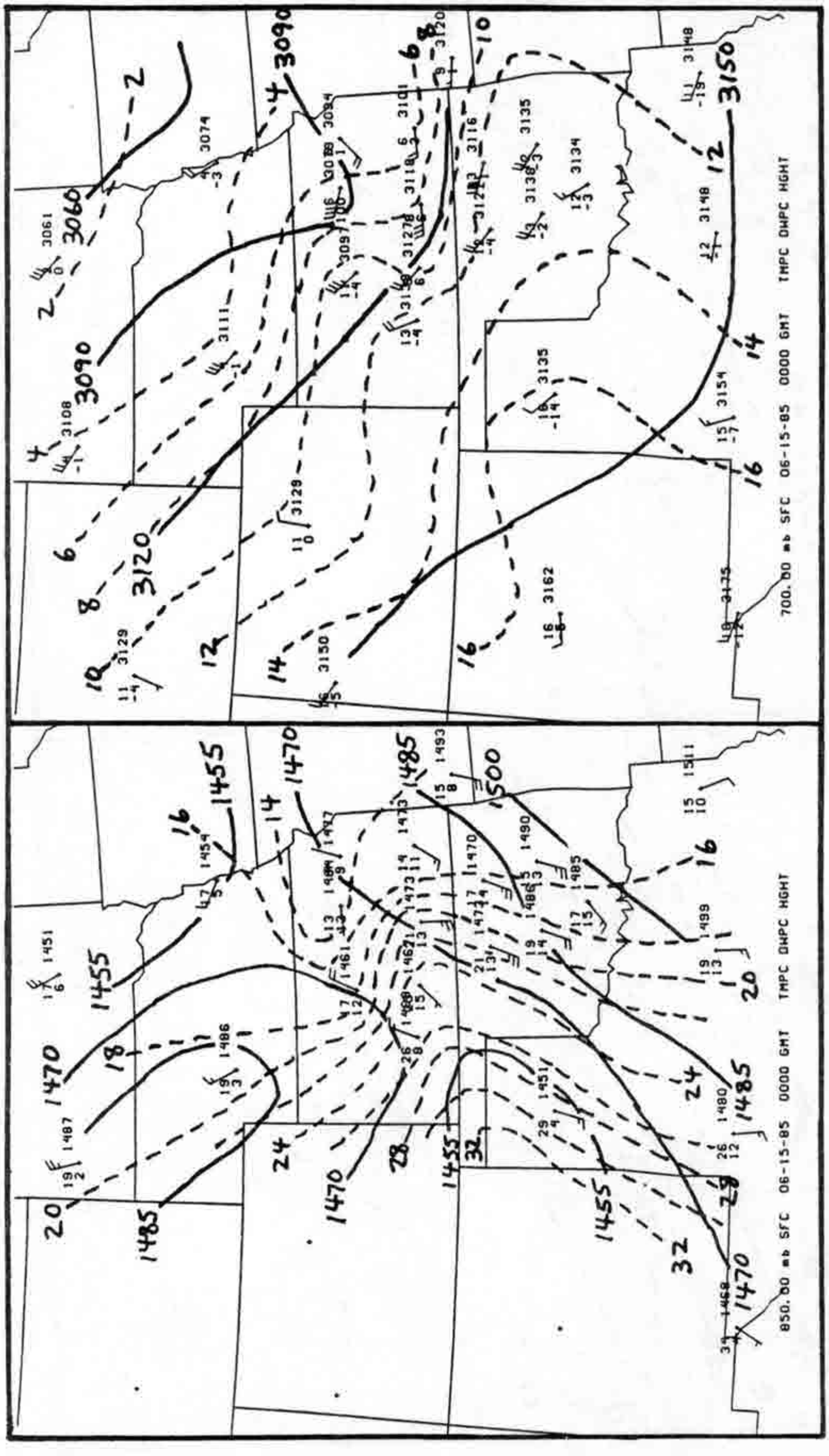

Figure 3.4: Same as Fig. 3.3, but for 0000 UTC 15 June 1985.

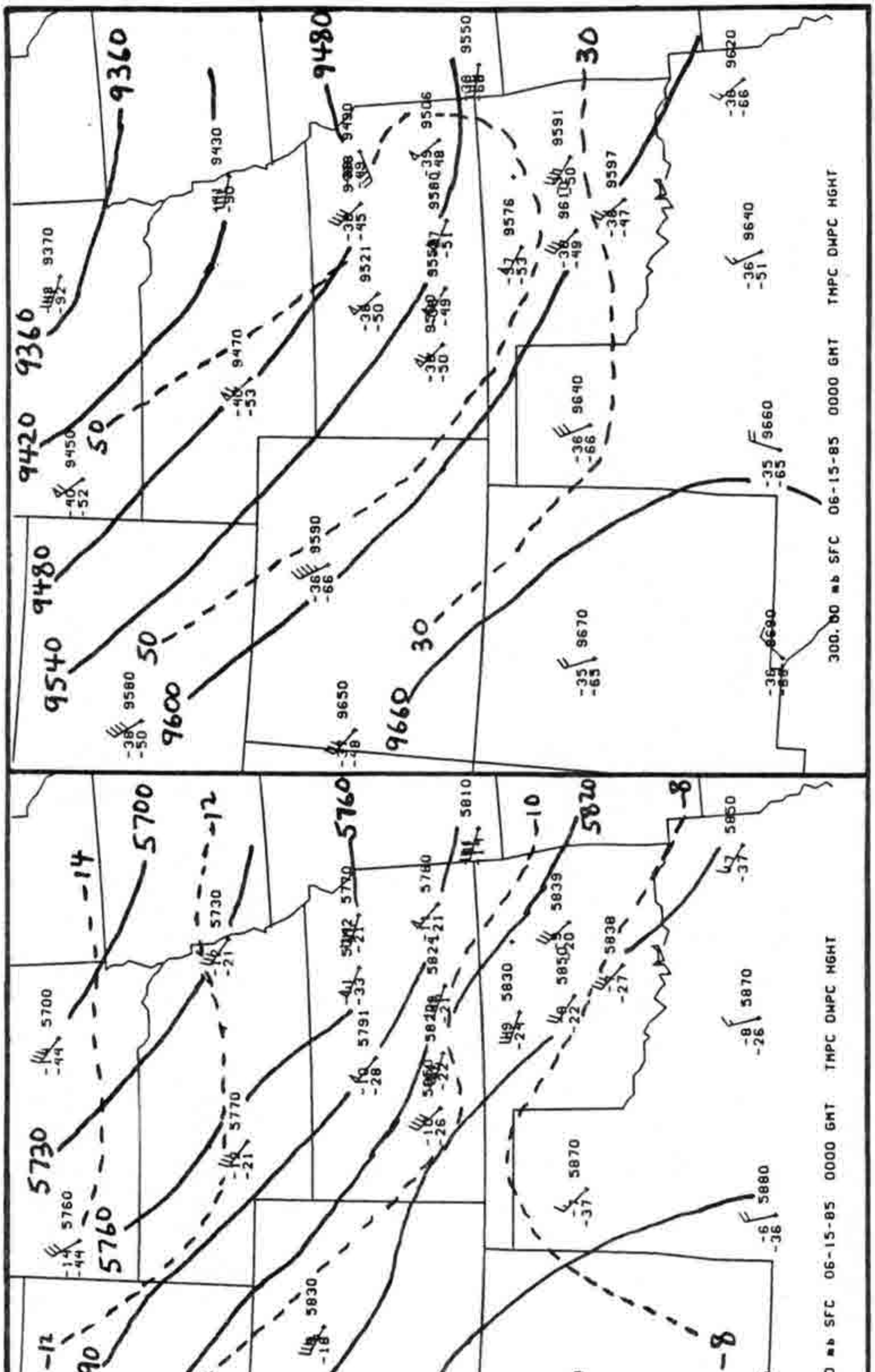

Figure 3.4: continued

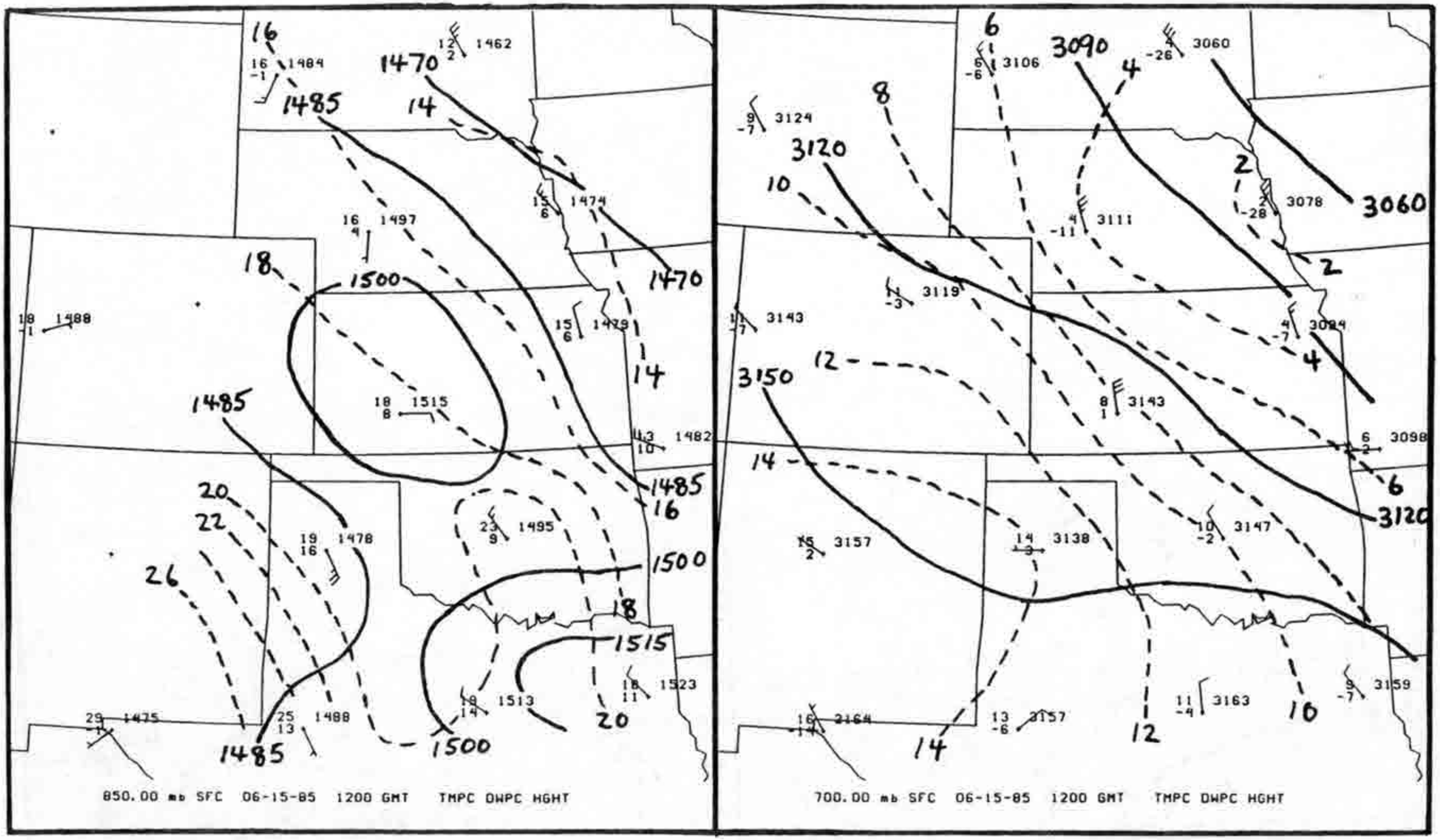

Figure 3.5: Same as Fig. 3.3, but for 1200 UTC 15 June 1985.

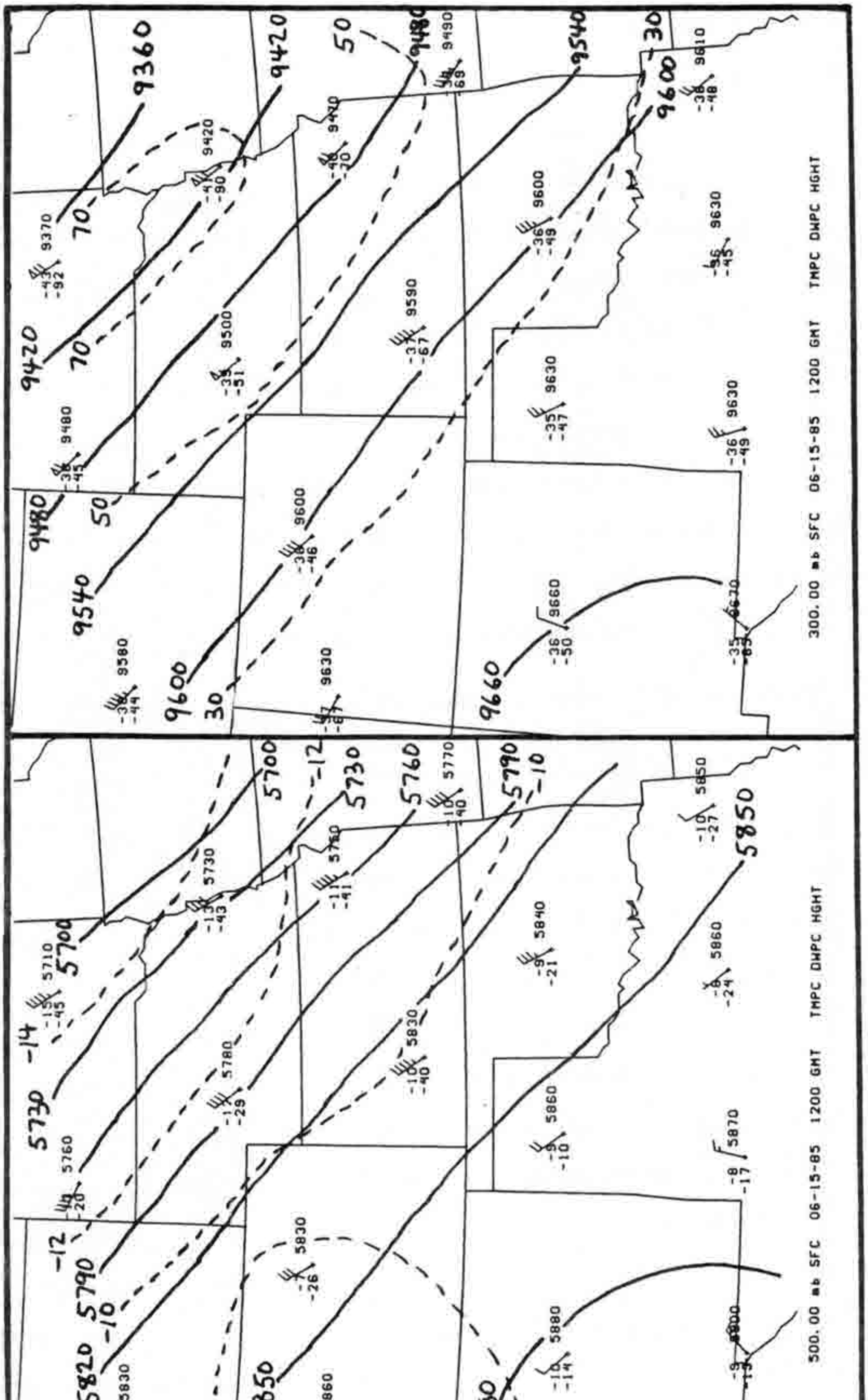

Figure 3.5: continued

convective system, the data have been analyzed to reflect the passage of the short wave trough between FRI and TOP at 70 and 30 kPa. At 85 kPa, the trough has split into two low centers, one over the Texas panhandle, coincident with the thermal ridge, and the other far to the northeast. Cold advection at 85 kPa appears to be strong in western Kansas. The thermal pattern at 70 kPa is somewhat misleading, since it reflects the changing depth of the inversion ahead of the trough. This behavior will be discussed in more detail in section 3.5. By the following morning (Fig. 3.5), the 85 kPa temperature gradients are strong only in western Texas and eastern New Mexico. Even in this area the gradient is no stronger than it was the previous morning. At 70 kPa, temperatures have cooled over most of Kansas, resulting in a strong temperature gradient over western Kansas. Over the remainder of the area, 70 kPa temperatures have remained constant or warmed slightly. There is still some upper-air support for a surface front, but NMC's dropping of the front after this time appears reasonable.

3.3 Development of mesoscale convective systems

A weak convective system was already present at mid-morning in northcentral Kansas. By mid-afternoon, new convection developed in the same area (Fig. 3.6a, 2130 UTC; 1530 local standard time), apparently tied to the approaching short wave trough. Thunderstorms had developed over the southern Colorado mountains and were beginning to move east into the plains. But there is no indication of cloud cover over the plains directly associated with the surface cold front. By late afternoon (Fig. 3.6b) several intense thunderstorms had developed over northeast Kansas. Isolated patches of towering cumulus now appear along the front/trough extending southeast to extreme southern Colorado. There are at least three cloud bands in southwest Kansas and the Oklahoma panhandle (Fig. 3.6c) oriented parallel to the surface front. The convection moving off the Colorado mountains appears to be developing a cyclonic rotation (Fig. 3.6d) as it interacts with the cloud bands oriented parallel to the surface front. As predicted by PRE–STORM forecasters (Meitín and Cunning, 1985), these features evolved into a mesoscale convective system which then propagated southeast into western Oklahoma.

a

c

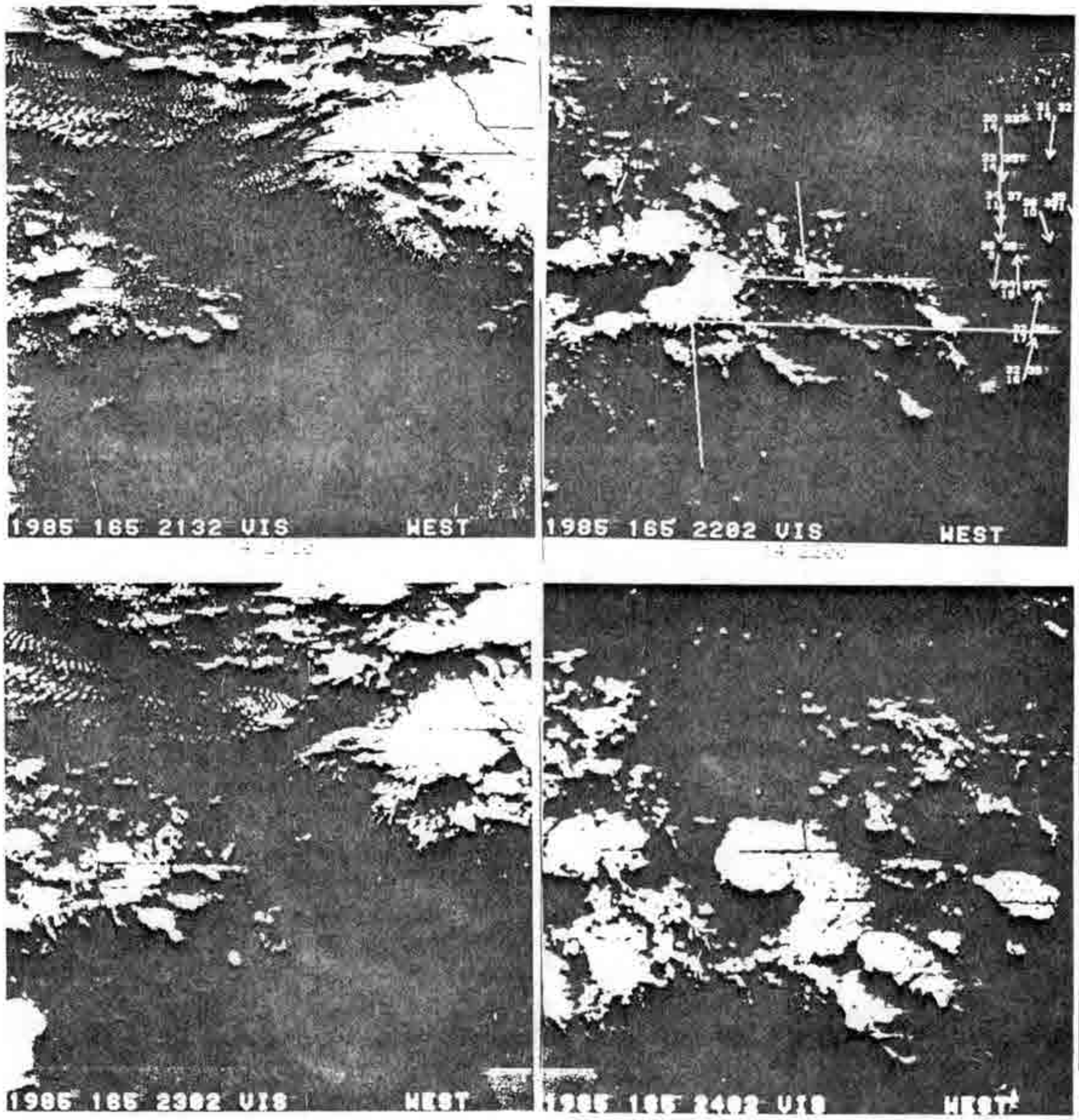

b

d

Figure 3.6: Visible satellite images on 14-15 June 1985 for (a) 2130 and (b) 2300 UTC, both at 2 km resolution, and for (c) 2200 and (d) 0000 at full (1 km) resolution. Surface temperature, dewpoint and wind arrows for stations near the front have been added to the 2200 image (c).

The continued evolution of the convective systems during the evening hours is shown by composite radar reflectivity plots in Fig. 3.7. Although the most intense echoes became

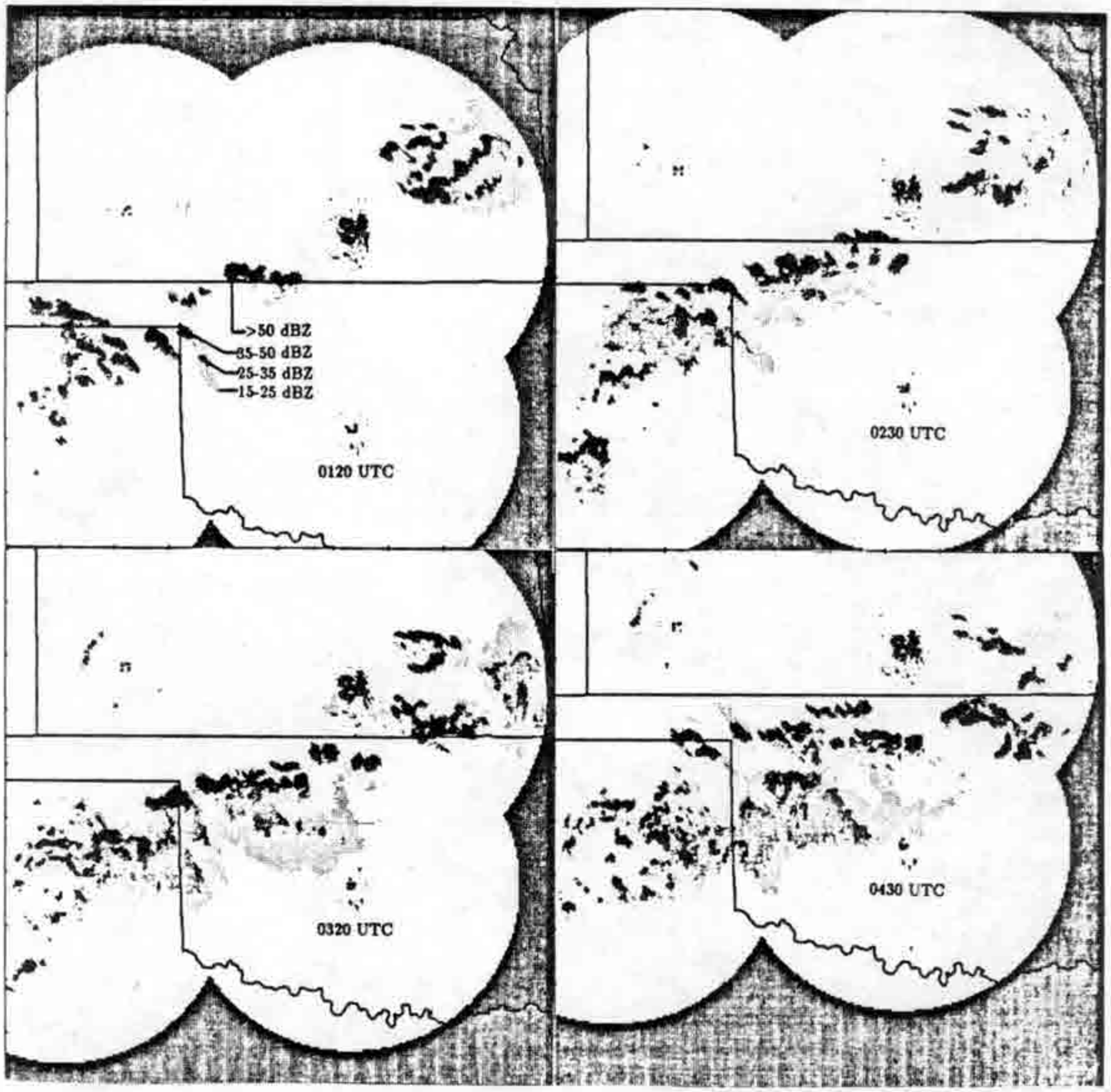

Figure 3.7: Composite (NWS WSR-57 radars at Garden City and Wichita, Kansas; Amarillo, Texas; and Oklahoma City, Oklahoma) digitized radar reflectivity factors on 15 June 1985 for (a) 0120 UTC (b) 0230 UTC (c) 0320 UTC and (d) 0430 UTC.

more evenly distributed along the trough, two broader areas of lighter, stratiform precipitation continued to delineate separate mesoscale convective systems. The first system, which produced intense thunderstorms in eastern Kansas during the afternoon, propagated south–southeast. The second system, which produced numerous reports of severe weather in the western portion of the PRE–STORM network (Meitín and Cunning, 1985), propagated southeast. With this movement, the two convective systems almost perfectly avoided the PRE–STORM dual–Doppler radar coverage near IAB. This was a case when strong low–level convergence was observed by the Doppler radars, yet the convergence, at least locally, did not result in new convection.

In summary, two convective systems developed with and ahead of the trough/front. Behind it, where the air was much drier, there was very little moist convection. Surface dewpoints (not shown) decreased rapidly from 10–15 °C ahead of the western portion of the front to < 8°C behind. It is clear that the synoptic-scale cold advection over Colorado and extreme western Kansas during the daylight hours was uncomplicated by the effects of moist convection.

3.4 Regional surface analyses

Objective analyses at 2–3 h intervals of a surface potential temperature, along with the station wind vectors, are shown in Fig. 3.8. The data are from the PRE–STORM network, the PROFS network in northeast Colorado, and from the conventional surface airways reports. The potential temperature (°C) deviates from the standard definition in that it has been adjusted to an elevation of 500 m. Thus the analyzed temperatures near the middle of the PRE–STORM area are very close to the actual surface temperatures.

Obviously, the surface features are closely related to those already discussed for 85 kPa. The surface windshift line moving south through Colorado and Kansas corresponds to the NMC analyzed frontal positions (Fig. 3.1). But clearly, the potential temperature gradient is very nearly parallel to this line. Strong cold advection does not occur until after easterly and northeasterly flow develops immediately behind the front between 14/2000 and 15/0000 UTC. This development is probably due partly to the mesoscale convective system in northeast Kansas. The combination of the mostly weak cold advection behind the front, the inversion over all but the extreme western area ahead of the front, and the diurnal surface heating result in little change in the overall temperature gradient. Consider, for example, the 34° isotherm. Except for cooling immediately behind the front, the isotherm position changes little between 14/1800 and 15/0000 UTC. Farther

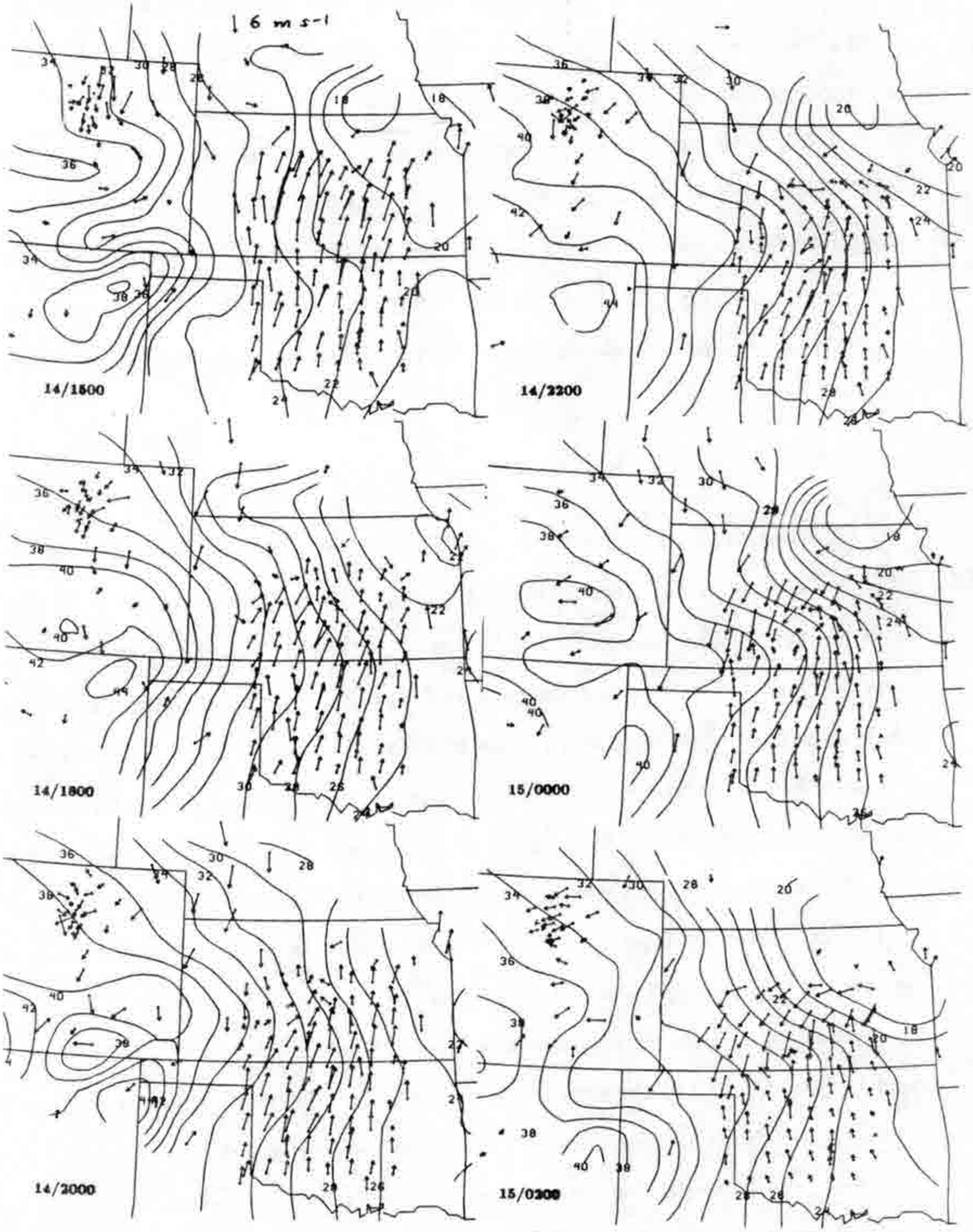

Figure 3.8: Surface wind arrows (scale indicated in top left panel) and objective analyses of the surface isentropes for selected times on 14–15 June 1985. Labels on the isentropes (°C) are equivalent to the actual temperatures at 500 m, the elevation near the middle of the PRE-STORM network.

west, the winds at the mountain PROFS stations are mostly northwest or north during the afternoon. After sunset, they become northeast, the same as at lower elevations, indicating that the northeasterly flow has now reached those levels and is fairly deep (> 1.5 km).

The surface pressure pattern resembles the 85 kPa trough and low centers discussed in section 3.2. The pressure changes (all changes are from 14/1500 UTC) as the trough moves south are shown in Fig. 3.9. There is a strong isallobaric gradient over the PRE–STORM area. But of more interest for this study is the pattern to the west. Since the 70 kPa heights are rising uniformly (Figs. 3.3–3.4) behind the trough, then if the net cooling were the same everywhere, the pressure rises should be fairly uniform. Instead there is an axis of maximum pressure rises near the Colorado–Kansas border. The implication of this is that the cold air in the lower troposphere has been able to penetrate south in this area. This is also suggested by the surface isotherms in Fig. 3.8. Farther west, the daytime surface heating more than compensates for the cold advection. For the same synoptic situation, the isallobaric pattern at night, as shown by the modeling simulations in the next chapter, would be quite different.

3.5 Details of the thermal structure

Vertical soundings at 15/0000 UTC from along the western edge of the cold front are shown in Fig. 3.10. For comparison, the solid circles at the mandatory levels are the temperatures 12 h earlier. The DEN sounding is dry–adiabatic through a deep layer, with the only suggestion of a frontal inversion being the stable layer near 60 kPa. Winds are light below this level, indicating weak cold advection. At DDC, the front has just passed (see Fig. 3.8), yet winds are north–northeast through a deep layer, up to almost 70 kPa, indicating that the front is very steep in this area. At AMA, there is an inversion just below 70 kPa that can be associated with a broad, diffuse warm front (Fig. 3.1). The directional shear across the inversion would correspond to the classic warm front if all the winds were rotated cyclonically by 90 degrees. The inversion is much stronger farther east, but even at AMA the 70 kPa warm advection has been strong enough to maintain the capping inversion in spite of daytime boundary layer warming.

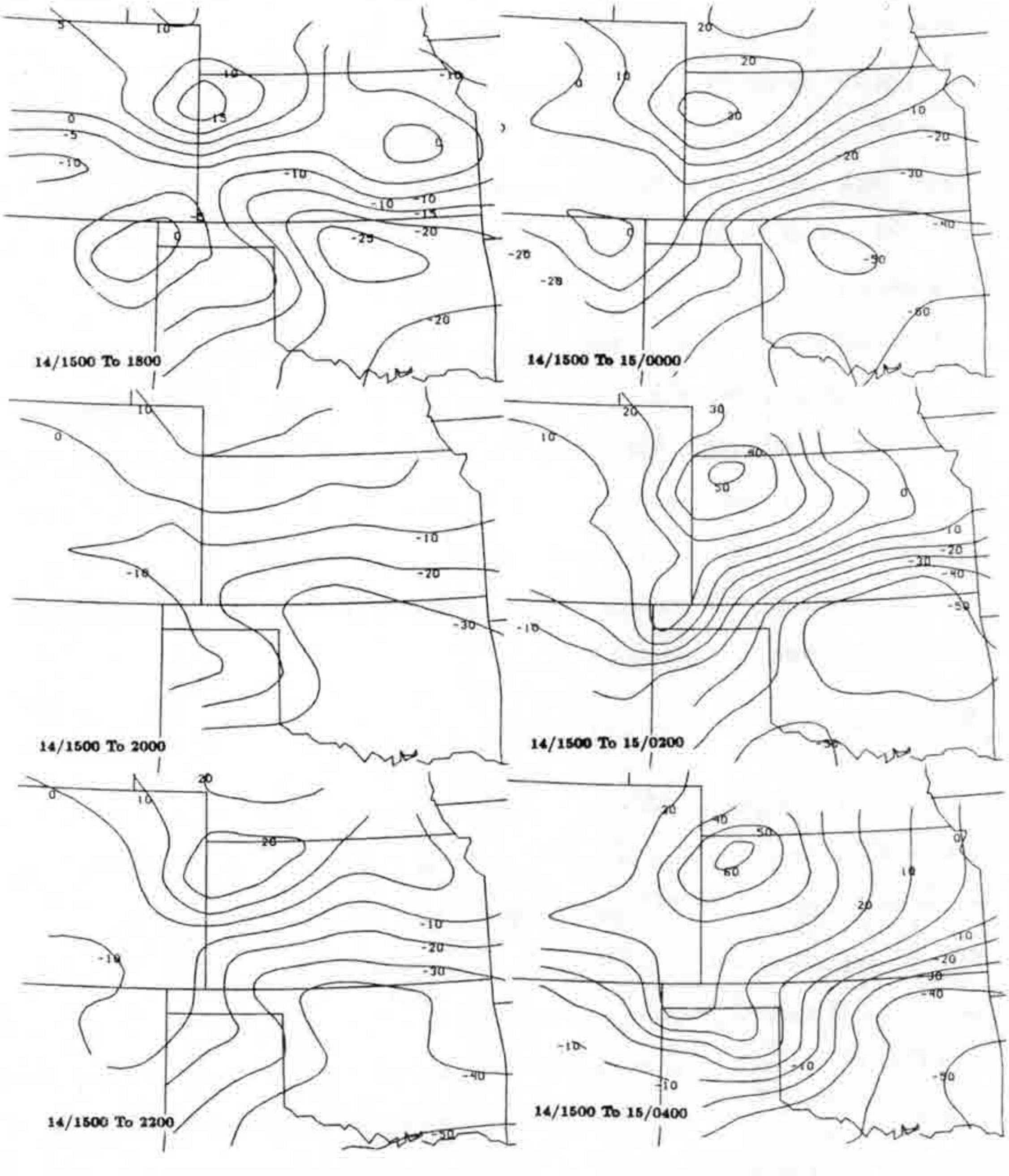

Figure 3.9: Objective analyses of the surface pressure changes during the periods labeled. The contour interval is 100 Pa, except for the top-left panel where it is 50 Pa.

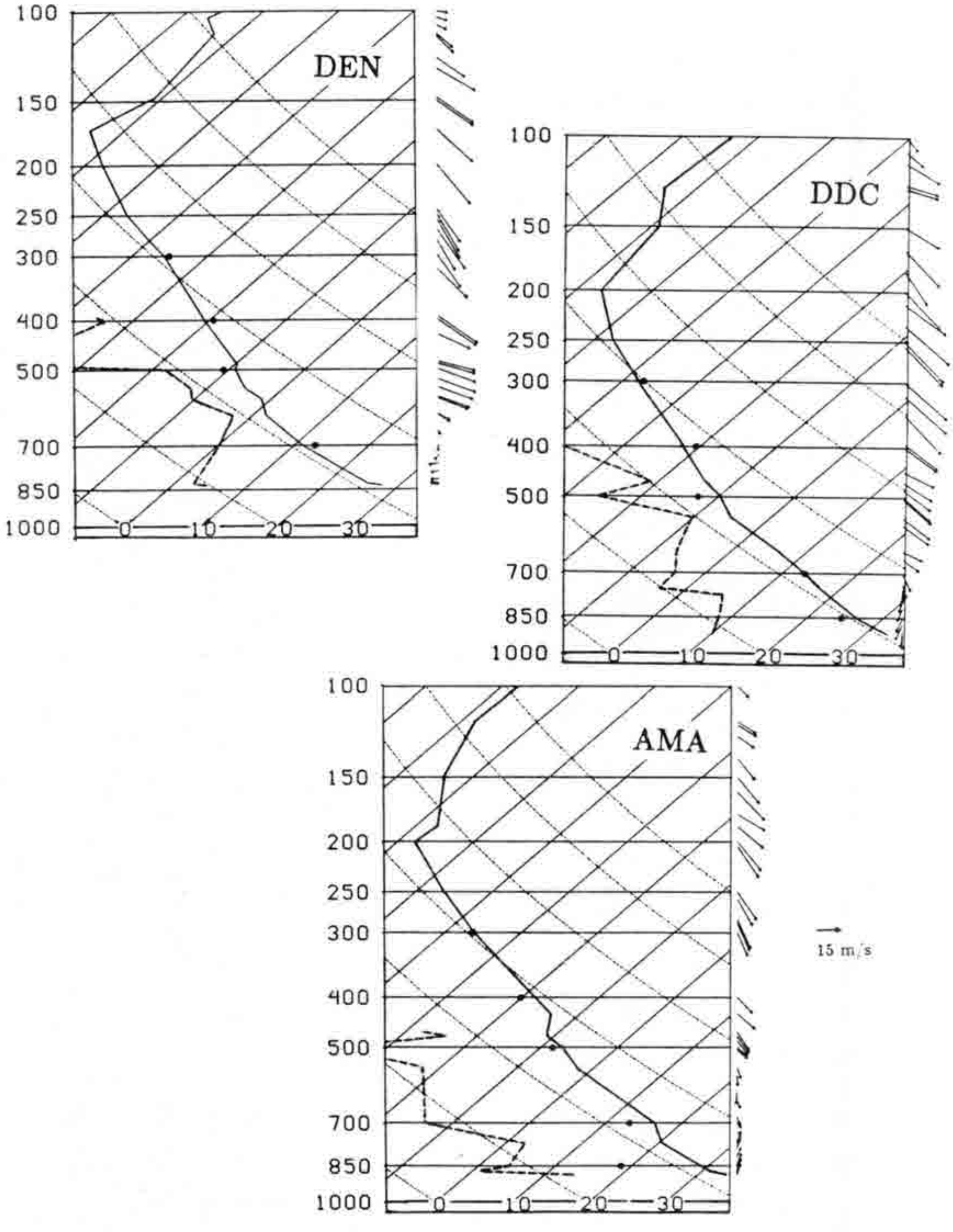

Figure 3.10: Radiosonde soundings near the cold front at 0000 UTC 15 June 1985. Solid dots at mandatory levels are the temperatures 12 h earlier. The scale for the wind arrows is shown to the right of the AMA sounding.

A view of the evolution of the thermal structure near the higher terrain can be seen in the southeast–northwest cross-sections in Fig. 3.11. At 14/1200 UTC, in spite of the nocturnal inversions, the low-level warm tongue between AMA and DEN is prominent. The thermal structure during the late-afternoon (15/0000 UTC) between AMA and DEN is not resolved by the sounding network, but the lower isentropes have been subjectively adjusted to be consistent with the surface observations. By 15/1200, the nocturnal inversions are dominant; there is no support for a front in the vicinity of AMA (see Fig. 3.1).

Additional cross-sections with a general north–south orientation are shown in Fig. 3.12. East of the DEN-AMA line, the cold front is distinct as it moves past DDC (top). If better resolved, the front would probably be steeper, as it is farther east approaching PTT (middle). The warm sector is very narrow near PTT. Still farther east (bottom), the warm sector has vanished at the surface, but the front aloft remains between 70 and 50 kPa. It is not clear whether the FRI sounding is representative of the low-level thermal structure; the broader temperature difference between HON and IAB is only 2°C. The east- west thermal structure (Fig. 3.13) is similar north (top) and south (bottom) of the front. Just ahead of the front (middle), the east–west slope of the baroclinic zone is much steeper.

The depth of the front with time can be inferred from the wind profiler (Augustine and Zipser, 1987) time series (Fig. 3.14) at Liberal, KS (between AMA and DDC, Fig. 3.2). The wind shift associated with the frontal passage reaches Liberal just before 2330 UTC, rapidly builds upward to ~4 km, then remains near this level, becoming more diffuse after 15/0230 UTC. During the period 0530-0730, the shear layer slowly drops to 3.0–3.5 km. So the top of the cold air is never more than 3 km above the surface. Another feature that can be seen in the profiler time series is the southwestward advance and retreat of the upper tropospheric jet. This occurs smoothly and appears to evolve independent of the surface features.

Subjective low-level analyses of the PRE-STORM sounding data are presented in Figs. 3.15 and 3.16. (The fields at higher levels changed very little). The heights from

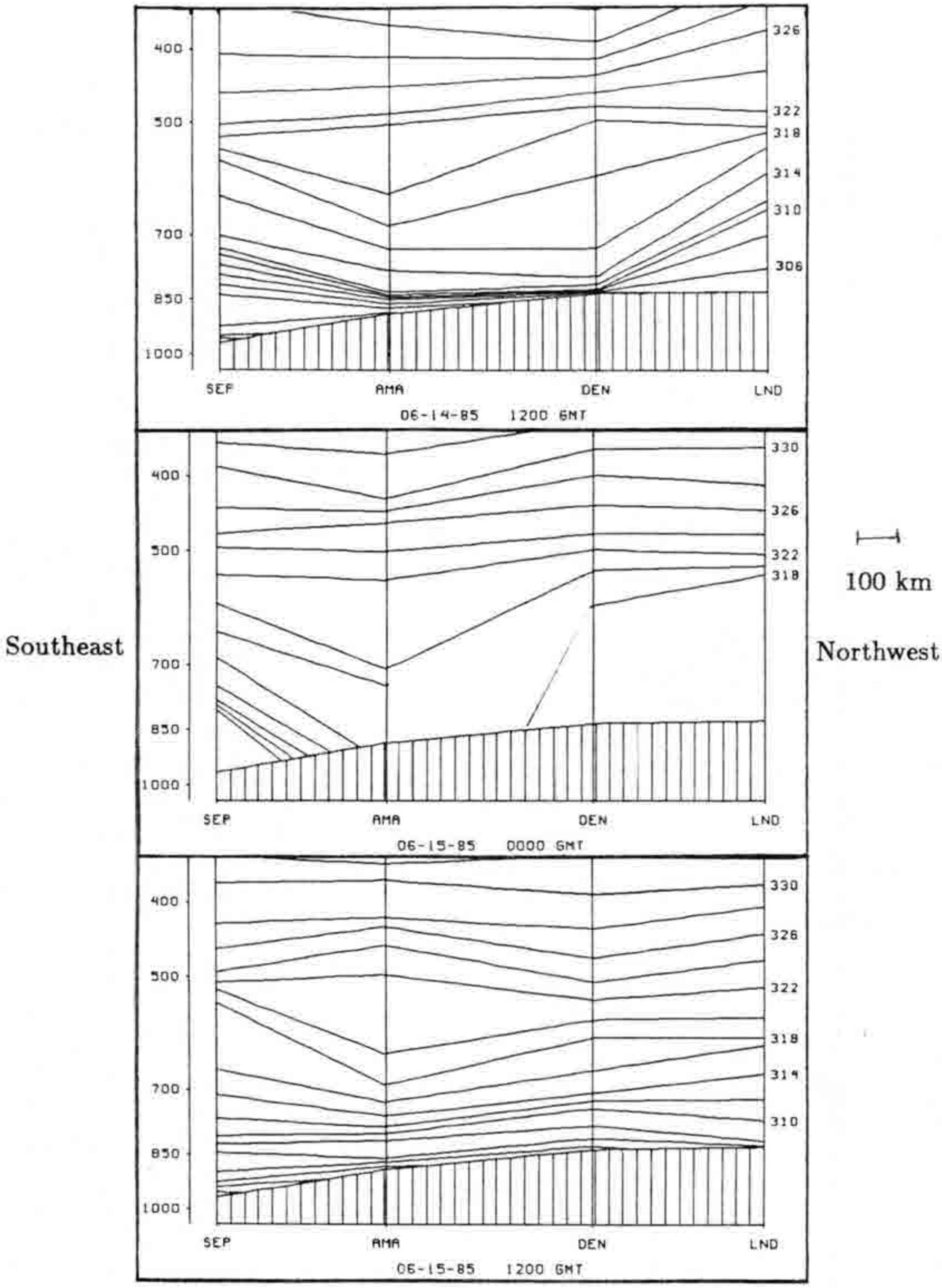

Figure 3.11: An isentropic cross-section roughly parallel to the Continental Divide (see Fig. 3.2) for three different times. The cold front lies between AMA and DEN in the middle panel at 0000 UTC 15 June 1985.

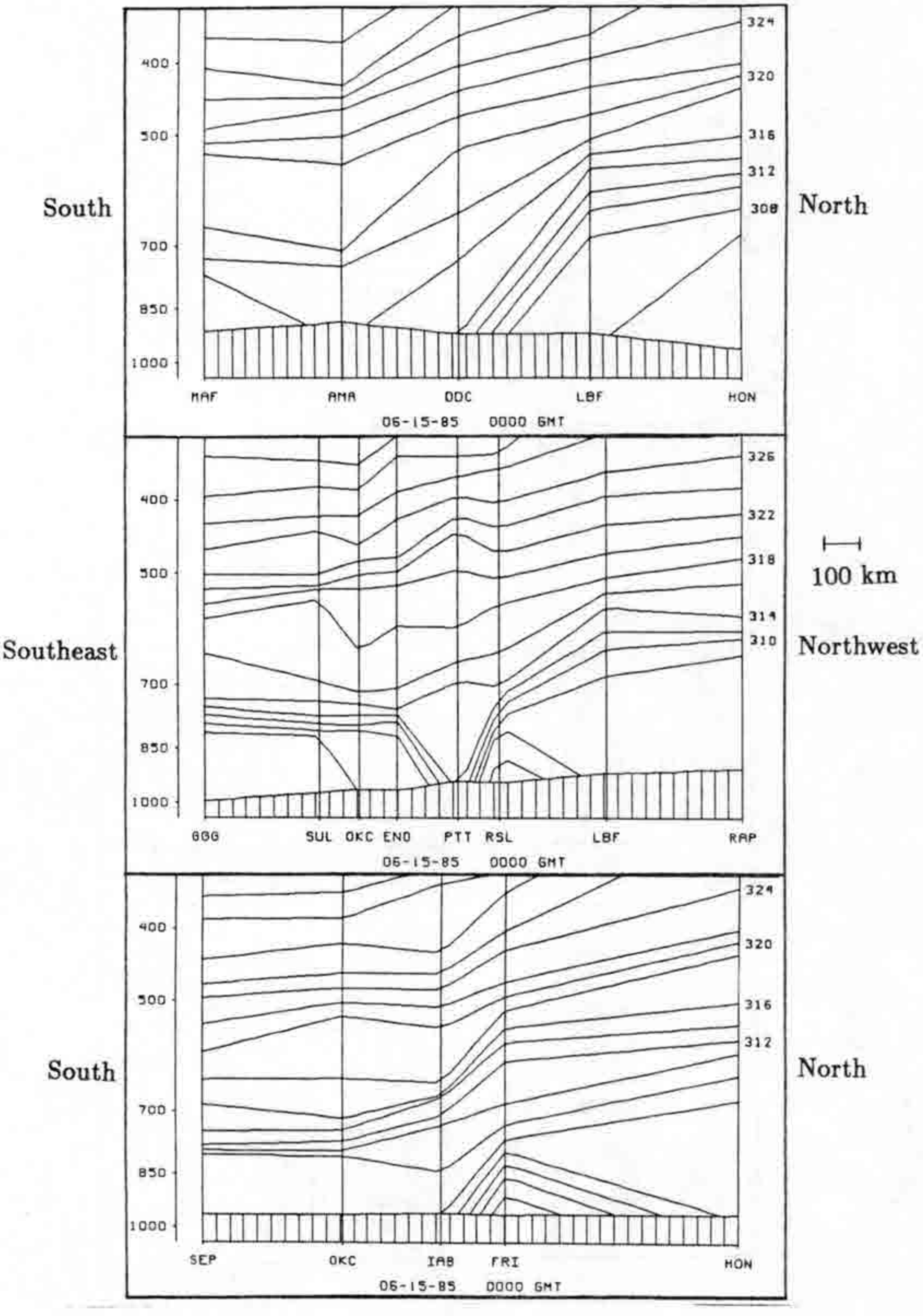

Figure 3.12: North-south cross-sections for 0000 UTC 15 June 1985. The cross-sections lie progressively farther east moving down from the top panel to the bottom one.

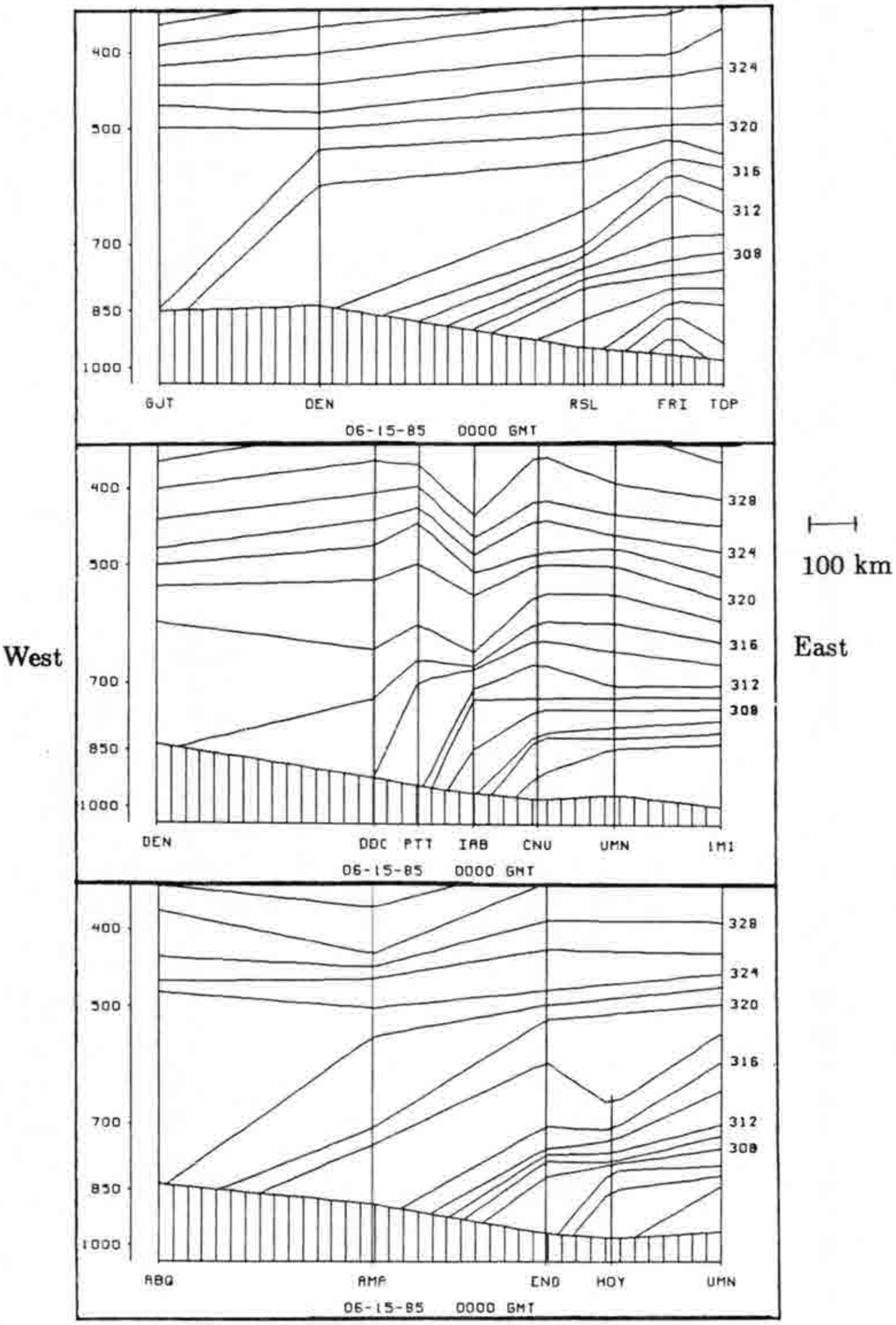

Figure 3.13: East-west cross-sections for 0000 UTC 15 June 1985. The cross-sections lie progressively farther south moving down from the top panel to the bottom one.

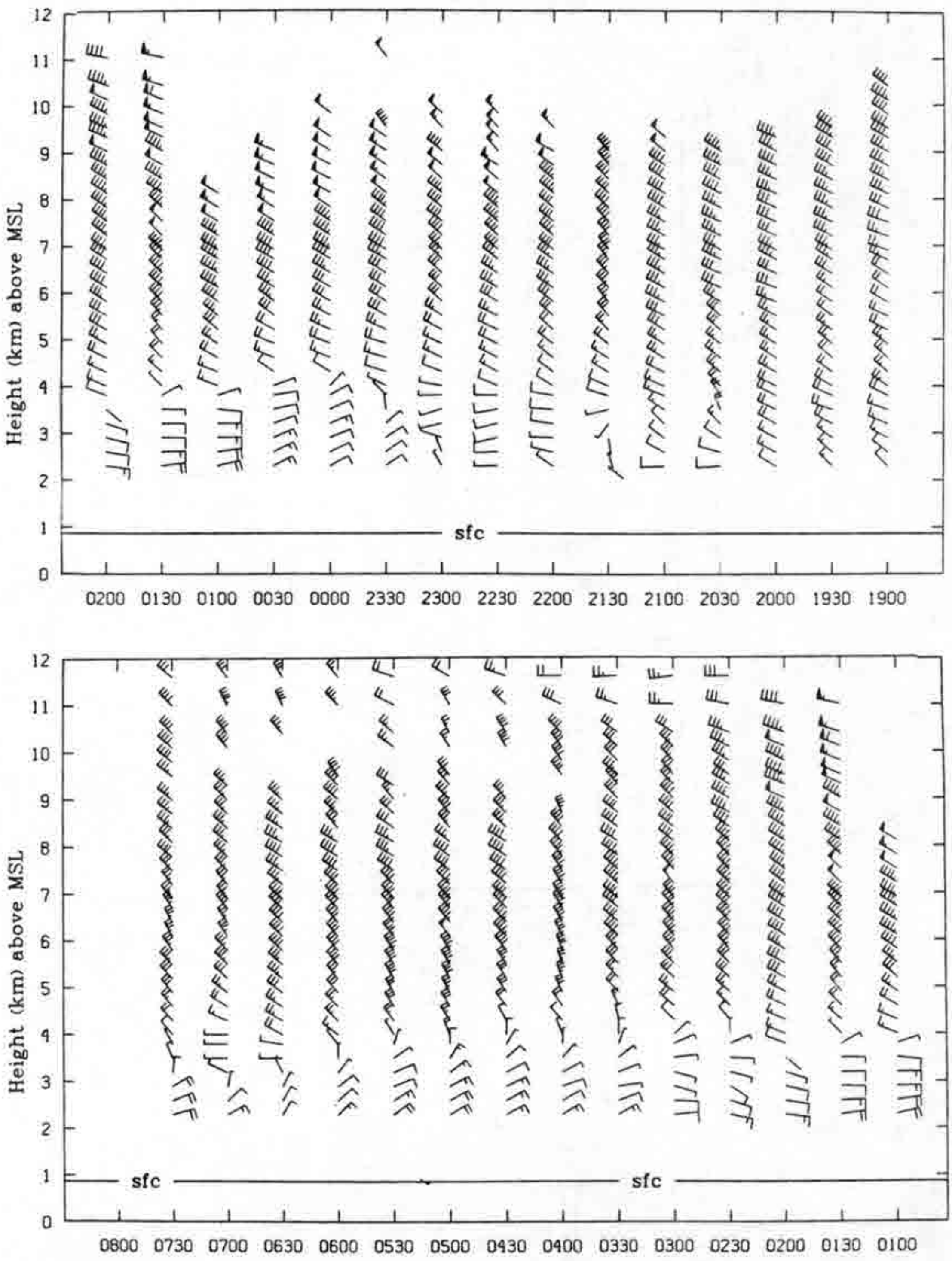

Figure 3.14: Time series from the Liberal, KS, wind profiler for 14–15 June 1985. One full barb = 5 m s^{-1}. Time (UTC) increases from right to left in the top panel, and then from right to left in the bottom panel.

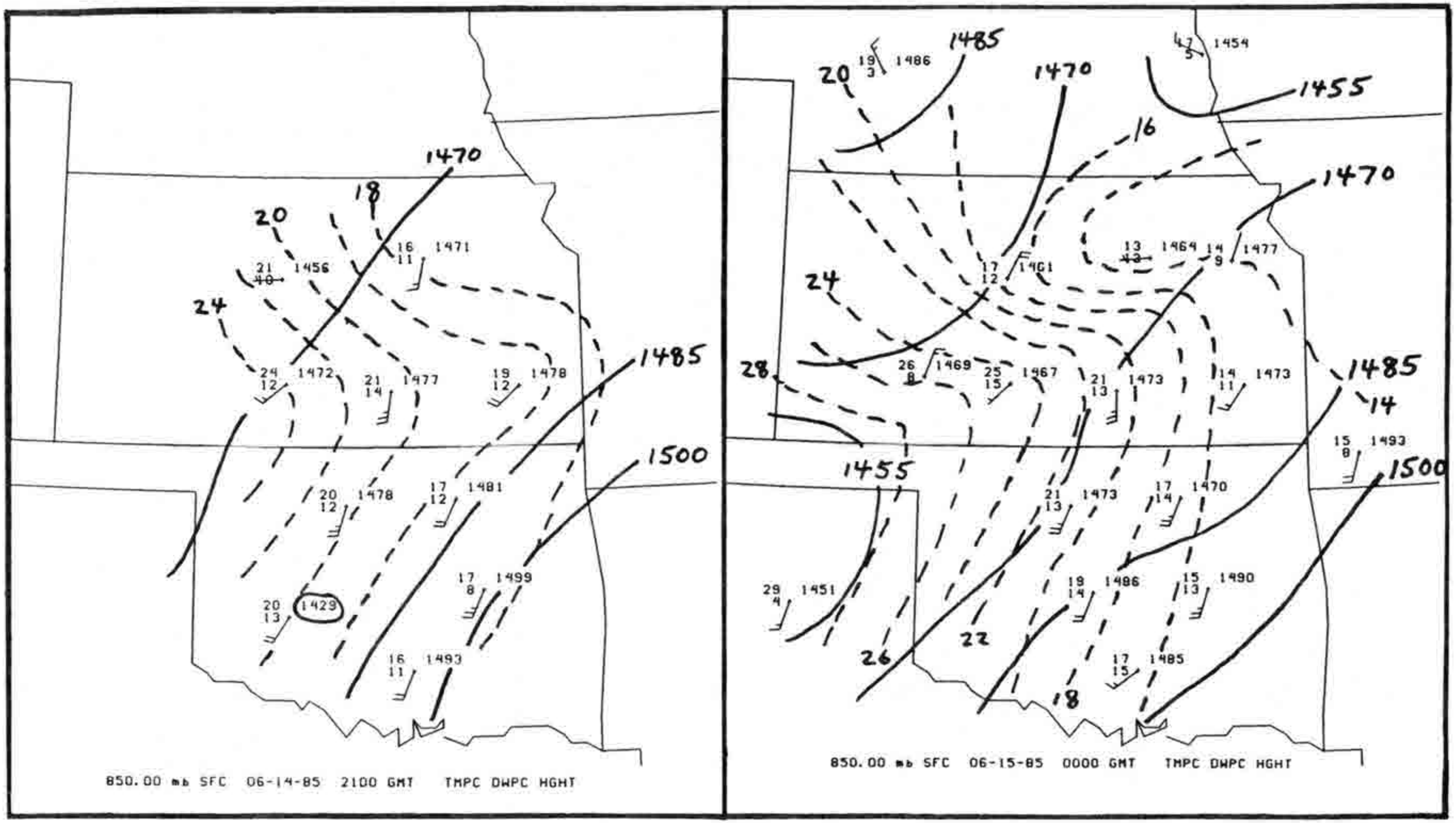

Figure 3.15: Analyses of the PRE-STORM sounding network data for the 85 kPa surface. Plotting and contours are the same as in Fig. 3.3. The circled heights are not correct and were subjectively adjusted.

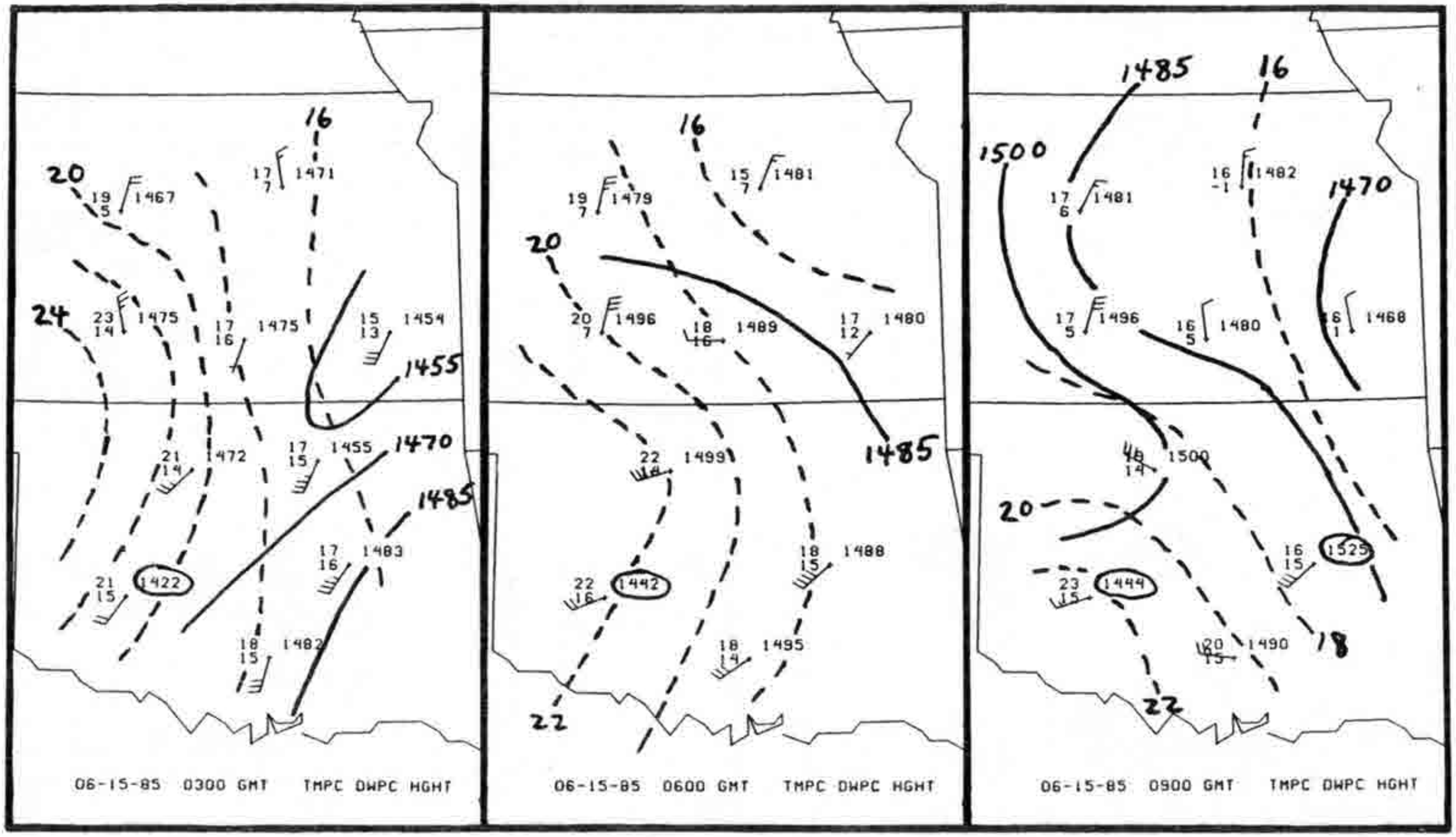

Figure 3.15: continued

FSB were discovered after the experiment to have a bias of ~50 m, and this has been taken into account in the analyses. The 85 kPa warm trough progresses from southcentral Kansas at 14/2100 UTC to southwest Oklahoma at 15/0900 UTC (Fig. 3.15), and is replaced by a cold ridge. The net result is 4-5°C cooling over southcentral and western Kansas, 3–4°C warming over southwest Oklahoma, and little change elsewhere. At 70 kPa (Fig. 3.16), the 80–60 kPa thickness pattern has been analyzed in lieu of the temperature. It was stated in section 3.1a. that the 70 kPa temperatures were misleading. The reason for this can be seen in the PTT and IAB soundings at 15/0000 UTC (Fig. 3.17). The warm sector air, barely reaching the surface at PTT, is above 70 kPa at IAB. In addition, it appears that the IAB inversion raised from below 70 kPa to above it as the surface trough approached (bottom panel of Fig. 3.12), probably due to the surface convergence ahead of the trough. Consequently, the thermal pattern along the Oklahoma–Kansas border at 70 kPa in Fig. 3.4 is representative of only a very thin layer near the inversion. The layer mean temperature gradient (Fig. 3.16), in fact, remains mainly northeast to southwest throughout the region. Winds become more northerly in Kansas late in the period, tending to shift the baroclinic zone to the southwest. Ahead of the northerly flow, there is a zone of cooling that propagates from eastern Kansas into central Oklahoma between 0300 and 0900 UTC. This feature may be a result of a cold outflow from the eastern mesoscale convective system (Fig. 3.8).

At 15/0000 UTC, the cyclonic shear of the short wave trough, acting geostrophically on the temperature gradient, is tending to increase, following an air parcel, the low–level horizontal temperature gradient perpendicular to the trough (Hoskins, 1982). (Because of the weak temperature gradients at 50 kPa and above, there is little, if any, geostrophic forcing at those levels.) The compensating low–level circulation results in quasi– geostrophic upward motion ahead of the trough, which is in agreement with the convective developments.

One way to compare the relative importance of geostrophic and ageostrophic temperature advection with diabatic effects is to look at the actual, local, layer–mean temperature changes (Fig. 3.18). During the day, there is a local increase in the low–level (80–60 kPa

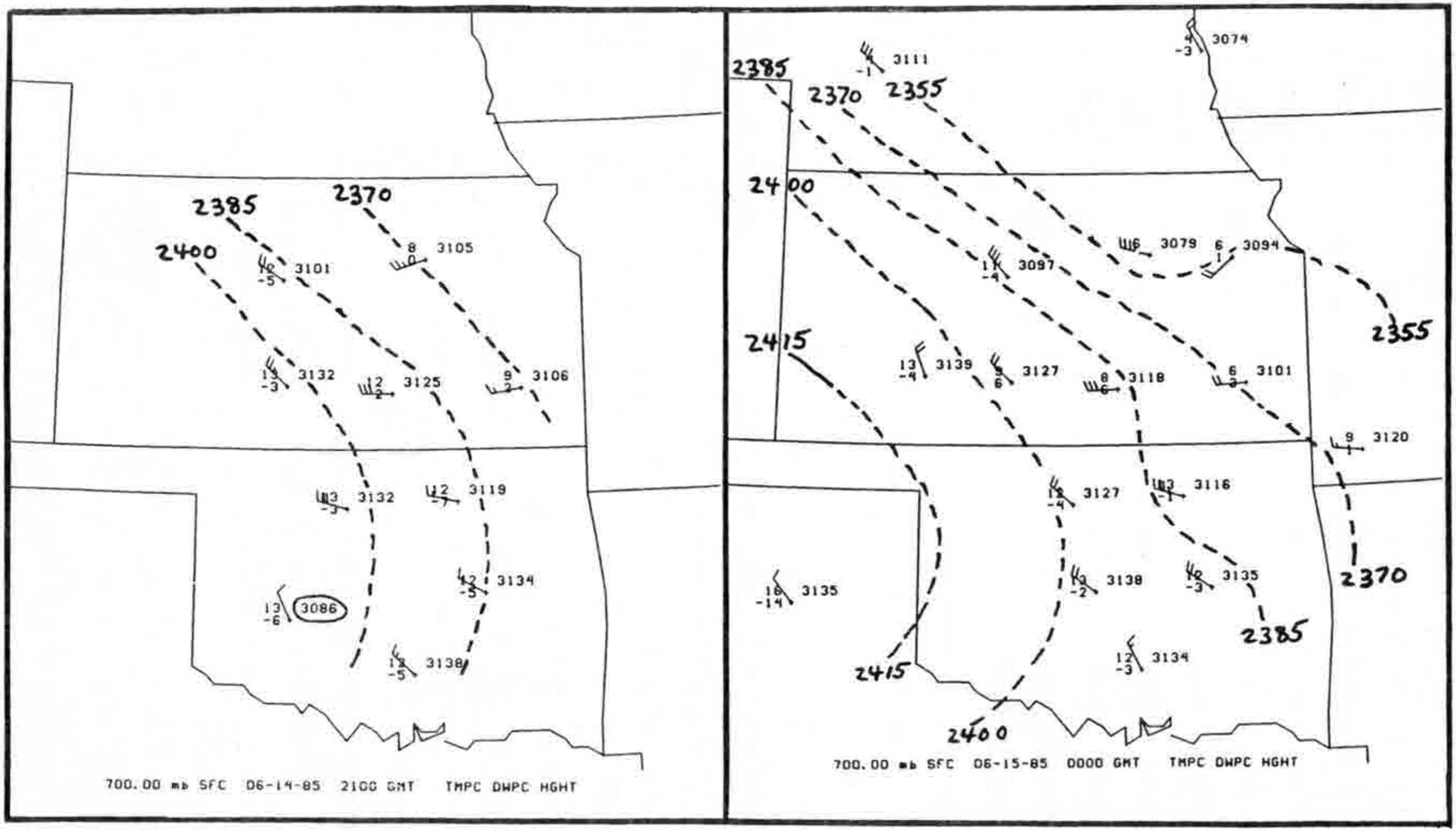

Figure 3.16: Same as Fig. 3.15, but for 70 kPa. Instead of isotherms, the 80–60 kPa thickness has been analyzed (15 m interval).

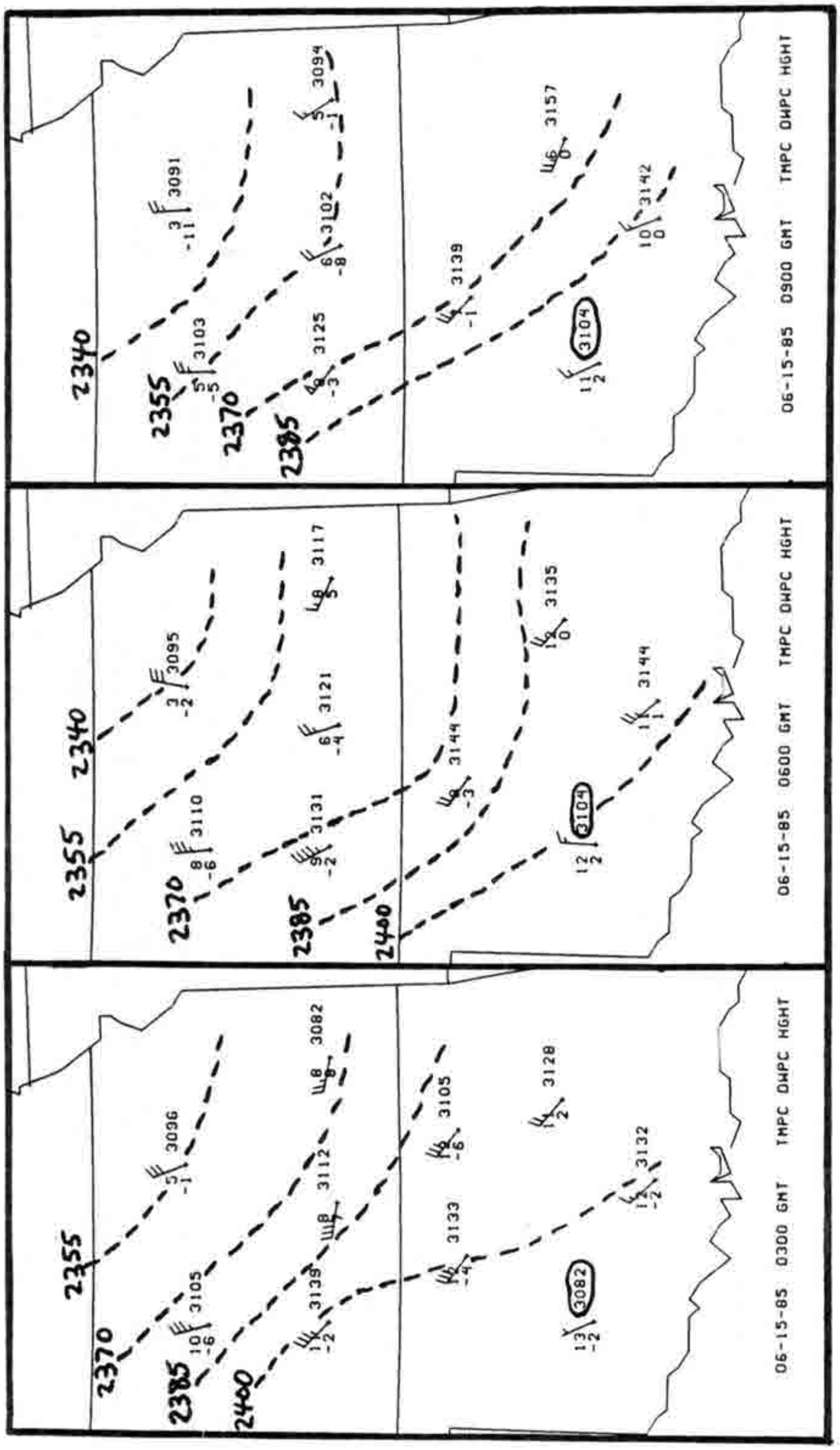

Figure 3.16: continued

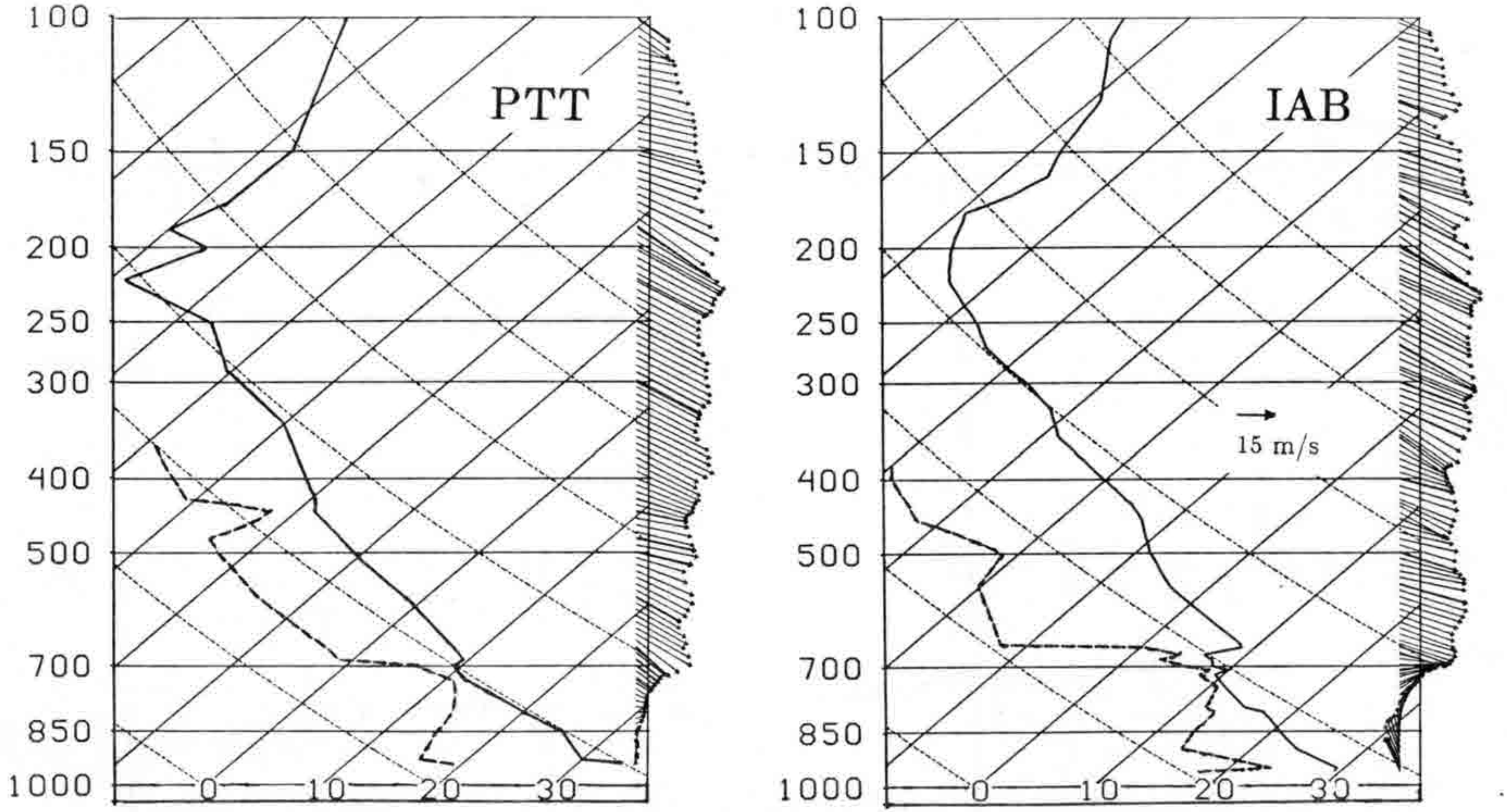

Figure 3.17: PRE-STORM soundings for PTT and IAB at 0000 UTC 15 June 1985, showing the slightly higher and more intense inversion at IAB just ahead of the surface windshift.

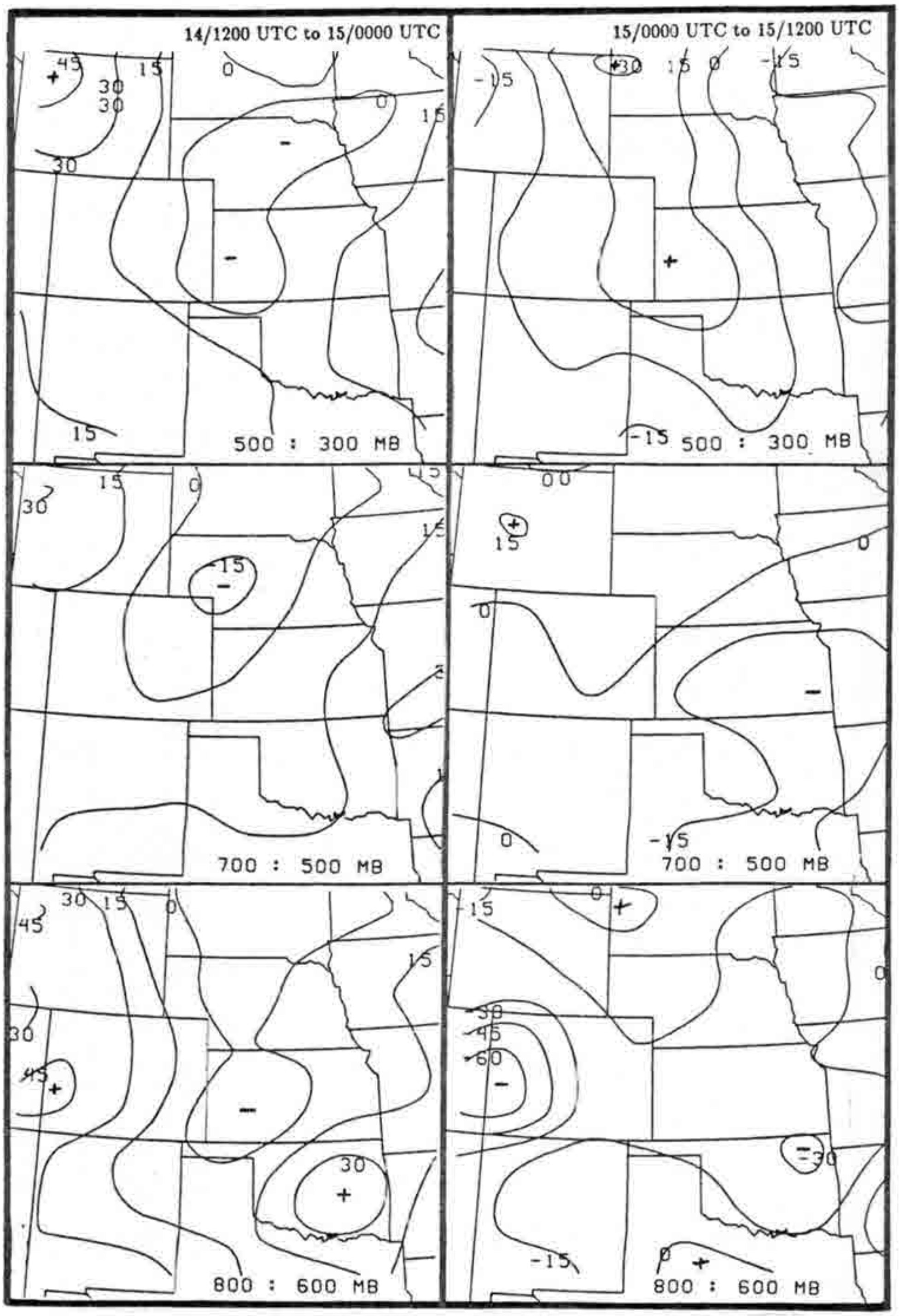

Figure 3.18: Thickness changes for the periods 1200 UTC 14 June 1985 to 0000 UTC 15 June 1985 (left) and 0000 to 1200 UTC 15 June 1985 (right). The contour interval is 15 m for all layers, equivalent to a layer mean temperature change of 1.8 °C for 80–60 kPa, 1.5 °C for 70– 50 kPa, and 1.0 °C for 50-30 kPa.

layer; bottom left panel) temperature gradient across the PRE–STORM network, likely due mainly to horizontal advection. However, in this layer there is also an increased gradient, of at least equal magnitude, generated by heating over the higher terrain, which forces a circulation with surface flow towards the mountains. The amplitude of the diurnal oscillation at GJT, west of the Continental Divide, is larger than at DEN since the modifying effect of the cold advection is not present. East of the Divide, horizontal advection is tending to intensify the east–west temperature gradient, and the impact of diurnal heating is to enhance this change. At night, the effect of cooling over higher terrain is to decrease the east-west horizontal temperature gradient in the lower troposphere (Fig. 3.17; bottom left). At higher levels (700:500 and 500:300; middle and top panels), there is little evidence of diurnal surface heating/cooling; the temperature changes are due mostly to horizontal advection and quasi–geostrophic processes.

3.6 Discussion

This case, occurring near the summer solstice, is an extreme example of the impact of surface heating on a shallow cold surge. On the other hand, this surge is a fairly deep one, and so the impact of the heating on a shallower surge might be even more significant. The synoptic pattern is a typical one favorable for the development of a shallow cold surge at any time of year. When there is a stable long wave pattern, with northwesterly or west–northwesterly flow, and the polar jet lies well northeast of Colorado, any short wave trough will have the potential to generate a shallow cold surge which then interacts with the mountains. In fact, the same pattern existed during the 1 August 1986 cold surge (discussed in the next chapter). The details of the interaction depend on the initial structure of the cold surge and vary from case to case. This makes it difficult when comparing day and night cases to determine to what extent the different behavior is due to surface effects rather than differences in the initial structure of the cold surge. The goal of the modeling efforts in Chapters 5 and 6 is to isolate the surface effects.

Chapter 4

OUTFLOW FROM A CONVECTIVE SYSTEM–1 AUGUST 1986

This second case is an example of a shallow cold surge generated by the outflow from a mesoscale convective system (MCS). As on 14 June 1985, this case occurred with northwesterly flow aloft and with the polar jet northeast of Colorado. Although the MCS developed in part due to frontal forcing, the cold surge appears to be driven primarily by the mesoscale outflow. This differs from the previous case, where a baroclinic wave moving along the polar front was the direct cause of the cold surge in northeast Colorado.

4.1 Synoptic situation

At 1300 UTC on 1 August 1986, an MCS over the northern Nebraska panhandle (Fig. 4.1, top left) was moving east and rapidly beginning to dissipate. Upper air support for the convective system had come from a short wave trough, evident at 70 kPa in Fig. 4.2b. As on 14 June 1985, the 50 kPa flow changed little during the day over northeast Colorado (Fig. 4.2a,c); to the west 50 kPa temperatures warmed and heights rose while to the east they changed little. There was cooling at 70 kPa between 01/1200 and 02/0000 UTC at DEN (Fig. 4.2b,d), in opposition to the normal diurnal heating, indicating that, as in the previous case, the cold surge had reached that level. This is confirmed by the afternoon DEN sounding (Fig. 4.3a), which shows an inversion slightly above 70 kPa. This cap marks the top of the cold surge, meaning that the cold air was about 1.9 km deep at DEN at this time.

Surface analyses for selected times before, during, and after the cold surge are shown in Figs. 4.4 and 4.5. As for the 14 June 1985 case, the plotted temperatures are potential temperatures, adjusted dry adiabatically to a constant elevation of 1600 m (approximate elevation of the foothills along the Colorado Front Range). The plotted pressure parameter

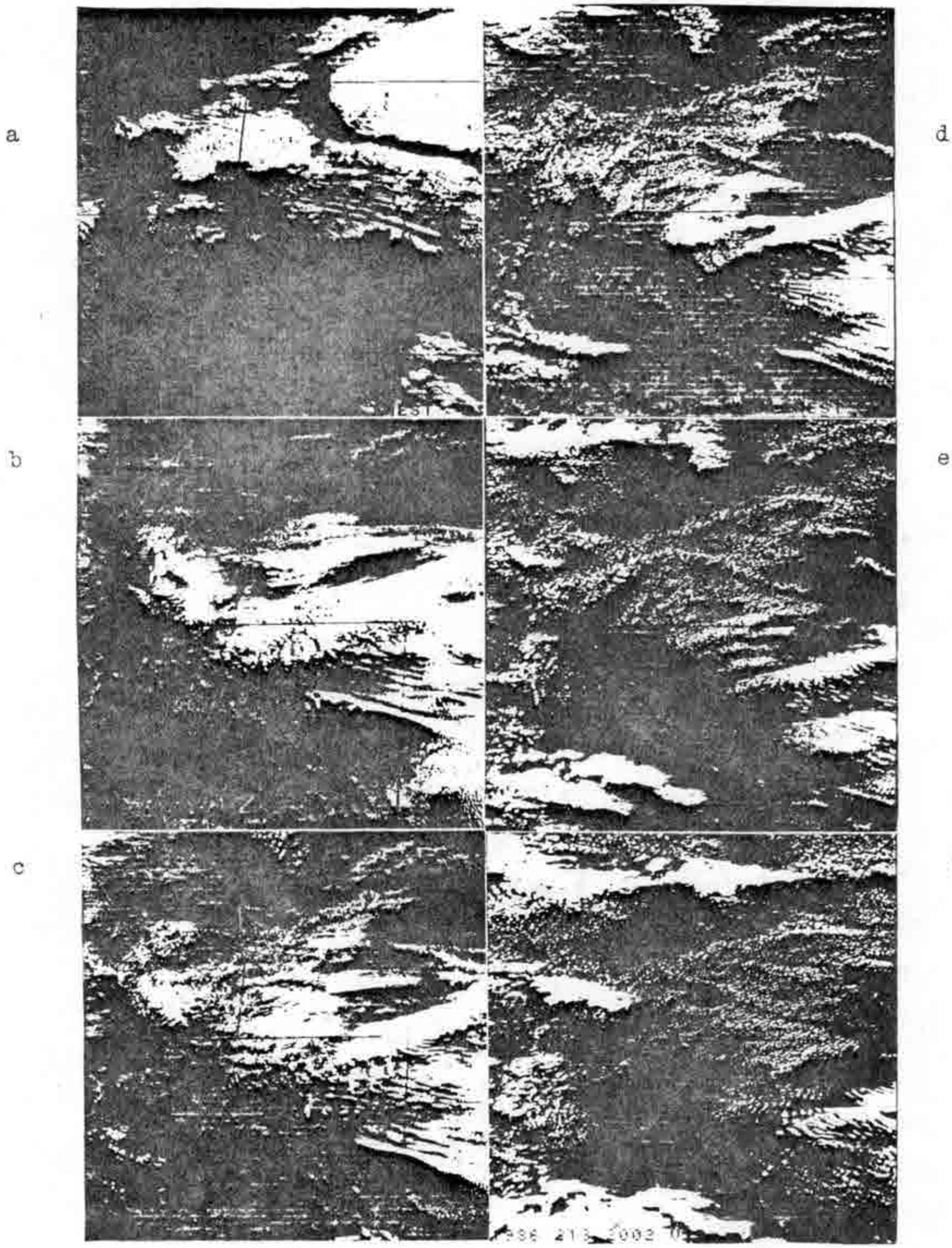

Figure 4.1: Full resolution visible satellite images on 1 August 1986 for (a) 1300 (b) 1600 (c) 1700 (d) 1800 (e) 1900 and (f) 2000 UTC. In addition to the state outlines, interstate highways 25 and 70 are shown in black (the city of Denver is near the intersection of the two highways).

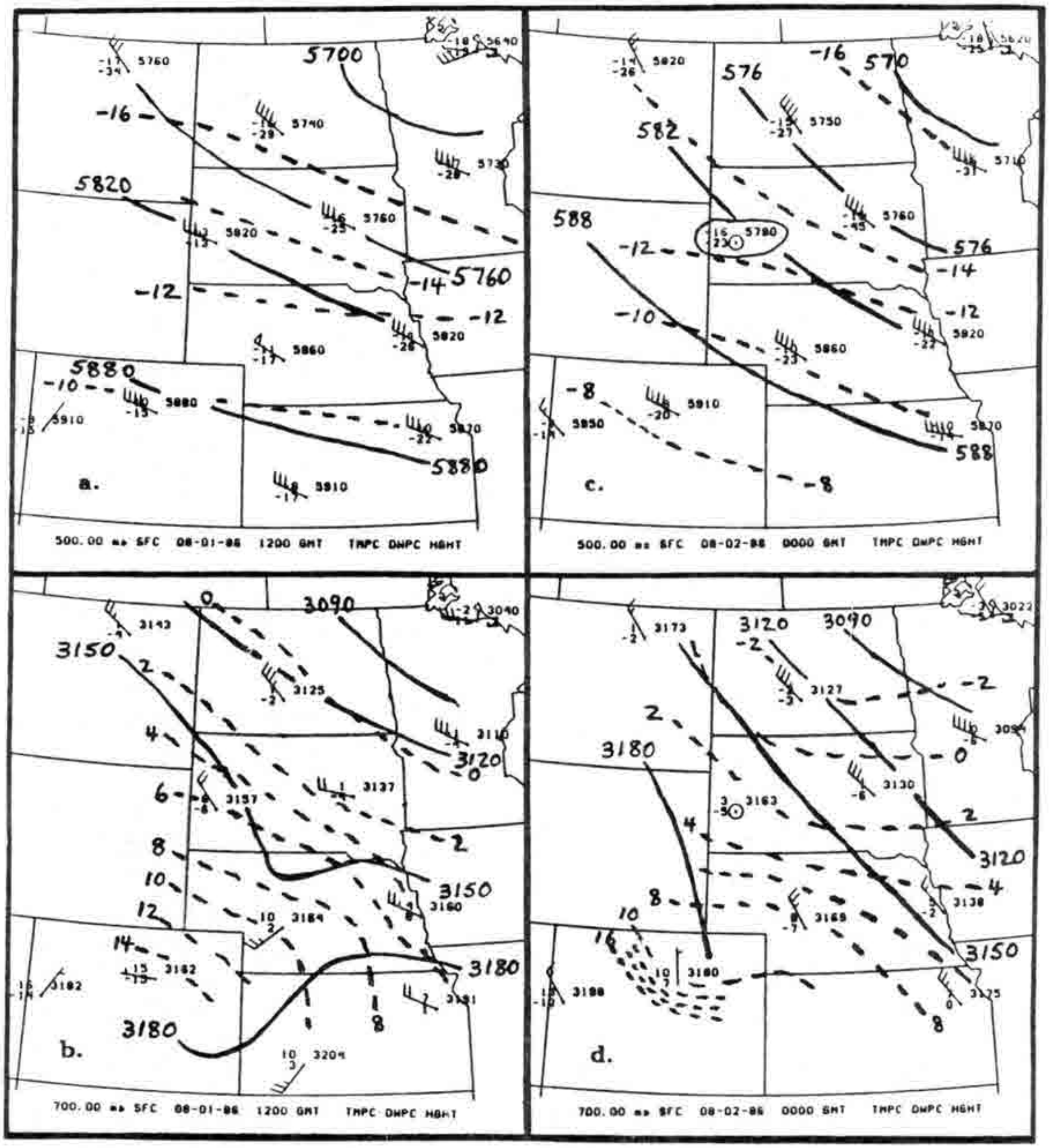

Figure 4.2: Upper air analyses at 1200 UTC 1 August 1986 for (a) 50 kPa and (b) 70 kPa and at 0000 UTC 2 August 1986 for (c) 50 kPa and (d) 70 kPa. The circled report at LBF at the later time appears erroneous. Plotting and contours are the same as in Fig. 3.3.

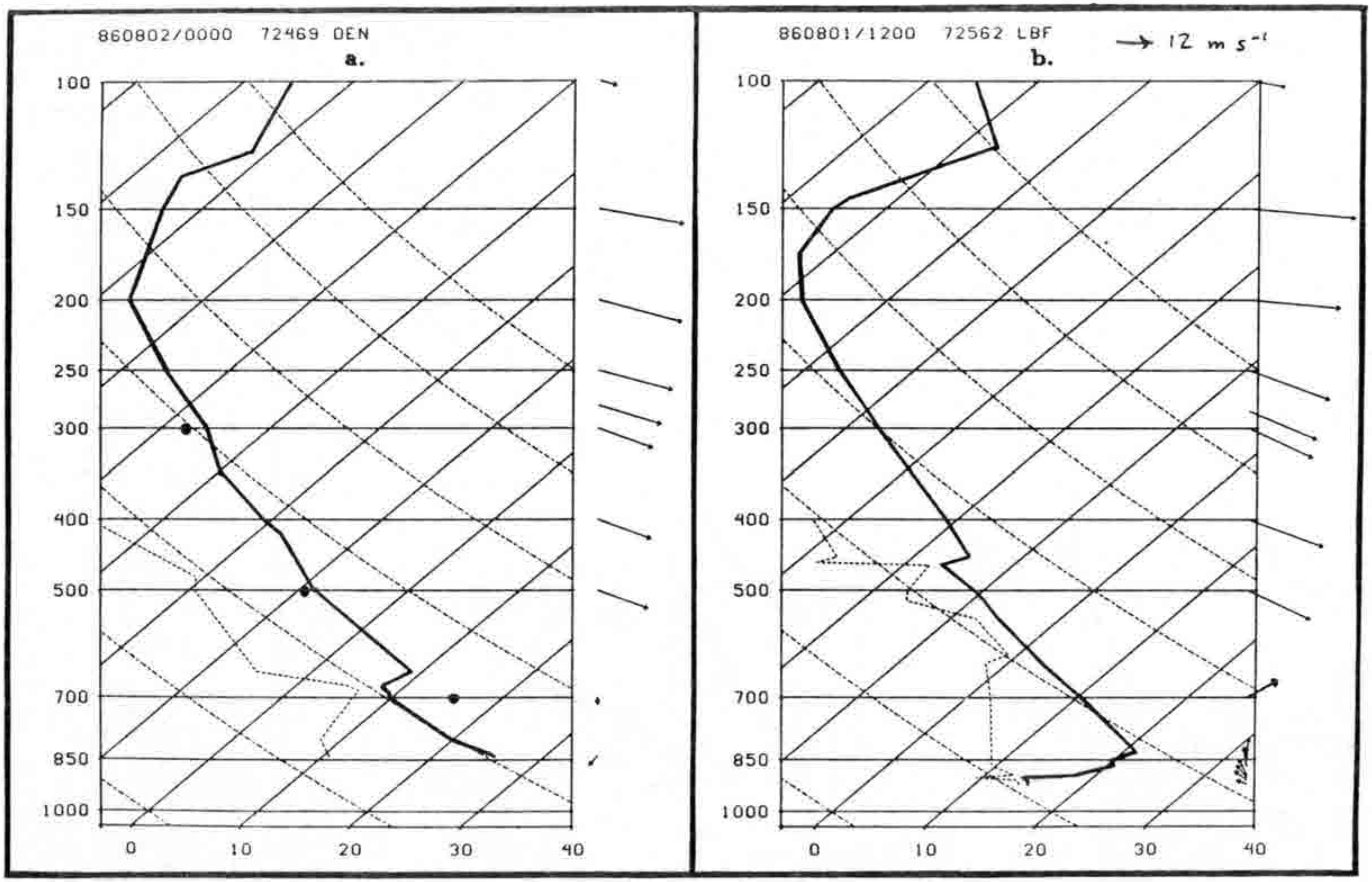

Figure 4.3: Temperature and dewpoint soundings for (a) DEN at 0000 UTC 2 August 1986 (solid dots at mandatory levels are the temperatures 12 h earlier) and (b) LBF at 1200 UTC 1 August 1986. Scale for the wind arrows is shown above the LBF sounding.

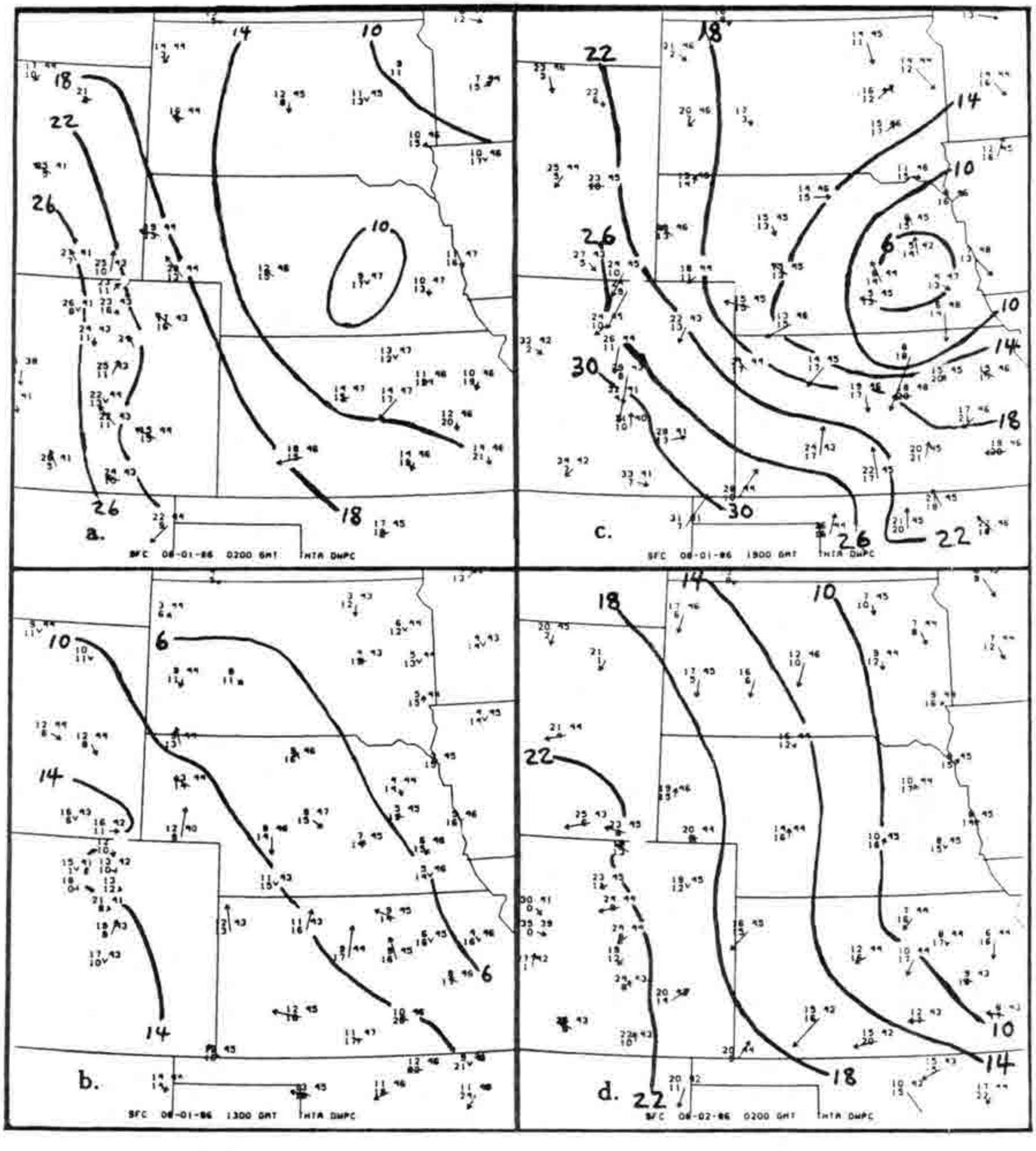

Figure 4.4: Surface plots with subjective analyses of the surface isentropes for (a) 0200 UTC (b) 1300 UTC and (c) 1900 UTC on 1 August 1986 and for (d) 0200 UTC on 2 August 1986. Plotted are wind arrows (scale at bottom middle), adjusted temperature [°C], dewpoint temperature [°C], and adjusted pressure [hPa, with the leading 8 omitted]. Adjustments to the temperature and pressure were made as described in the text.

(P_{adj}) is an adjustment of the station pressure (P_{sta}) to 1600 m using a form of the hypsometric equation

ln (P_{adj}) = ln (P_{sta}) + g(Station Elevation [m] -1600) $(R\overline{T})^{-1}$

where g and R are the gravitational force and the gas constant,

and $\overline{T}$ = 273.15 + (1/2)(Station Temperature [°C] + 25).

The adjusted pressure P_{adj} provides a good indication of the horizontal pressure gradient, especially where there are large differences in elevation between stations. It is based on a realistic (for this day) lapse rate passing through 25 °C at 1600 m, in contrast to, for example, the altimeter setting which is based on temperatures ~20 °C colder.

As in the previous case, the large scale northeast to southwest potential temperature gradient was nearly the same before (Fig. 4.4a) and after (Fig. 4.4d) the cold surge. Unlike the 14 June 1985 case, when much drier air accompanied the cold surge, moisture remained abundant over all but northern Wyoming and western Montana. The significance of the high moisture was that a severe weather pattern was maintained east of the Continental Divide. In fact, two separate thunderstorms deposited large hail on and around several Front Range cities during the following afternoon and evening. On this day, however, afternoon convection was suppressed, although not entirely absent, over northeast Colorado.

Prior to the cold surge (Fig. 4.4a,b and Fig. 4.5, top panel), a weak surface high persisted over eastern Kansas and Nebraska, with lower pressure over northeast Colorado. At later times, after the cold surge entered Colorado (Fig. 4.4c,d and Fig. 4.5, bottom panel), the pressure perturbations were mainly short–lived mesoscale features. The pressure changes during the period of the cold surge are discussed in the next section.

4.2 Importance of the convective system

The primary role of the MCS in generating the cold surge, making the synoptic scale cold advection much more intense, is supported by two observations. First, the morning sounding at LBF (Fig. 4.3b), which ascended just south of the MCS, exhibits an onion–shaped pattern (Zipser, 1977); i.e., a shallow, cold, saturated surface layer that is capped

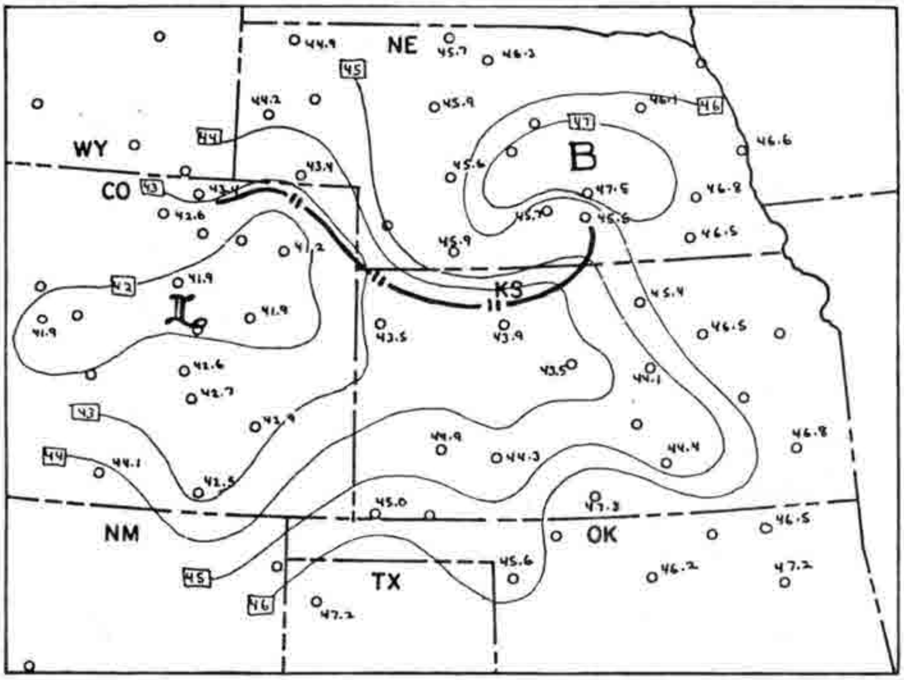

08-01-86 1500 UTC

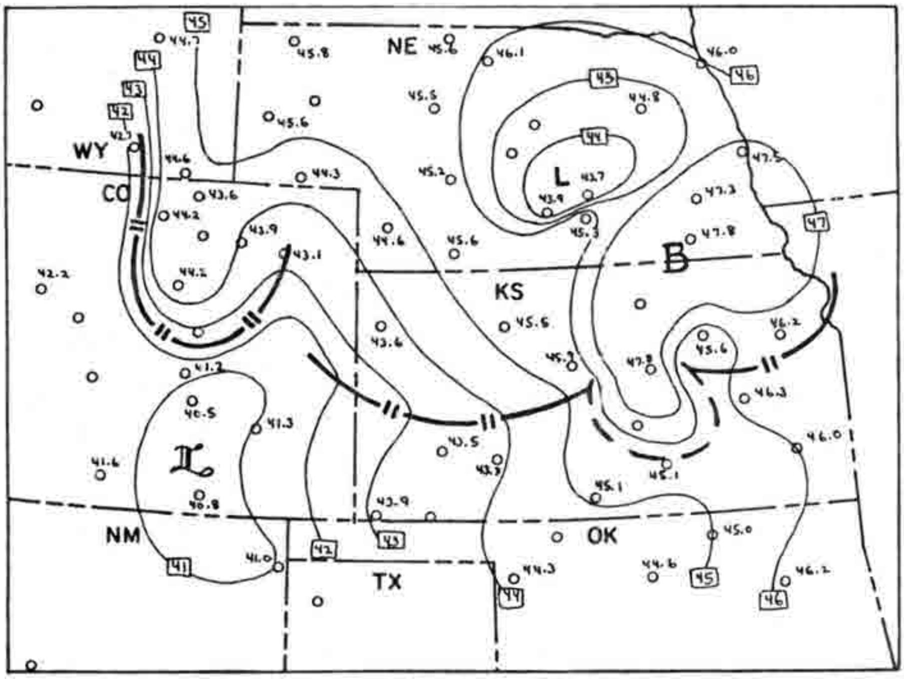

08-01-86 1900 UTC

Figure 4.5: Subjective analyses of the adjusted pressure for times shown. "B" indicates mesohigh (from Weaver and Toth, 1988).

by a deep warm layer. The warm layer is very dry below the melting level, but the dewpoint curve returns to near saturated conditions at higher levels. The onion–shape signature is typical of the stratiform precipitation region of a mature MCS. In this case, the MCS circulation had probably not quite reached LBF (the surface wind was northerly at LBF two hours later, Fig. 4.4b). The warm dry air between 85 and 60 kPa was advected in by the synoptic scale trough, and the cold air at the surface was due to nocturnal cooling. Nevertheless, the dry air is representative of the environment of the MCS, and because of this, convective scale downdrafts within the MCS could have been effective in generating a large pool of cool, moist air near the surface. This would explain the high dewpoints in the cold surge air. High surface dewpoints would not be expected if the cold air had simply been advected from northeast Wyoming and western Montana.

The second point illustrating the importance of an MCS outflow is the surface analysis for 01/1900 UTC (Fig. 4.4c, and Fig. 4.5, bottom panel). During the same period when the MCS in the Nebraska panhandle was dissipating, another MCS, not shown in Fig. 4.1, continued to develop farther east. At 01/1900 UTC, the outflow from this MCS was spreading over eastern Nebraska and the northern one-third of Kansas. The thermal and flow patterns in this area clearly deviate far from what would be expected simply from synoptic–scale cold advection. In a sense, this MCS, and likely the earlier one in the Nebraska panhandle, acted in a cooperative manner with the large–scale temperature gradient to locally advance the propagation of the cold air to the southwest. The cooperative interaction of synoptic–scale cold advection with diabatic cooling due to precipitation processes is the same mechanism described by Carbone (1982), but operating on a much larger scale.

The surface pressure changes (Fig. 4.6) also confirm the importance of mesoscale processes vs. advection of a synoptic air mass. The analysis is of the station pressure at the indicated time minus that at 01/1300 UTC. A V–shaped band of pressure change maxima expands and moves south, closely following the series of convective system outflows. The pattern evolved rapidly between 01/1600 and 1900, but became quasi–stationary between 1900 and 02/0200 UTC. The overall result was an increase in pressure towards the west,

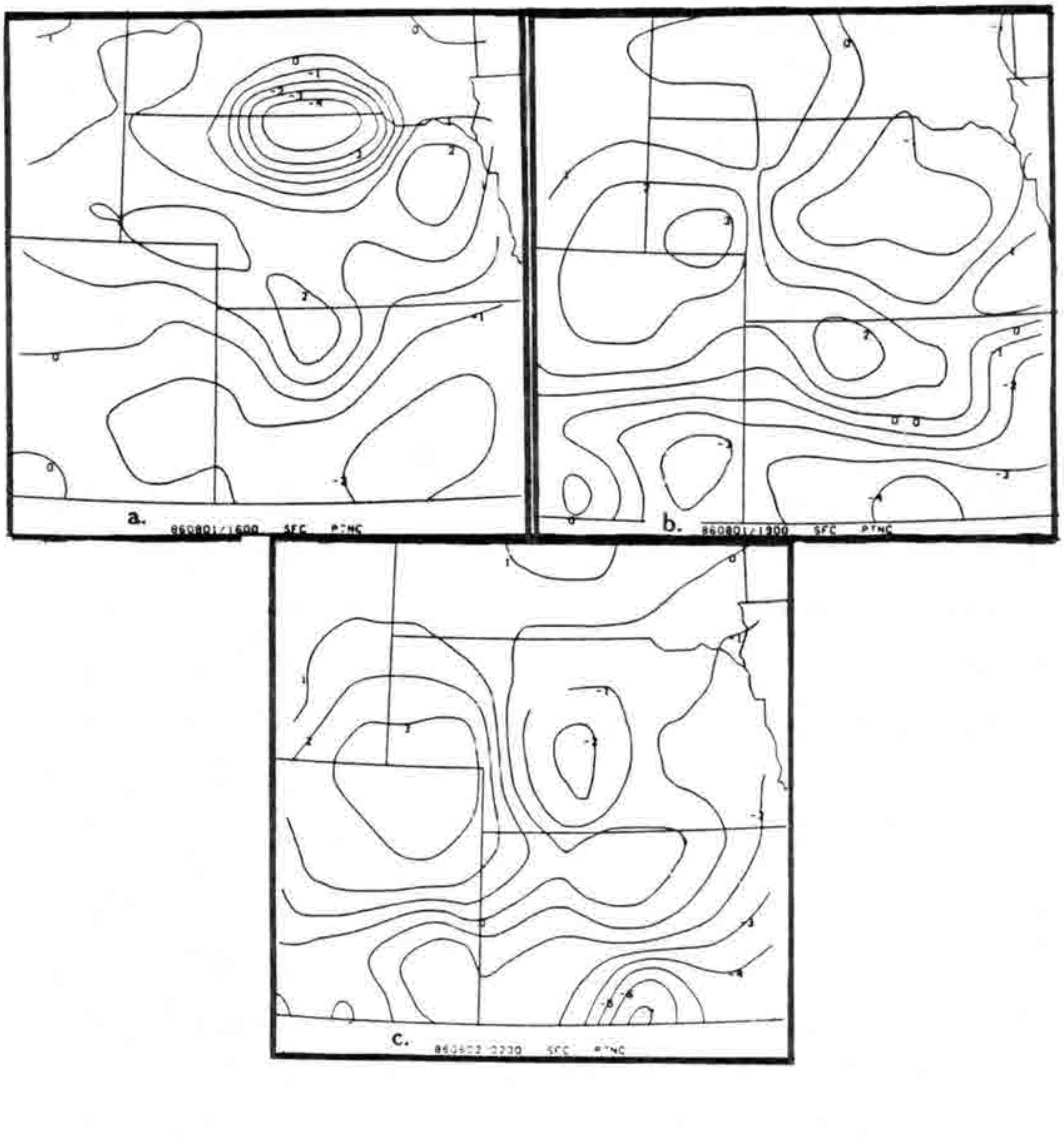

Figure 4.6: Surface pressure changes (contour interval 100 Pa) on 1–2 August 1986 for (a) the 3 h period 01/1300-1600 UTC (b) the 6 h period 01/1300-1900 UTC and (c) the 13 h period 01/1300-02/0200 UTC.

resulting in a reduction of the pressure gradient (Fig. 4.5) between northeast Colorado and eastern Nebraska/Kansas.

4.3 The outflow boundary over northeast Colorado

The effects of the cold surge were pronounced in the visible satellite imagery (Fig. 4.1), and in the surface observations over northeast Colorado (Fig. 4.7), including the PROFS mesonet. Subjective analyses of the pressure change (solid lines, difference from 01/1300 UTC = 0600 local time) and of the potential temperature (dashed lines) are shown in Fig. 4.7. The cold surge can be seen entering northeast Colorado from the north and propagating southward at 10-15 m s^{-1}. Ahead of the surge, there is southerly flow well east of the mountains (Fig. 4.7a,b), with light and variable flow closer to the foothills. As the surge moves through the PROFS mesonet (Fig. 4.7c,d), isolated clouds near the leading edge can be seen in the satellite images (Fig. 4.1b,c). The clouds are initially most numerous in a north–south band along the foothills east of the Continental Divide, but as the boundary reaches the Palmer Lake Divide (Fig. 4.7d), clouds develop rapidly there along an east–west line (Fig. 4.1d,e). At the same time, the north–south band of foothills cloud coverage increases slightly.

Inspection of the afternoon surface winds and temperatures (Fig. 4.7d,e,f) reveals that the cold surge potential temperatures were in the range 23-29°C, with the highest temperatures just behind the leading boundary. Temperatures in the warmer air were mostly 31-32°C, except for higher temperatures at the three PROFS mountain-top stations (Fig. 4.7d). The broad horizontal temperature gradient at the surface is in agreement with the vertical gradient in the afternoon sounding at DEN (Fig. 4.3a), which shows a temperature difference of 4-5°C between the cold and warm air. This amount of cooling up to the height of the DEN inversion would yield a hydrostatic increase in pressure at the surface of 200-300 Pa, again in good agreement with the horizontal gradient of pressure change. (As shown by Wakimoto, 1982, the pressure change at the leading edge of a cold outflow is not hydrostatic. But well behind the leading edge, and for the 5-minute averaging periods at the PROFS stations, non-hydrostatic effects should be insignificant.)

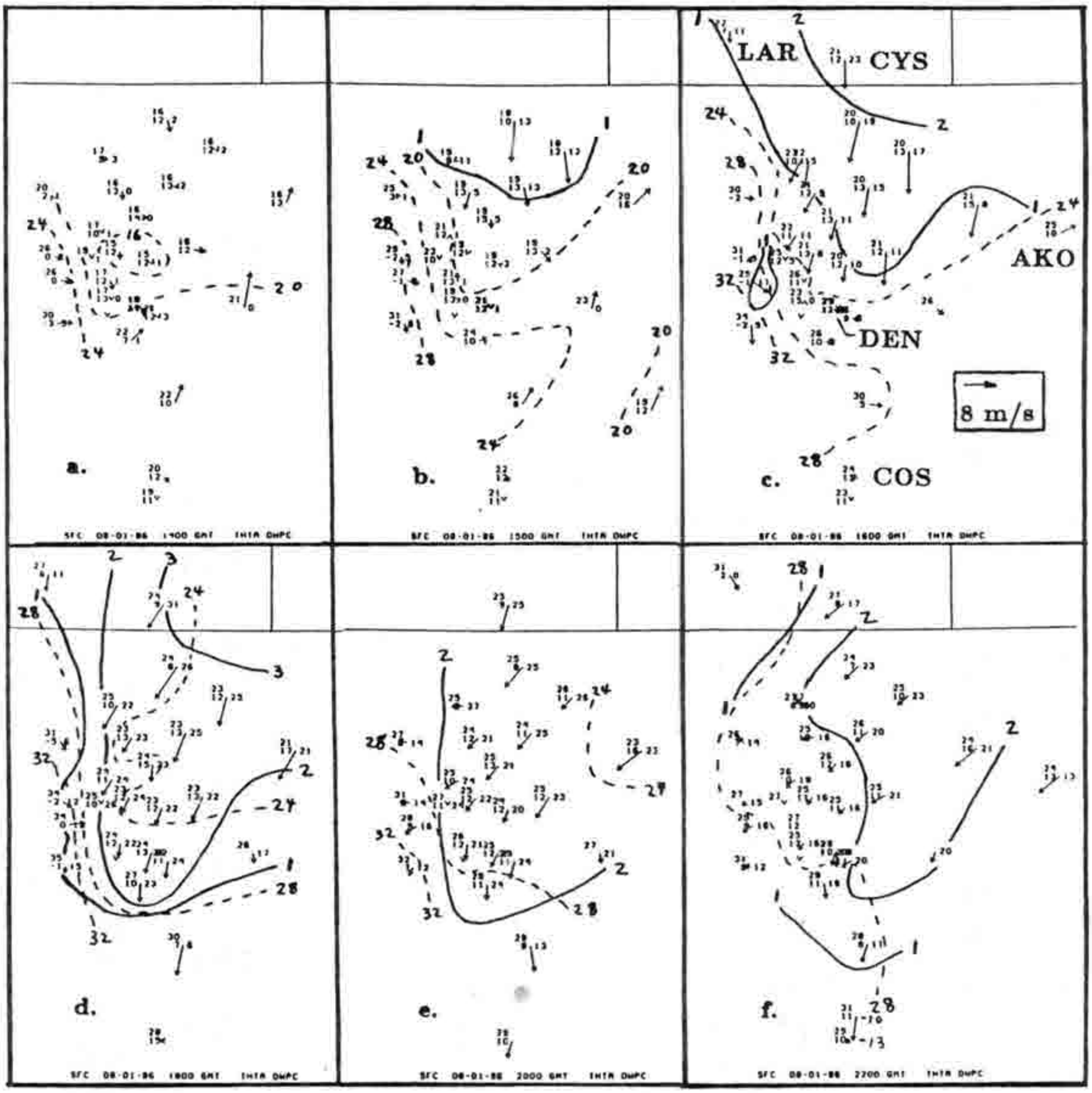

Figure 4.7: Surface plots on 1 August 1986 for the PROFS mesonet region at (a) 1400 (b) 1500 (c) 1600 (d) 1800 (e) 2000 and (f) 2200 UTC. Plotted are the adjusted temperature [°C], the dewpoint temperature [°C], and the pressure change [dPa] since 1300 UTC. Solid contours are pressure change (100 Pa interval); dashed contours are isentropes (2°C interval).

By late afternoon both the temperature gradient and the pressure change gradient at the southern leading edge of the cold surge had become very diffuse. For example, prior to 1900 UTC the wind at COS shifted to northerly (Figs. 4.4c and 4.7f) in response to the changing pressure gradient. Thus there was cold potential temperature advection at COS. In spite of this, and even with the effects of cloud shadowing (Fig. 4.1f), the COS temperature remained more representative of the warm air (e.g., the air above the DEN inversion) than of the cold surge air.

In Wyoming, the sequence of observations at LAR provides a glimpse of conditions at the western edge of the cold surge. The cold air retreated from LAR shortly after 1900 UTC (Figs. 4.4c and 4.7f). This occurred as the wind shifted from north-northeasterly to northwesterly. Along with a temperature increase of 4°C, the dewpoint temperature decreased 3-4°C and there was a pressure drop of 100 Pa. Warming lasted until 2300 UTC, at which time northeasterly flow returned to LAR accompanied by a 2°C temperature decrease. The short period of warming at LAR occurred even as the cold air farther south near the Front Range was becoming deeper (Fig. 4.3a), enough so that the air was finally able to reach the PROFS mountain-top stations (Fig. 4.7d,e). Evidently the impact of the Front Range on the structure of a cold surge can be highly localized.

4.4 Discussion

This case illustrates several features typically observed with shallow cold surges over northeast Colorado. There is a tendency for the surge to slow during the afternoon hours and become "hung-up" on the Palmer Lake Divide. The 1 August 1986 boundary, like most others, not only slowed, but its surface gradients became more diffuse. A similar effect appeared on 14 June 1985. Then the retardation took place at the Raton Mesa, 200 km south of the Palmer Divide.

Before the slowing of this boundary, station pressures immediately behind it rose by 100-200 Pa within 1-2 h. This indicates that the depth of the cold air increased fairly rapidly to $\sim$1 km. Yet it took several hours for the cold air to reach the PROFS mountain-top stations, meaning that further deepening developed slowly. In addition to synoptic-scale cold advection, the near-vertical wall of the Front Range probably controls the deepening of the cold air. It should be recognized that the grid spacings used for the numerical simulations in the later chapters (25-70 km) are not able to resolve the regional details of the interaction of the cold air with individual mountain ranges and valleys (e.g., the differences noted above between LAR and the Front Range). Similarly, it should also be recognized that the DEN radiosonde may not always be representative of regional conditions during a cold surge.

The slowing during the afternoon hours of both this cold surge and of the cold front on 14 June 1985 are further examples of the effect documented by Wiesmueller (1982), and also observed along the east coast of China in the vicinity of Taiwan. In Wiesmueller's case study, the cold front stalled just north of the Cheyenne Ridge. He did not comment on its importance, but the presence of an east-west ridge in each of the three Colorado case studies would seem to be important. In the numerical simulations of the 14 June 1985 case, however, afternoon slowing developed even with only minor north-south variations in the smoothed topography. Furthermore, the slowing in Taiwan cannot be attributed to an east-west ridge. The east-west ridges, although they generate important local effects, and block extremely shallow (< 1 km) cold surges, perhaps play an auxiliary but not crucial role in the large- scale slowing of cold surges that are 1–2 km deep. The important mechanisms involved in the movement of cold surges are investigated numerically in the remaining chapters.

Chapter 5

MODEL SIMULATIONS OF THE 14 JUNE 1985 CASE

Observations, even numerous and frequent ones such as during the PRE-STORM experiment, seldom provide a complete data set for studying mesoscale features. In contrast, the data set from a numerical simulation has good temporal and spatial resolution and can be used to further understand the important physical processes operating during the evolution of phenomena such as shallow cold surges. The first section of this chapter is a general description of a hydrostatic version of the RAMS numerical model, which was used for all simulations. After that, a realistic simulation of the 14 June 1985 case incorporating detailed model physics is compared with the observations from Chapter 3. The roles on this day of the surface fluxes of heat and momentum are then explored in the final section with a less complex form of the model.

5.1 The hydrostatic version of the RAMS model

Essential features of this hydrostatic version of the model are described in Tremback *et al.* (1985). Other details not unique to the hydrostatic version are given in Tripoli and Cotton (1982). The model provides for either two- or three-dimensional simulations; only the three-dimensional ones are discussed in this study.

The model has a modular design so that physical processes may be added or deleted as desired. Only the most essential processes were retained so that interpretation of the results could be as straightforward as possible. The convective cloud parameterization was never used. The surface energy budget and the short– and longwave radiation parameterizations were used only for the simulation of the actual 14 June 1985. The specific features of each simulation will be listed as each is discussed. But it is appropriate to note at this point details of processes that appear to be crucial in the evolution of cold surges, and that were common to all simulations. Probably the most important of these processes are the surface heat and momentum fluxes.

5.1.1 Model treatment of surface fluxes

Surface fluxes in the hydrostatic version of the model as developed by Tremback are based on the parameterization of Louis (1979), which, in turn, is based on Monin-Obukhov similarity theory for the constant-flux layer. This theory states that there is always some portion of the boundary layer near the ground where it is appropriate to assume that the vertical turbulent fluxes of heat and momentum are each constant through the layer. The vertical gradients of the mean temperature and momentum through this layer are not independent; both depend on the nature of the turbulence which is determined by the ratio of the heat to the momentum flux. Thus it is physically unrealistic, for example, to assume that the surface heat flux increases linearly with increasing wind speed.

More realistically, the drag coefficients (C_{D_M}, C_{D_H}) in the model expressions for the momentum and heat fluxes

$$\rho\overline{u'w'} = -\rho C_{D_M} u^2,$$

$$\rho c_p \overline{w'\theta'} = -\rho c_p C_{D_H} u \Delta\theta,$$

are not treated as constants; instead, they vary with the bulk Richardson number

$$Ri_B = \frac{gz\Delta\theta}{\overline{\theta} u^2},$$

where z, $\Delta\theta$, and u are determined between the surface and the first model layer above the surface. Varying C_{D_M} and C_{D_H} according to the gradients at the surface estimates in a simple way the ratio of the heat to the momentum flux and accounts for combined thermal and mechanical contributions to turbulent fluxes. The model roughness length (4 cm) and the vertical grid spacing were never changed (there is a slight decrease in z with the coordinate system over higher terrain). As a result, the dependencies of the drag coefficients on u and $\Delta\theta$ were essentially the same in all simulations and are plotted in Fig. 5.1.

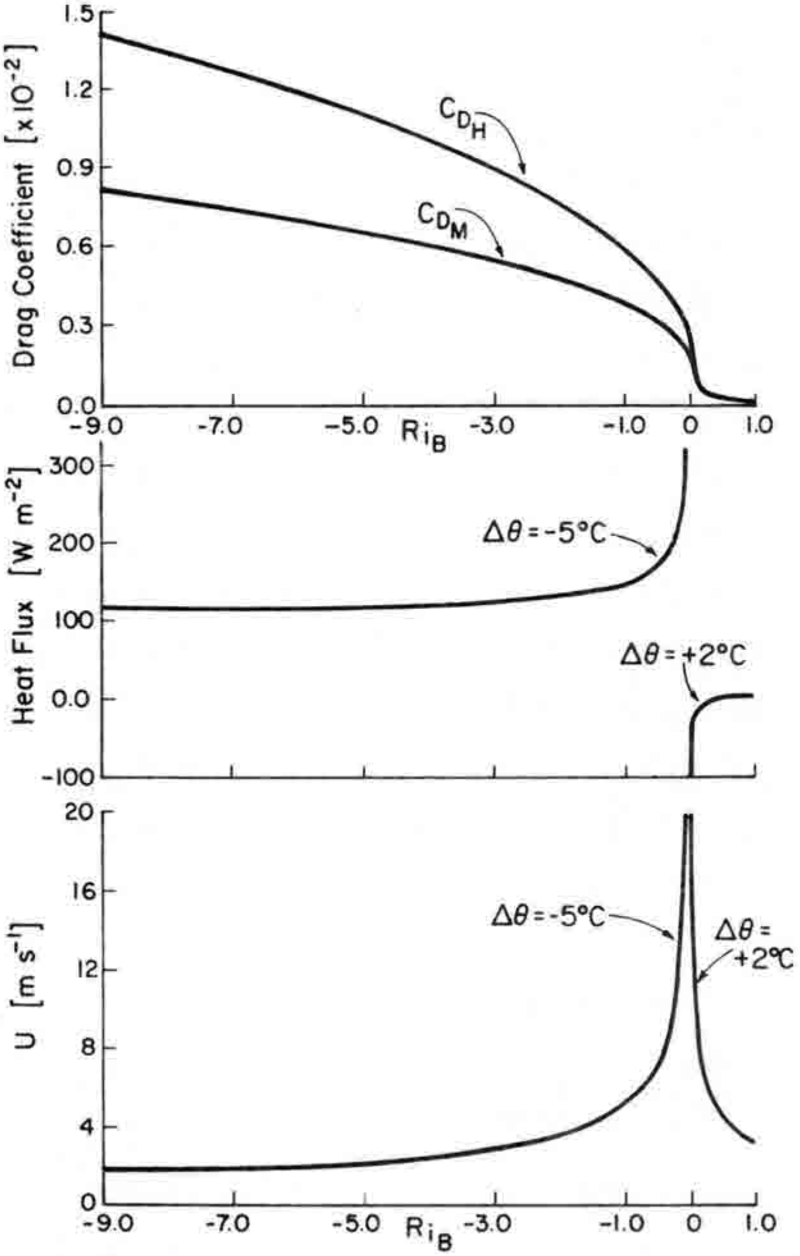

Figure 5.1: Drag coefficients for heat and momentum as a function of the bulk Richardson number (top). For the fixed atmosphere to ground temperature differences indicated, the corresponding heat flux (middle) and surface windspeed (bottom) are also shown.

In general, $\Delta\theta$ depends at each grid point on the surface energy budget and on the model atmosphere advection and thermodynamics. With $\Delta\theta$ specified, as it is for the simpler simulations described in the final sections of this chapter, the fluxes revert to a dependence only on the wind speed u.

For the simple cases, with a fixed temperature difference of 5°C in the unstable simulation and of 2°C in the stable one, the wind speed and the corresponding heat flux have been included in Fig. 5.1. In the unstable case, the heat flux is virtually constant for wind speeds below 8 m s^{-1}, increases only slowly with wind speed, and averages close to 150 W m^{-2}. In the stable case, the heat flux is roughly proportional to the square of the wind speed. At large Ri_B, the Louis fluxes become small but, contrary to theory (e.g., Panofsky and Dutton, 1984), do not vanish. There is always some small distance above the ground where the fluxes do not vanish in the real atmosphere, and since the model parameters are layer averages, unresolved gradients justify the non-vanishing fluxes. At the other extreme, near $Ri_B = 0$, the large heat fluxes in Fig. 5.1 exist only because the temperature differences are fixed. Thus, extreme wind speeds are necessary in order for Ri_B to approach 0. Given very high speeds, the heat flux would be as indicated. But of course the momentum flux (proportional to the square of the speed), prevents such winds. Realistically, Ri_B approaches 0 only when $\Delta\theta$ does the same, and in that case the heat flux also vanishes.

The horizontal and vertical turbulent fluxes above the surface are calculated with locally diagnosed eddy exchange coefficients, with the coefficients based on the Richardson number. Vertical diffusion is calculated implicitly.

5.1.2 Vertical coordinate

The vertical coordinate was the same in all experiments and is illustrated in Fig. 5.2. Vertical spacing in the layers closest to the ground averages near 300 m; the spacing increases gradually to 2000 m above the tropopause. There are 8 layers below 70 kPa–approximately 50% greater than the resolution of the operational Nested Grid Model (NGM, Phillips, 1979; McPherson, 1986). The coordinate system follows the terrain, using the sigma-z system as described by Clark (1977).

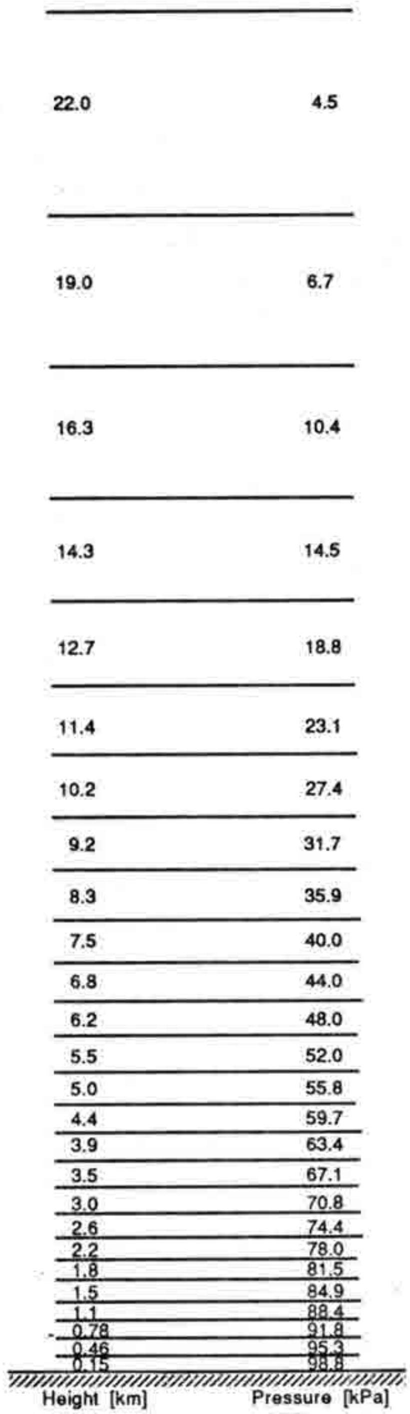

Figure 5.2: The 26 vertical levels used in all model simulations. Heights and pressures are for the middle of each layer.

It is possible to express and evaluate the horizontal pressure gradient directly in sigma coordinates. This method may introduce errors when the terrain slopes steeply (Tremback, personal communication). A less efficient but more accurate alternative is to vertically interpolate between model grid points so that the gradient of pressure between horizontally adjacent points is evaluated at a common elevation. This second procedure is a model option and was used in all simulations.

5.1.3 Sensitivity and adequacy of the model

The large–scale ($\sim$ 300 km) evolution of cold surges in the model was found to be relatively insensitive to the horizontal resolution. A wide range of resolutions, as low as 25 km and as high as 70 km, were used in two and three dimensions. In all cases, a smooth, physically realistic outflow gradually evolved. For the idealized simulations, a 30 km grid spacing offered excellent resolution of the cold surges over time periods ($\sim$ 3h) for which the Coriolis force was important. The density current structure (e.g., the nose of a density current) was, of course, not resolved. However, to do this, not only increased resolution but also a non–hydrostatic model would be required.

The grid spacing for the simulations of the 14 June 1985 case, incorporating boundary conditions from analyzed data, was increased to 70 km. This was done so that the model boundary could extend as far northwest ($\sim$ 1400 km) of Colorado as possible. A jet–stream disturbance at the northwest corner of the model, propagating at 30 m s^{-1}, could reach the area of interest near the end of the 12 h simulation. There was no disturbance traveling this fast, and so, although increases in both resolution and domain are desirable, this combination of the two was adequate for simulating the 14 June 1985 cold surge.

5.2 Simulation of the 14 June 1985 cold front

For this case, parameterizations of short– and longwave radiation were included as described by Chen and Cotton (1983). These parameterizations consider absorption, scattering, transmission, and emission by both clear and cloudy layers. The ground temperature is determined from a surface energy budget incorporating the soil model described by Tremback and Kessler (1985). Moisture is included in the model because of its impact on radiation. Otherwise, it is effectively a passive tracer. Since the convective parameterization was not included, the model can be expected to deviate from reality in areas where moist convection was important (northeast Kansas). Other specific features of this simulation are listed in Table 1.

Table 1

Horizontal Domain	119.0–91.8 W Longitude ; 30.0–52.8 N Latitude
Horizontal Grid Size; Spacing	34×35; 0.80° Longitude, 0.65° Latitude (≈70 km)
Timestep	Long 90 s, Short 30 s
Start Time	1200 UTC 14 June 1985
End Time	0000 UTC 15 June 1985
Lateral Boundaries	Sponge; Boundary values interpolated between analyses of radiosonde data at the start and end times
Top Boundary	Prognostic surface pressure; upward integration of hydrostatic equation

The model was initialized from isentropic analyses of significant level radiosonde data. The analysis area, model domain, and model topography are shown in Fig. 5.3. Gridpoint data from the National Meteorological Center (NMC) operational analyses were not included. Although the initialization package for the RAMS model contains this option, adding the smoothed NMC constant pressure data would have degraded the sharp frontal gradients (horizontal and vertical) that were obtained from the isentropic surfaces by using the significant as well as the mandatory level sounding data (Tremback, personal communication).

5.2.1 Coarse model analyses

Analyses of the 1.8 km geopotential height surface for selected times are shown in Fig. 5.4. Wind arrows at each gridpoint and contours of potential temperature have

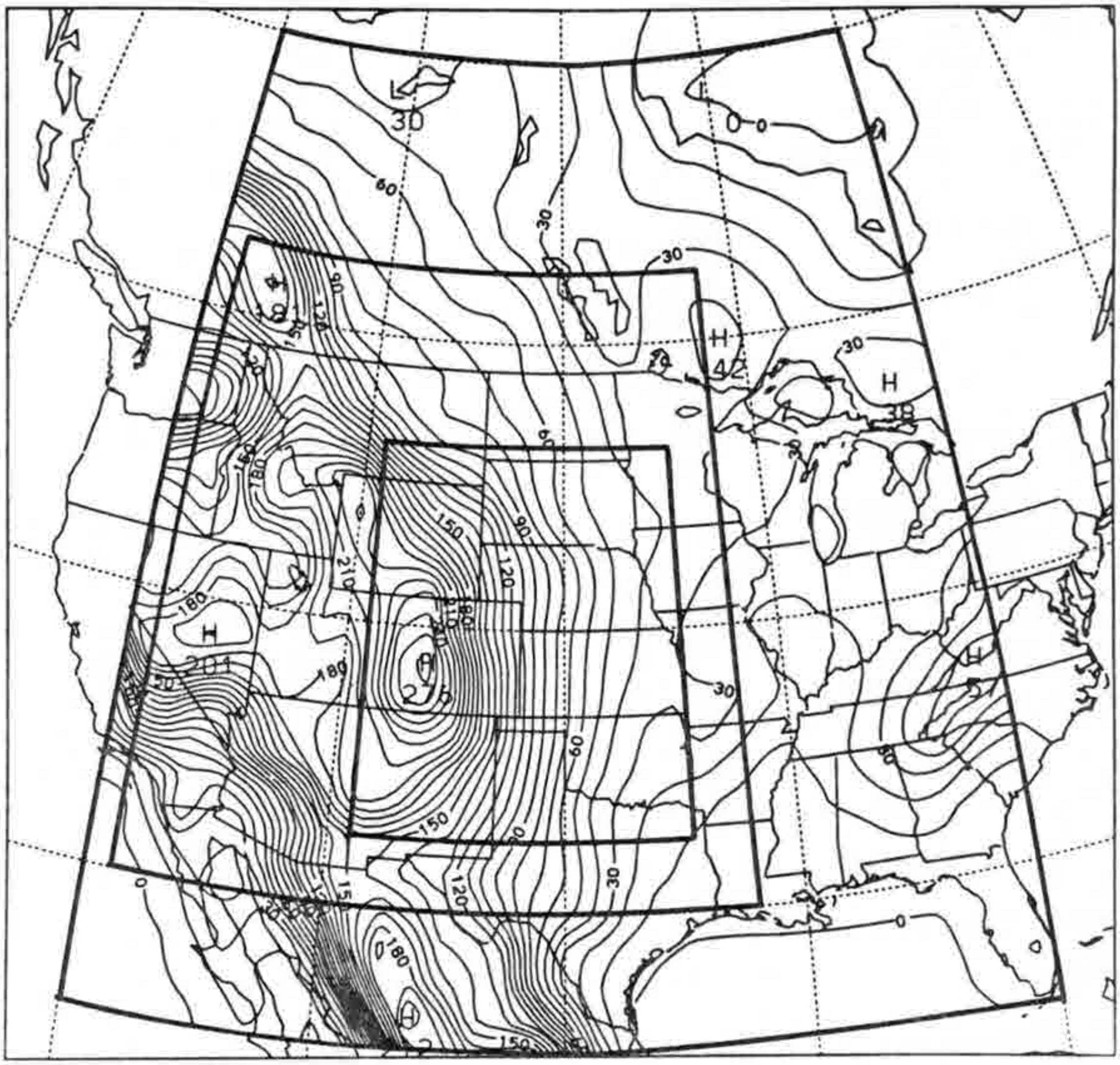

Figure 5.3: Smoothed topography used in the model for the 14 June 1985 case. The outer box indicates the area used in the objective analyses of the radiosonde data. The middle box is the domain of the coarse grid model. The inner box is the domain of the nested, fine-grid model. Contour interval 100 m; labels in decameters.

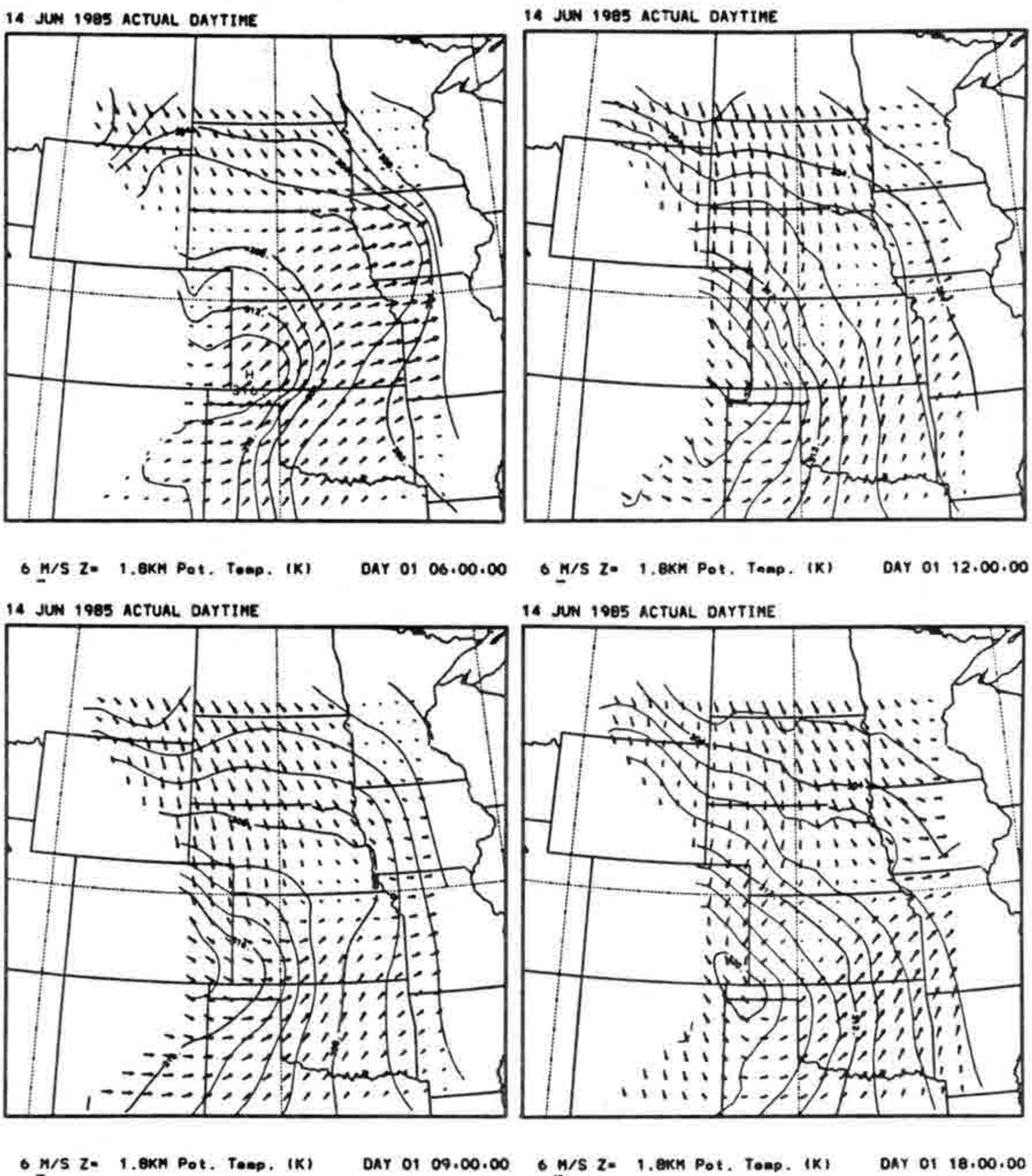

Figure 5.4: Isentropes (2 K interval) and wind vectors at a constant geopotential height of 1.8 km for (a) the beginning of the model simulation at 0600 local time = 1200 UTC (b) 0900 local = 1500 UTC (c) 1200 local = 1800 UTC and (d)1800 local = 0000 UTC.

been interpolated from the model terrain-following levels to this constant height, which intersects the ground near the Front Range. A constant height offers the advantage in later analyses of a direct presentation of the horizontal pressure gradient. Since over Colorado, and over at least western Kansas, the daytime boundary layer extends to 1.8 km, the surface isentropes must be virtually the same as shown at this height. This assumption is less valid over the lower terrain farther east.

The model initially (Fig. 5.4a; 1200 UTC/0600 local time) contains a somewhat distorted baroclinic zone, a result of the radiosonde spacing. After a three-hour period of adjustment (Fig. 5.4b), and for later times (Fig. 5.4c,d), the model baroclinic zone closely resembles the surface features described in Chapter 3 (add 283 to the contours in Fig. 3.8 to convert to absolute potential temperature). Evidently because of surface heating, the model isentropes made little southward progress over northeast Colorado and, in fact, retreated slightly northward by noon (Fig. 5.4c). There is little further change over eastern Colorado between then and the end of the simulation (Fig. 5.4d). Cold advection (maximum 0.85°C h^{-1} at the surface) appears to have been approximately canceled by surface heating. The details of this process are discussed in Section 5.3.

Comparison between the model soundings (Fig. 5.5) and the upper-air observations (Fig. 3.10) near the western edge of the cold air is possible only at 15/0000 UTC. The model DEN sounding is 1–2°C warmer in the lower troposphere. Correspondingly, the dry-adiabatic layer extends to 54 kPa, slightly higher than observed. In contrast to the observed light easterly flow, the model developed light northerly flow below 70 kPa. This discrepancy may be partly due to the smoothing of the topography (Fig. 5.3) near the Continental Divide. Otherwise, the vertical shear, although heavily smoothed, closely resembles the observed wind profile. The model temperature profile for the gridpoint closest to DDC is also too warm and not stable enough. However, this is an area where moderate cold advection was just beginning in both the observations and in the model. Adjacent model points to the north and east better resembled the DDC observation. The AMA area also was the site of large low-level gradients in the model. To the east, a deeper layer of stable, southerly flow existed that more closely resembled the AMA observation.

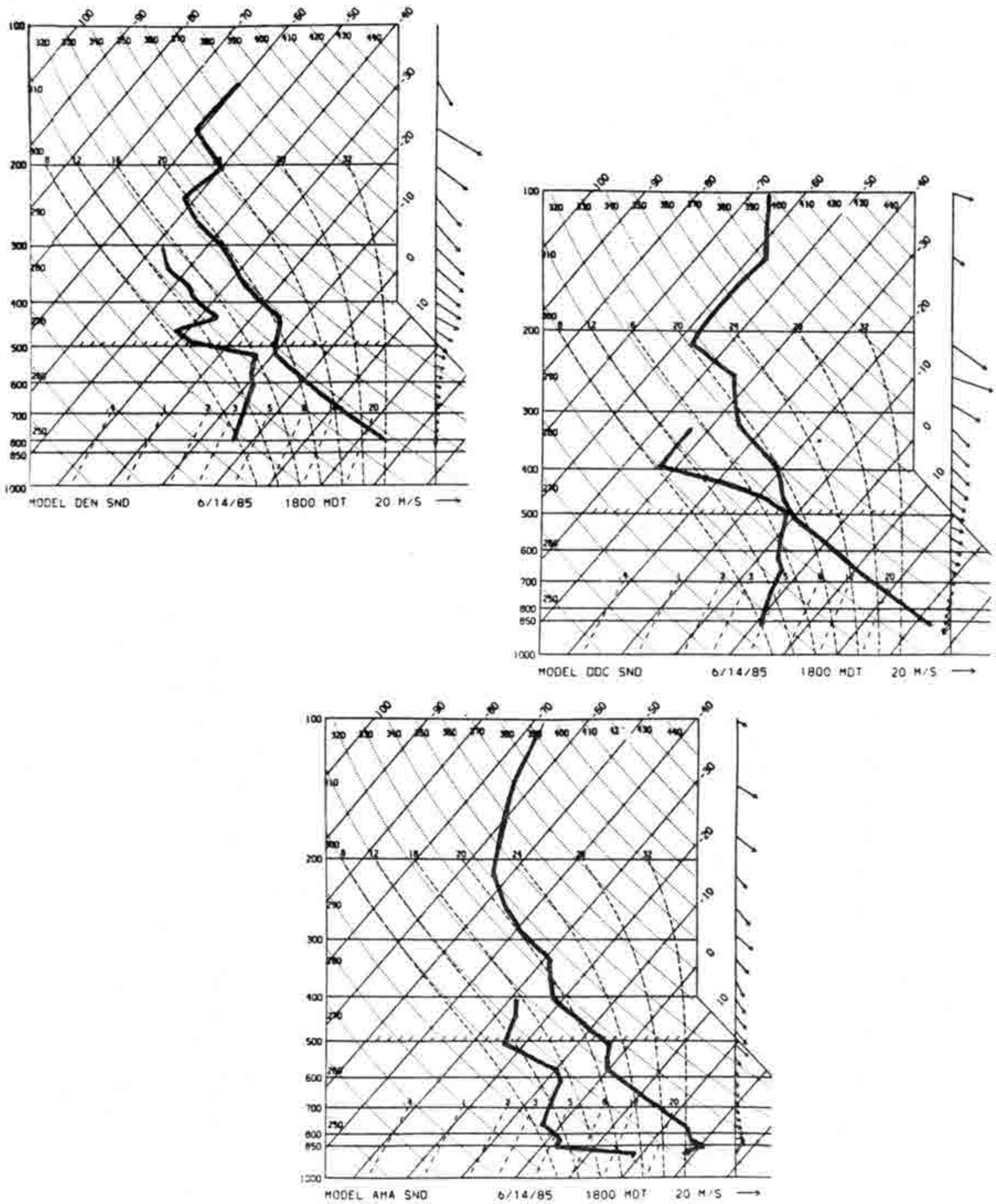

Figure 5.5: Soundings as in Fig. 3.10 (1800 local time = 0000 UTC), but for the model output.

To the west, the surface temperatures were warmer, the shallow surface inversion vanished, and northwesterly flow extended to the surface, consistent with the observations.

The development of a deep boundary layer along the western edge of the cold air may also be inferred from a comparison of the 3.0 km analysis at the end of the 12 h simulation (Fig. 5.6b) with the 1.8 km analysis for the same time (Fig. 5.4d). The isentropes at the two levels are nearly coincident over eastern Colorado, western Nebraska, and western Kansas. This was not the case at the beginning of the simulation (Figs. 5.4a and 5.6a). Moving north and east from the western edge, farther into the cold air, there are larger temperature gradients at the lower level and, therefore, increased stability between the two layers.

5.2.2 Nested grid model analyses

In the belief that increased resolution would improve the model agreement with observations, and also to test the impact of varied horizontal resolution, a one-way nested-grid simulation was done for this case. The grid spacing was reduced by a factor of 3 to $\approx$25 km. The domain for the fine grid is shown in Fig. 5.3. The boundary values were obtained from the coarse model grid using model analyses at 3 h intervals. Other features, including the smooth topography, were identical to the coarse model. Although the finer grid is capable of adequately resolving smaller-scale topographical features, it would be difficult to determine if atmospheric features developed differently only because they were better resolved or whether they were forced by different terrain features. Leaving the topography unchanged eliminates one possible contribution to any differences. Since there was a period of adjustment during the first three hours of the coarse model run, this was not repeated for the fine run. Instead, only the last 9 h were simulated in the nested run.

The result by the end of the simulation (Figs. 5.7 and 5.8) was an increase in the easterly component of the flow at the surface in eastern Colorado (in better agreement with the observations), cooling of 4–6°C in eastern Colorado and western Kansas compared to the coarse run (not in agreement with observations), and much higher wind speeds in the same area (also not in agreement with observations). In contrast to the coarse run, the coincidence of isentropes at 1.8 and 3.0 km occurred only in a narrow north–south strip

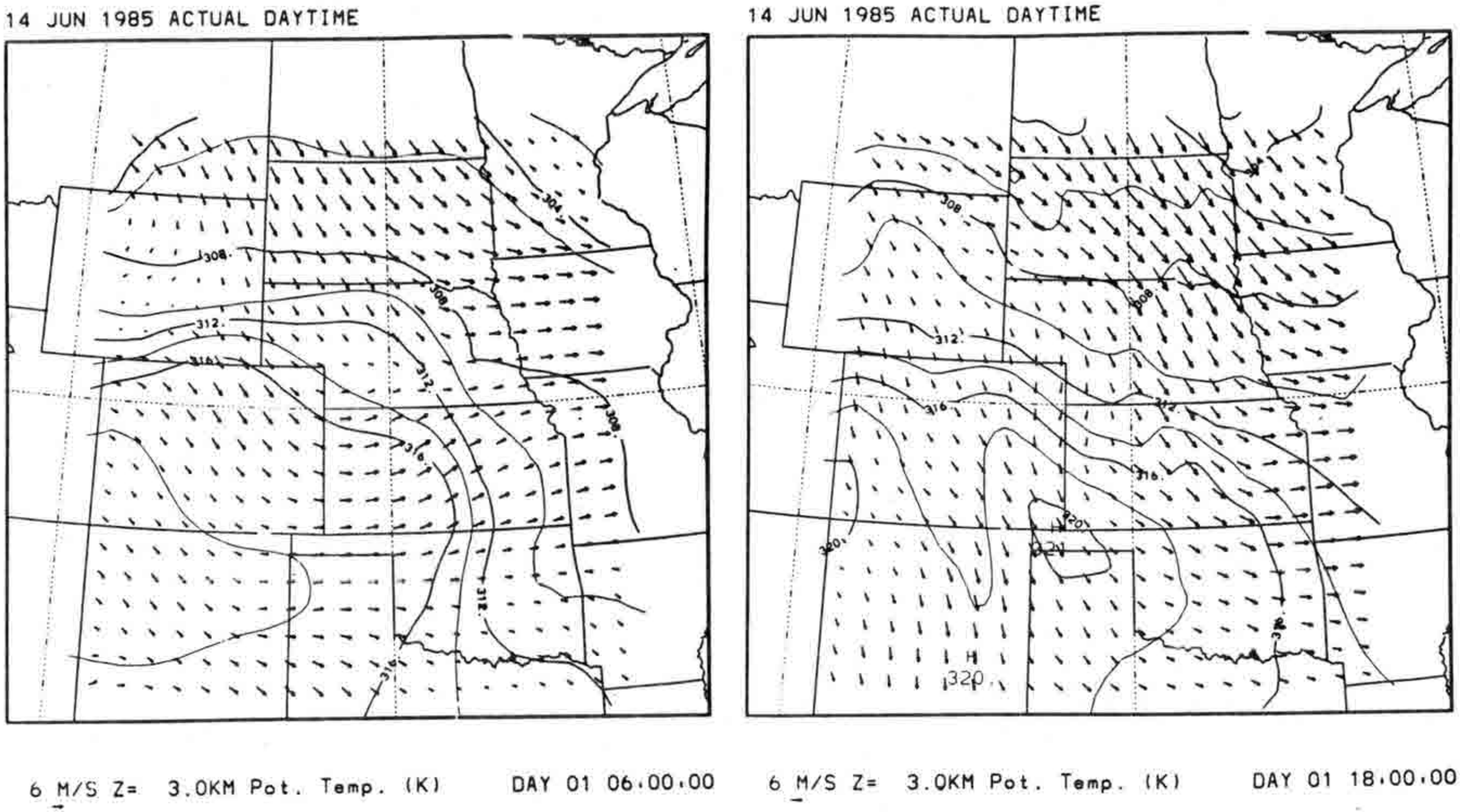

Figure 5.6: Constant height analyses as in Fig. 5.4 but for 3.0 km at (a) beginning and (b) end of simulation.

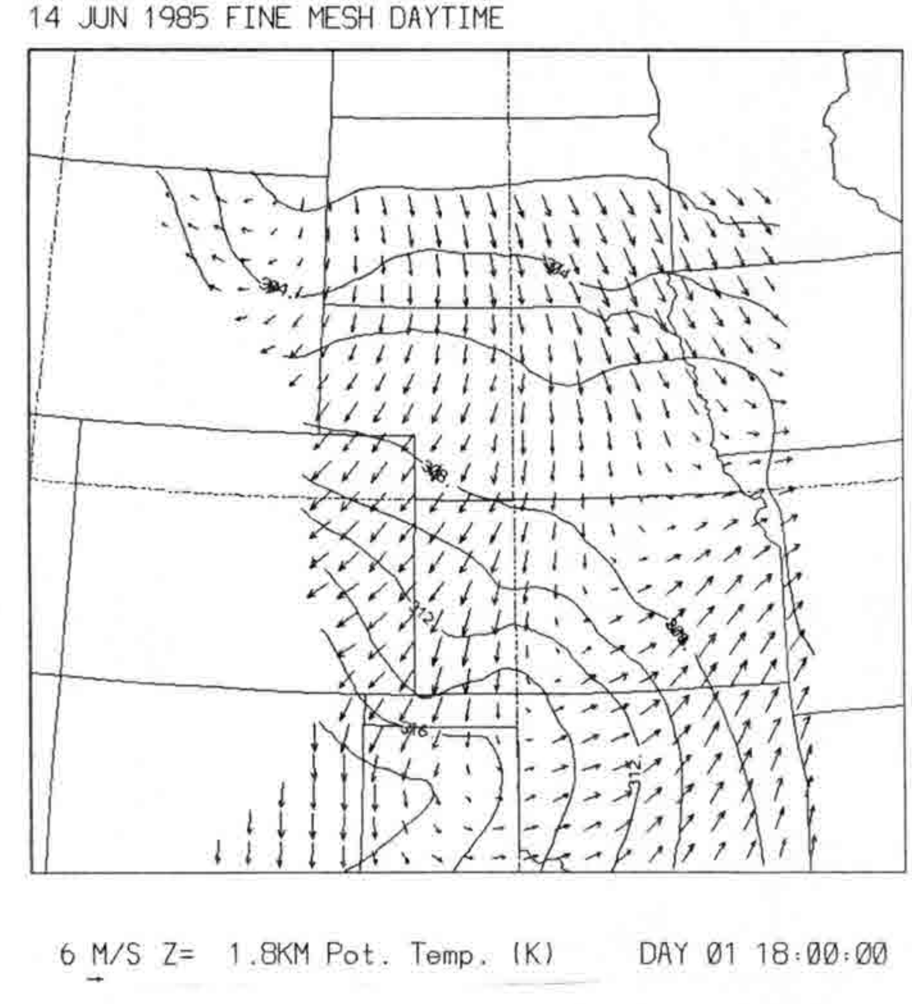

Figure 5.7: As in Fig. 5.4d, but for the nested, fine-grid simulation. Wind vectors are plotted at every other grid point horizontally and vertically.

very close to the Front Range in Colorado. East of this strip, the boundary layer was much more shallow and did not quite extend to 3.0 km. Large amplitude gravity waves can be seen in the isentropes at 3.0 km (Fig. 5.8). Waves at the top of the boundary

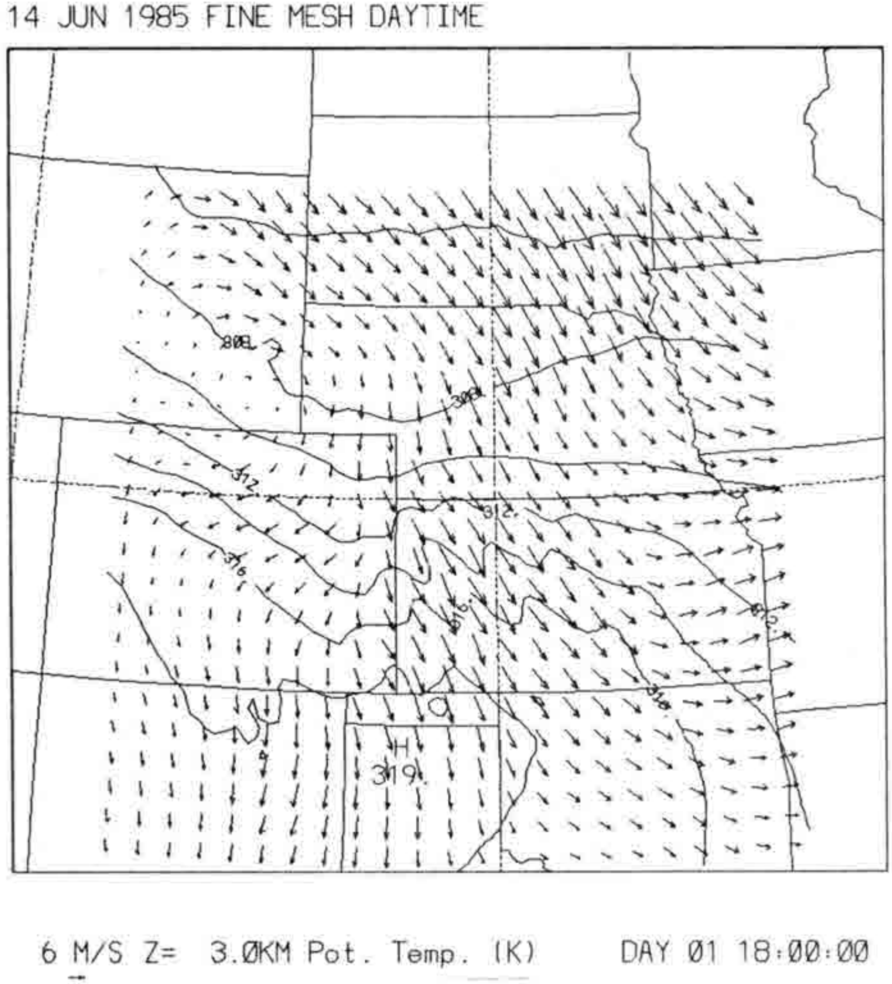

Figure 5.8: Same as Fig. 5.7, but for 3.0 km.

layer would likely be present in the real atmosphere for a similar situation (Kuettner, *et al.*, 1987), although such large amplitudes would probably not be observed. These model amplitudes are, however, consistent with the discrete vertical spacing in the model.

The differences between the coarse and the fine run are likely attributable more to the domain and boundaries instead of the resolution. In retrospect, the boundary of the nested model did not extend far enough west, and was not updated frequently enough, to allow it to resolve correctly the synoptic-scale evolution of the baroclinic zone in the middle troposphere. Unlike the coarse run, which contained both the trough and the upstream ridge, only the trough was contained in the nested domain. The increased troughing in the isentropes east of the mountains, which could be a realistic modification by the mountains, is instead probably only an indication of the difficulties of the boundary conditions for the one-way nested grid. In spite of these problems, the nested run appeared to handle the trough moving through the PRE-STORM area reasonably well and additional details of the thermal structure could be seen that were not resolved by the coarse run. But the one-way nest is inadequate for interactions between the synoptic-scale cold advection and much smaller terrain features. A two-way nested grid for the RAMS model has recently been developed by Tremback, but it has not yet been used for this study. For now, the resolution and domain of the coarse model seems to have been the best compromise allowing for both synoptic-scale forcing of the cold surge as well as the interaction with the terrain.

Well east of the mountains, the coarse and the fine model results were similar. North-south cross sections corresponding to the observed data in Fig. 3.12 are shown in Fig. 5.9 for the fine model data. The model supports the conclusion reached from the observed data that there was an important difference in the near-surface temperature structure of the front/trough over the eastern half of the PRE-STORM network compared to the western half. To the west (Fig. 5.9 top), the model developed a clear surface cold front. There is low stability through most of the troposphere ahead of the surface front and the air is convectively unstable. In contrast, farther east (Fig. 5.9 bottom), there is a surface wind shift but almost no north-south surface temperature gradient. Furthermore, the air above the surface wind shift is very stable, preventing the release of convective instability. In the real atmosphere, the stability in this area was probably the main factor in suppressing the moist convection over the middle of the PRE-STORM area.

In summary, reducing the grid spacing in the model increased the resolution of the leading edge of the cold surge, and provided results consistent with the surface and upper-air observations over the PRE-STORM network. But at the same time, the necessary reduction in the domain of the model was detrimental to the evolution of the large-scale features. The correct way to explore this problem would be with a two-way nested grid.

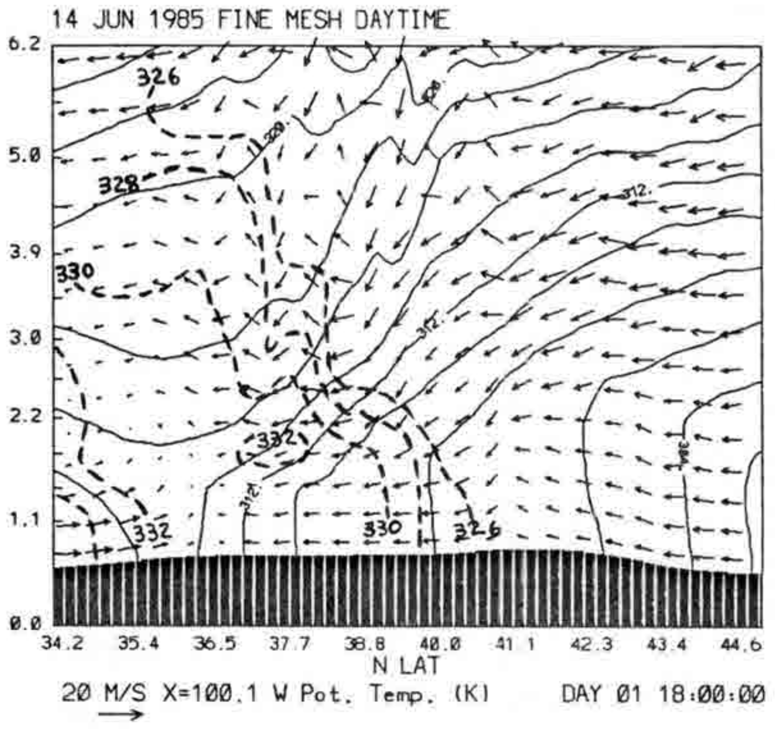

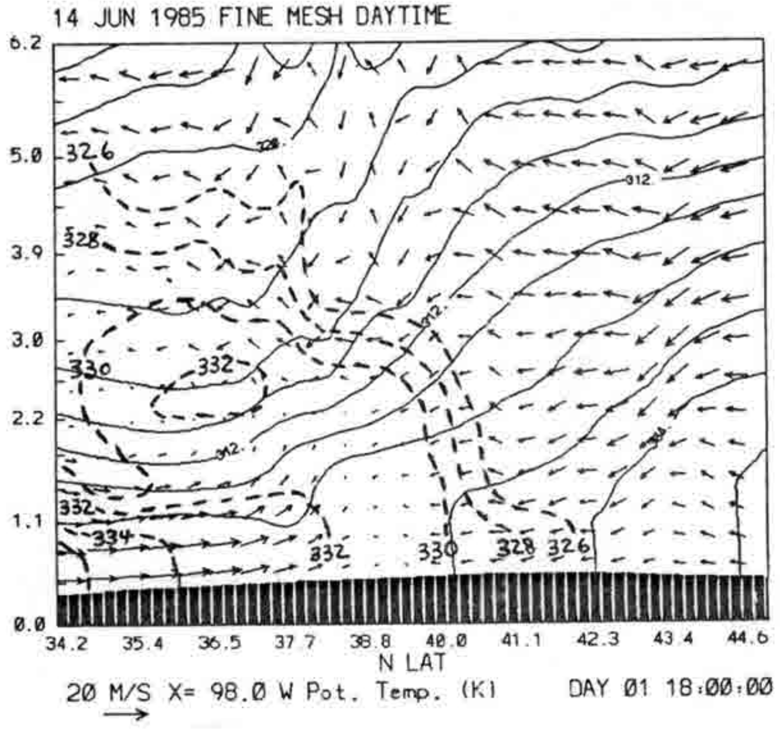

Figure 5.9: North-south cross-sections near the middle of the PRE-STORM network. Wind vectors plotted at every grid point vertically and at every other grid point horizontally. Isentropes are solid (2K interval). Near the surface front, countours of equivalent potential temperature are dashed

It should be realized, however, that a further reduction of the smallest grid by an order of magnitude would be necessary before density current features such as observed by Shapiro (1984) and by Young and Johnson (1984), or simulated by Droegmeier and Wilhelmson (1985) could be resolved.

5.2.3 Impact of short-wave radiative heating on cold surge evolution

As a first step in assessing the importance of surface heat flux, and to test whether there would be increased southward propagation of the front at night, in agreement with the observations of Wiesmueller (1982), the coarse model was rerun for the last 9 h with simulated nighttime conditions. This was done by changing the model local time. Beginning from the model fields at 0900 in the actual simulation, the local time in the simulated night case was set to midnight. This changed the parameterization of short wave radiation for the last 9 h of the simulation. The 0900–1800 period of strong solar heating was replaced by a 0000–0900 period of predominant cooling. The results at the end of the period are shown in Figs. 5.10 and 5.11.

The nighttime analyses for the 1.8 and 3.0 km surfaces in Fig. 5.10 can be compared with the daytime case in Figs 5.4 and 5.6. At night there was more cooling at both levels just east of the mountains, associated with an increased southward propagation of the front. In addition, the magnitude of the temperature gradient increased at both levels and, in fact, throughout the lowest 3.0 km of the model troposphere. Another change that occurred as the front propagated to the south was a decrease in its slope. At 1.8 km, the zone of maximum baroclinicity along the eastern Colorado border propagated farther south by ≈300 km. But at 3.0 km, the southward advance was limited to to a maximum of ≈200 km near the Continental Divide. Farther east, the advance at 3.0 km was limited to only 100 km. Thus the near vertical isentropes during the day became more horizontal at night. The front became very shallow, with a slope typical of a warm front.

The differences in temperature gradient do not result directly from changes in diabatic heating. The processes involved will be discussed in the next section. In the night case, the baroclinic zone did not merely shift to the south, but also intensified. Associated with this, the horizontal pressure gradient (Fig. 5.11; perturbation pressure is defined simply

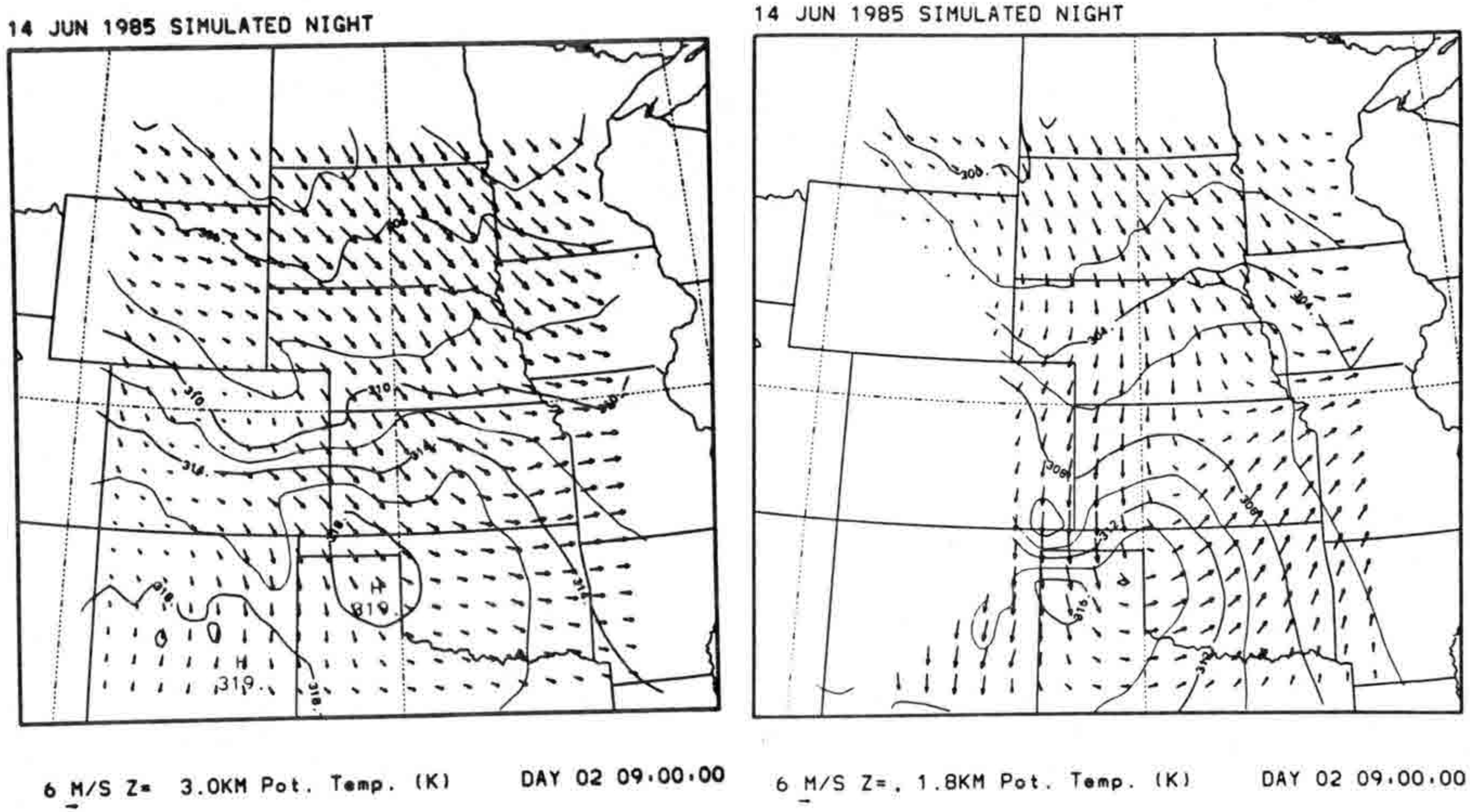

Figure 5.10: Constant height analyses as in Fig. 5.4 but for the simulated night case at 3.0 km and at 1.8 km.

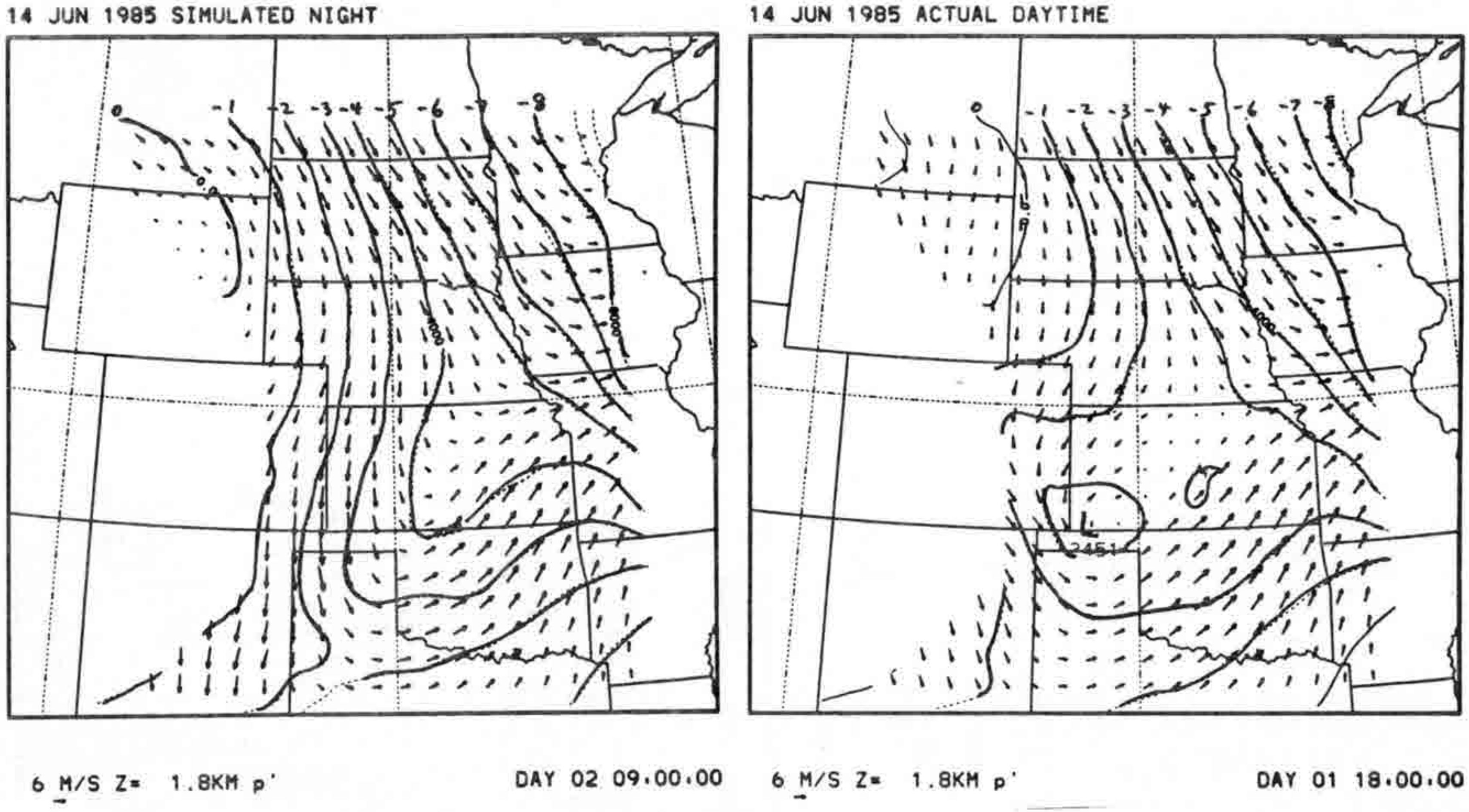

Figure 5.11: Isobars (100 Pa interval) of the perturbation pressure for the simulated night case and for the actual daytime case at 1.8 km. Wind vectors are identical to those in Fig. 5.4d and in Fig. 5.10.

as the deviation from an arbitrary reference pressure at that level) evolved differently at night, consistent (given that the pressure gradients at higher levels were nearly the same) with much colder air near the surface along and to the east of the Continental Divide. The nighttime flow, in contrast to the daytime, has a significant component parallel to the Continental Divide in near geostrophic balance. The evolution of the northerly, approximately geostrophic flow for the stable night case can be explained by the analytic models for cold air damming as discussed in Chap. 2. Near the end of the simulation, the leading edge of the cold surge was propagating southward at a speed of 18 m s^{-1}. The model had developed a temperature near–discontinuity of 9°C. Although the model is not able to resolve the leading edge of any density current structure, the depth of the cold air behind the leading edge in the model rapidly increased to approximately 1.0 km. This depth, combined with a temperature discontinuity of 9°C, yields a gravity wave speed of 16 m s^{-1}. Thus the speed of the northerly, nighttime flow is consistent with a rotating gravity current description.

5.3 Comparison of the impact of idealized surface fluxes

There are many feedback processes that in general make it difficult to interpret the causes for the differing evolution of the cold surge described in the previous section. The 14 June 1985 case was chosen so that the feedback effects of moist convection would be minimized over eastern Colorado. For example, moist convection in reality did not develop until near the end of the period simulated in the model. Still, it might be argued that the model generated slightly different cloud cover at night, and that this then modified the surface energy balance. For the nighttime case, increased northerly flow advected not only cooler but drier (not shown) air over the area east of the Continental Divide, and this alone would have increased the surface radiative cooling. In order to isolate the roles of the surface fluxes of heat and momentum, simpler model runs with fewer physical processes are described in this section. In these simulations, the radiation parameterizations and surface energy budget calculations were eliminated. Instead, a constant surface temperature difference was set and used for the calculation of fluxes from the ground to the first model layer. All other model parameters were unchanged. Although highly simplified, these simulations yielded results very close to those discussed in the previous section.

5.3.1 Analyses

Three surface temperature differences of −5°C, 0°C, and 2°C were used. Upward heat flux in the −5°C case and downward flux in the 2°C case, discussed at the beginning of this chapter, simulated daytime and nighttime conditions respectively. Atmospheric absorption and emission are of course not present. But the essential difference between day and night appears to be contained in the surface fluxes alone, as indicated by the results at the end of each simulation (Fig. 5.12). As before, the nighttime case yielded an increase in the

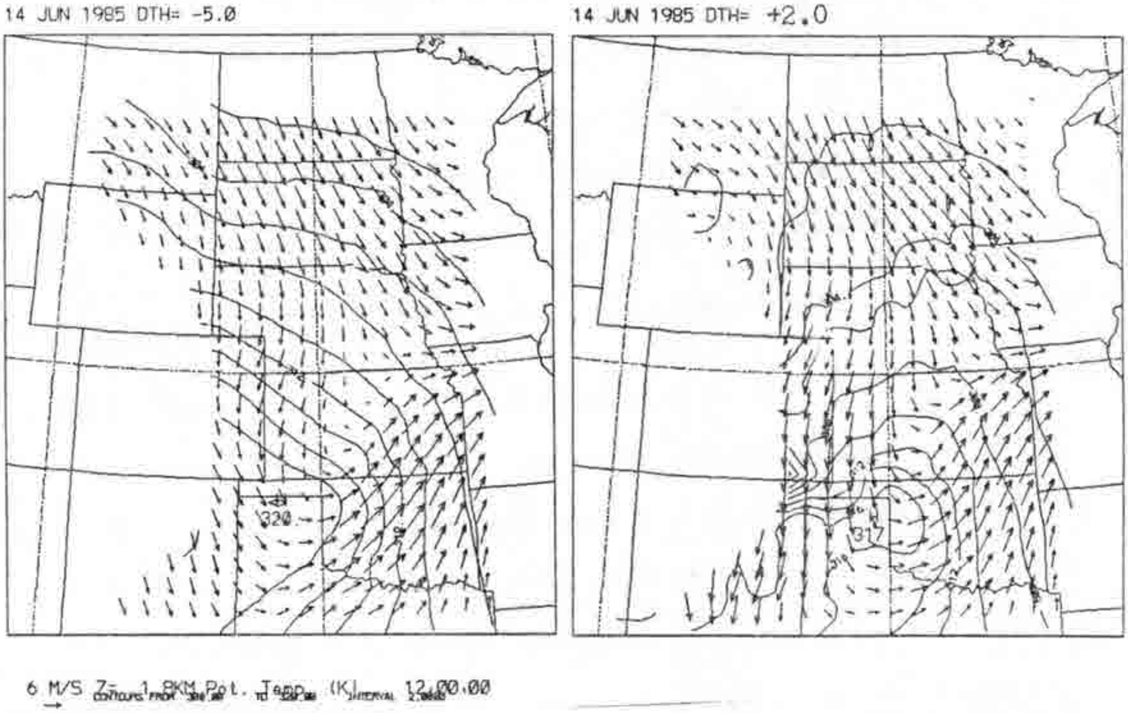

Figure 5.12: Temperature analyses at 1.8 km as in previous figures but for specified surface temperature differences of −5°C (day case, left) and 2°C (night case, right) at the end of each simulation.

southward propagation of the baroclinic zone. Fields at all levels were similar to those discussed for the cases with radiation and a surface energy budget. Furthermore, since the case with no heat flux was very similar to the one with downward heat flux, the presence or absence of upward heat flux is apparently the crucial element.

5.3.2 Trajectories

The baroclinic zone propagated farther south in the night case, and this means that at least some of the air parcels must have increased their southward movement. The movement of a chain of air parcels during the last nine hours is shown in Figs. 5.13 and 5.14 for the day (–5°C) and night (2°C) cases. The initial positions of the parcels extend along an east-west line (Fig. 5.13) near the baroclinic zone in northeast Colorado. The western parcel starts at the 3.0 km level; the eastern one starts at 1.4 km. Because of the terrain slope, all parcels start ≈0.5 km above the ground. There are large differences in the speed of the eastern parcels from the day to the night case. During the 9 h period, they moved south ≈300 km during the day, averaging a speed of 9 m s^{-1}, and ≈500 km during the night, averaging 15 m s^{-1}. The vertical movement of the parcels (bottom panel of Figs. 5.13 and 5.14) is also different. All parcels except for "A" rise by 400–1100 m during the day. At night, the eastern parcels stay near the ground, while the western ones travel southeast, up and over the cold air.

Parcel temperature changes (not shown) also differed moving west to east. The western parcels traveled southeast during both periods. The terrain sloped rapidly down under them so that by the end of the period they were roughly 2.0 km above the ground. As a result, and also because the parcels started well within the warm air, turbulent heat flux was small and diabatic temperature changes were <1°C. In contrast, the eastern parcels started within the baroclinic zone and were strongly affected by differences in surface fluxes. Largest temperature changes were 3.5°C warming for parcel "I" during the day and 7.1°C cooling for parcel "G" during the night case. Even at night, parcels "D" and "E" warmed by 1.4°C. Clearly, the heat fluxes were determined not only by the surface fluxes but by the parcel position relative to the baroclinic zone. Ironically, because of the large movement at night of the warm air parcels relative to the cold ones, transport and diffusion actually increased the magnitude of the vertical temperature gradient. For example, the final night position of parcel "D" is 190 km north of and 1.4 km higher than parcel "G". Relative motion of the two parcels contributed to the gently-sloping (1:330), intense baroclinic zone in this area. But the temperature difference between

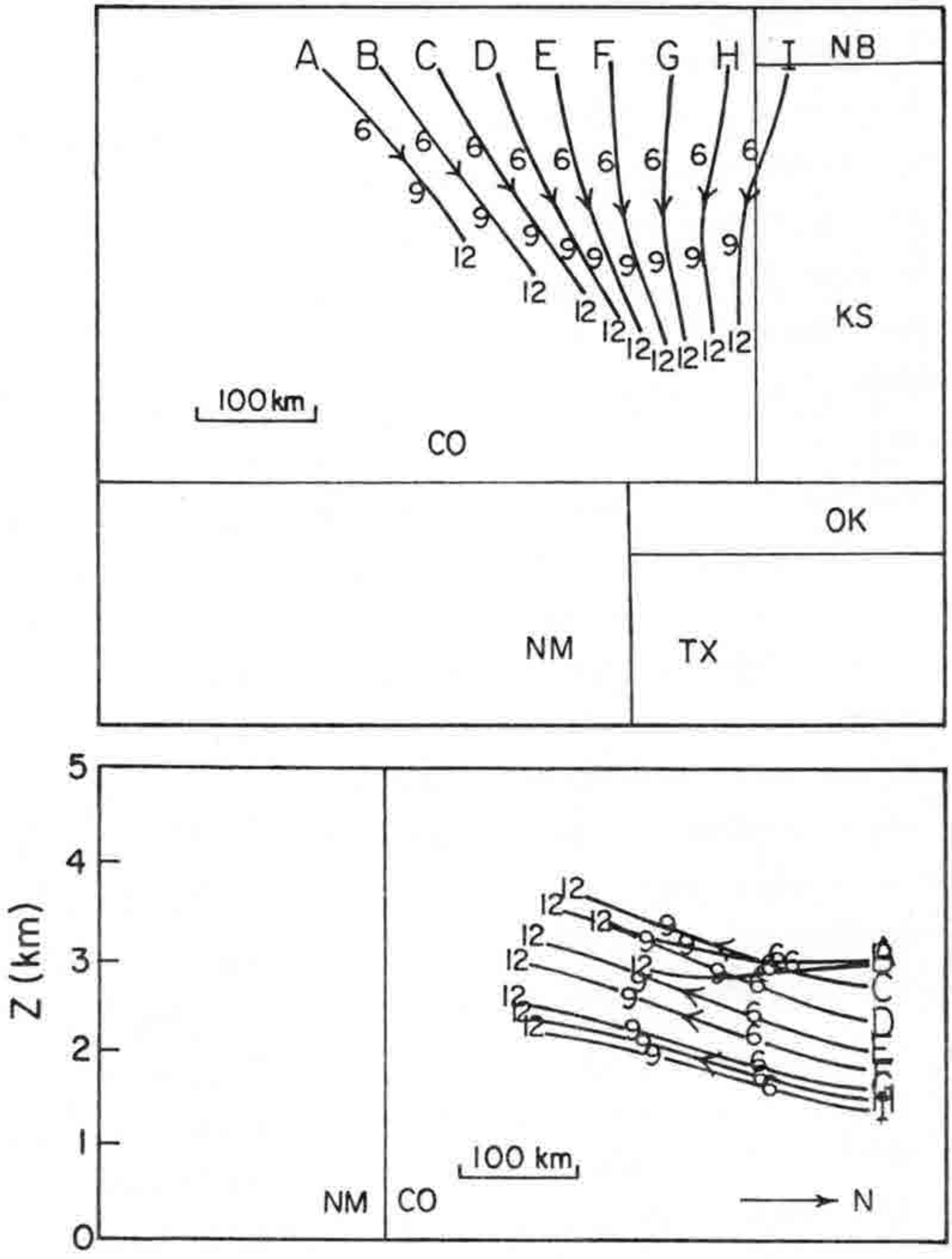

Figure 5.13: Trajectories for the day case (–5°C). Letters indicate initial position of the parcels starting at a point 3 h into the simulation. Positions at later times are labeled at 3 h intervals. In the bottom panel, the positions have been projected onto a vertical plane, viewed from the right side of the top panel.

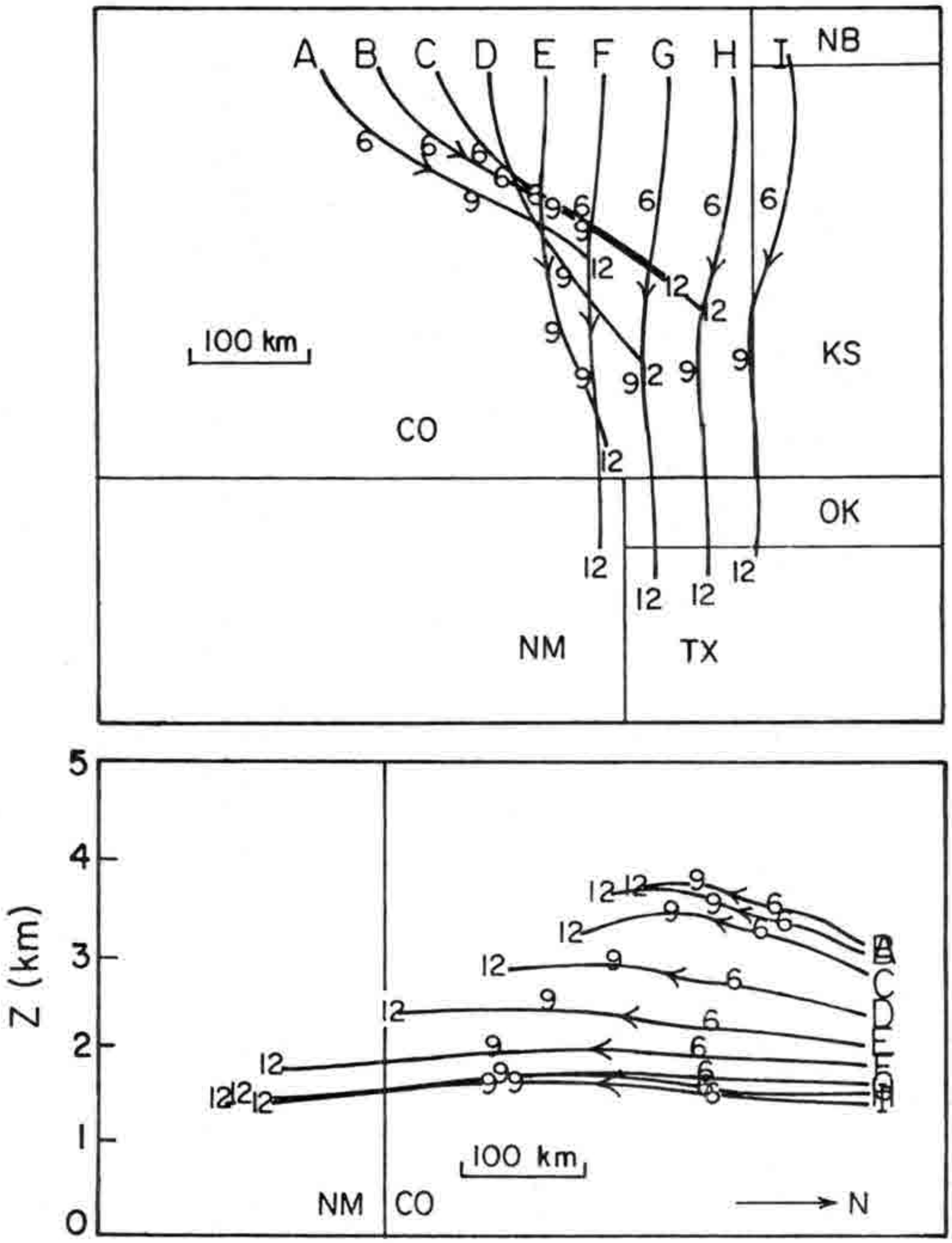

Figure 5.14: Same as Fig. 5.13, but for the night case (2°C).

these two parcels was further enhanced by parcel "D"s earlier proximity to much warmer air (turbulent heat flux that reduced the local mean temperature gradient but warmed "D") and "G"s proximity to even colder air (turbulent heat flux that cooled "G").

The impact of surface heat flux in modifying the horizontal temperature gradient near the surface for the day case is further illustrated using the trajectories shown in Fig. 5.15. In this case, the movement of two sets of parcels near the area of maximum surface

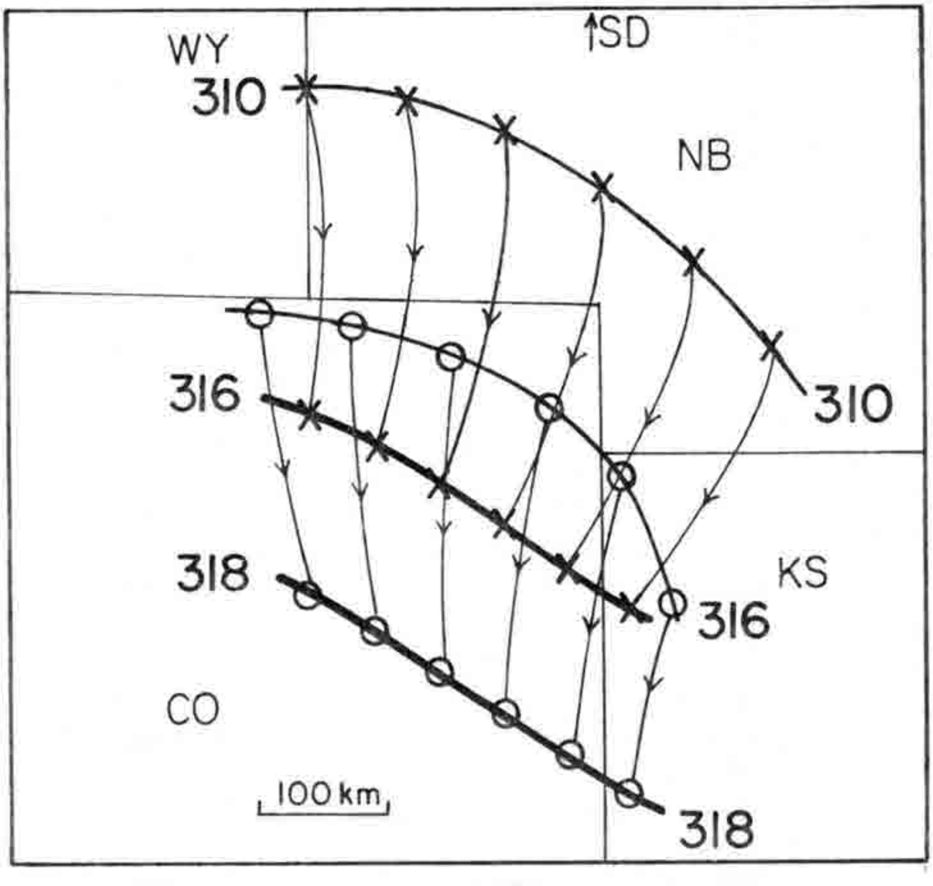

Figure 5.15: Additional trajectories for the day case. Initial positions are near the thin isentropes; final positions are near the thick isentropes.

baroclinicity is examined. The positions of the parcels were evaluated at the end of the nine hour period (the end of the simulation). A set of parcels at the leading edge of the baroclinic zone at this time lies approximately along the 318 K isentrope. Another set of parcels, reaching at the same time points 140 km north of the first ones, lies along the 316 K isentrope. The magnitude of the horizontal temperature gradient in this area was 1.7×10^{-2} °C km^{-1}. Nine hours earlier, the gradient between the two sets of parcels had been 3.6×10^{-2} °C km^{-1}. It can be seen in Fig. 5.15 that there was weak (10^{-5} s^{-1}) horizontal convergence between the two sets of parcels during the period, yet the temperature gradient was reduced by a factor of 2. This was because the northern parcels warmed diabatically 6°C, while the southern ones warmed only 2°C. Surface heat flux was approximately uniform horizontally, yet it was confined initially to a much shallower layer beneath the frontal inversion to the north. Thus the northern parcels became almost as warm as the southern ones. A uniform heat flux resulted in a much more diffuse surface temperature gradient. This process was absent and to some extent reversed at night. Decoupling of the mid-level flow from the surface flow at night also contributed to large differences. The next section contains additional discussion of both diabatic and adiabatic processes contributing to differences between the day and night cases.

5.3.3 Frontogenetical processes

In addition to the southward acceleration of the baroclinic zone, there were also changes in the intensity of the front for the night case. The diabatic and adiabatic contributions to the changes of the temperature gradient for both day and night are discussed in this section. For the y-component of the temperature gradient, the contributions, following the air parcels, are as follows:

$$\frac{D}{Dt}\left(\frac{\partial\theta}{\partial y}\right) = \left(\frac{\partial}{\partial t} + u\frac{\partial}{\partial x} + v\frac{\partial}{\partial y} + w\frac{\partial}{\partial z}\right)\frac{\partial\theta}{\partial y} = \frac{\partial}{\partial y}\left(\frac{D\theta}{Dt}\right) - \frac{\partial v}{\partial y}\frac{\partial\theta}{\partial y} - \frac{\partial u}{\partial y}\frac{\partial\theta}{\partial x} - \frac{\partial w}{\partial y}\frac{\partial\theta}{\partial z}\,.$$

There are similar equations for the x and z components. The first term on the right is the contribution from diabatic effects. For cases when the variables are average quantities, as they are in the model, this includes the effective contribution from turbulent fluxes. In fact, for the simple model runs, where actual diabatic effects have been eliminated, turbulent fluxes are the sole contribution to this term. The second term is the contribution from convergence, acting on the existing y-component of the temperature gradient. The last two terms are tilting (shear) terms acting on the perpendicular components of the temperature gradient.

As previously noted in the observational analysis in Chapter 3, an important process operating during the day in the lower troposphere was the synoptic-scale trough, and its associated shear (Fig. 5.12, top panel), acting on the temperature gradient that was originally oriented northeast-southwest. In the model there was a strong tendency (not shown) for a decrease in the magnitude of the x-component and an increase in the magnitude of the y-component of the temperature gradient near the west-central portion of the PRE-STORM area. This tendency forced upward motion along and ahead of the trough in that area.

The main difference between the day and night cases, however, occurred farther west in eastern Colorado. There was a near-vertical, diffuse baroclinic zone during the day, but it became much more shallow and intense, and propagated farther south at night (Fig. 5.16). Although the nocturnal inversion favors the development of a hydraulic jump or undular bore, this does not appear to be happening in the model. In addition to the lack of resolution in the model, the presence of slight vertical stability above the cold air, and the absence of an opposing jet in the same layer, both inhibit the trapping of wave energy near the surface (Crook, 1987). There were two dominant mechanisms that contributed to the evolution of the nighttime structure of the front. One was confluence in the north-south direction, acting to increase the existing horizontal temperature gradient (Fig. 5.17). This was as true for the case with no surface heat flux, shown in the bottom panel of Fig. 5.16, as it was for the case with downward heat flux. It can be seen in Figs. 5.16 and 5.17 that this process was particularly strong at the surface at night. The second process is not obvious in the cross-section, but was discussed in connection with the trajectory analysis. In the night case, directional shear between the near-surface cold air flow and the warm air flow aloft intensified the vertical temperature gradient. The combination of these two processes contributed to the shallow but intense baroclinic zone at night. They appeared to operate as positive feedbacks, becoming stronger as the baroclinic zone intensified, and as the surface flow became more decoupled from the flow aloft.

Once the difference between day and night becomes established, then the processes described above act to maintain and enhance the difference. But this does not explain why the difference initially develops. For this it is necessary to look back at an earlier time. The first few hours of model integration included a period of adjustment, yet it was

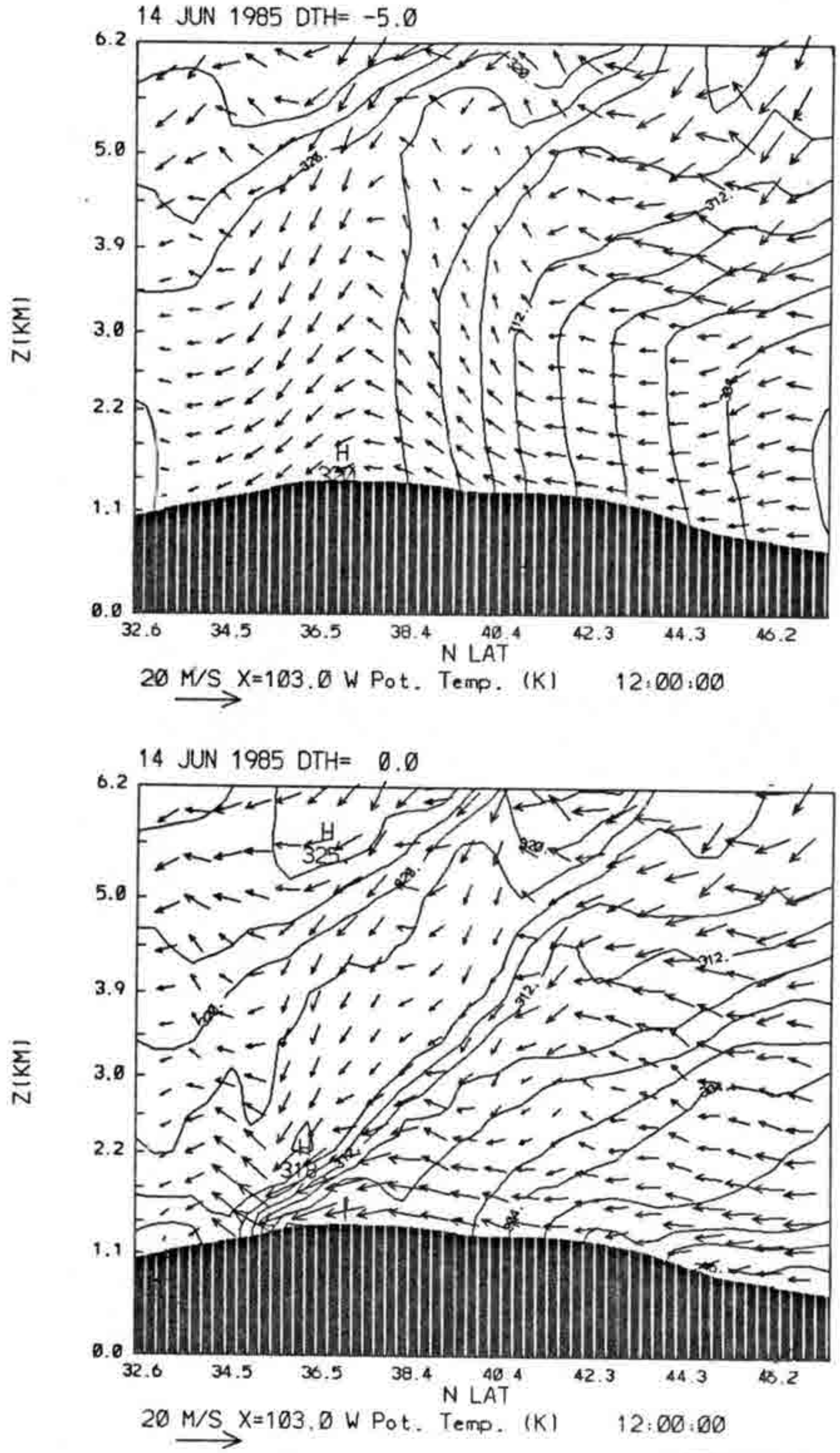

Figure 5.16: North- south cross-sections through eastern Colorado. The vertical plane lies approximately along the path of parcels "F" and "G" in Figs. 5.13/14. The top panel is for the day case; the bottom one is for the night case.

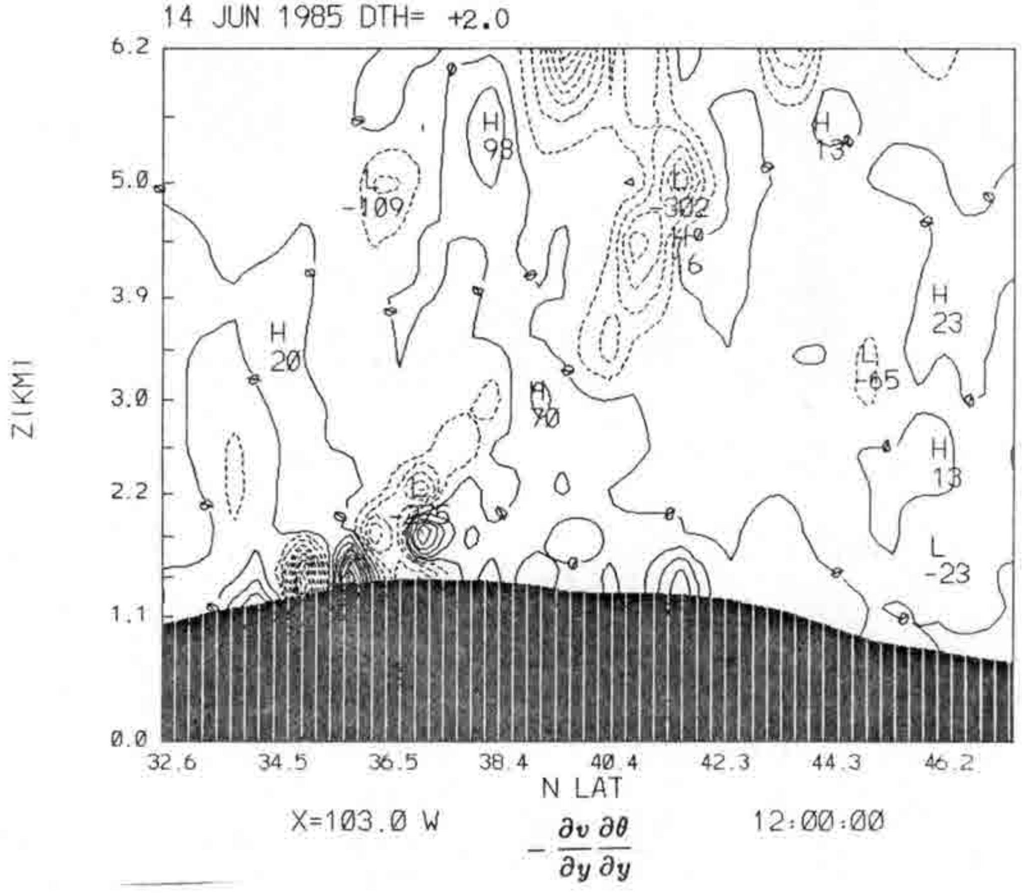

Figure 5.17: The convergence term, at the end of the simulation, contributing to changes in the north-south component of the temperature gradient. Contour interval is 1.8 X 10^{-3} °C km^{-1} h^{-1}.

the surface fluxes during this period that generated slightly different conditions favorable for the subsequent development of large differences between the day and night cases. Thus the key to understanding the differences between day and night lies in the developments early in the model integration.

After two hours of integration, the differences at 1.8 km (Fig. 5.18) were limited to

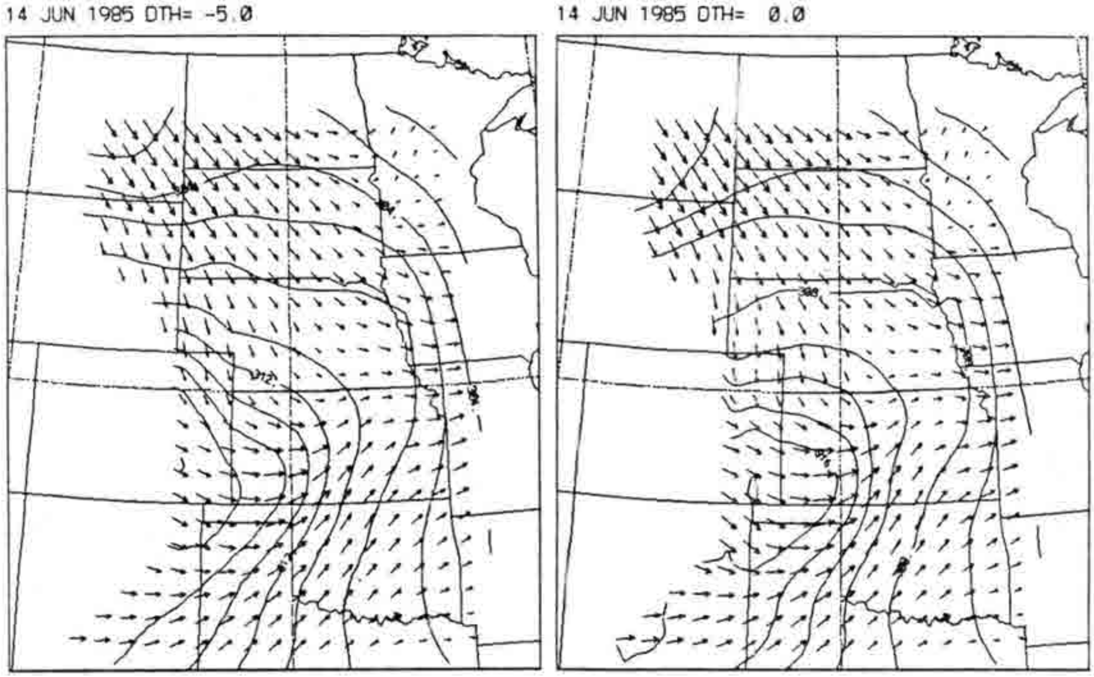

Figure 5.18: Same as Fig. 5.12, but after only 2 h of the simulation.

the extreme western portion, where the 1.8 km surface intersected the ground. North-south cross-sections at this time (Fig. 5.19) illustrate that significant differences in the isentropes are confined to a layer within 1200 m of the surface. The impact of a surface heat flux of 170 W m^{-2} (from Fig. 5.1, with a mean wind speed of 6 m s^{-1}) over a period of 2 h, assuming an average air density of 1 kg m^{-3}, would be to warm this layer by an average of 1.0°C or, equivalently, by 2.0°C at the surface decreasing to no warming at the top of the layer. The actual temperature differences between the day and night cases are slightly larger than this, particularly near the leading edge of the baroclinic zone, where the layer-average temperature difference is close to 2.0°C. Thus, a neutral layer developed within the baroclinic zone that was deeper than would result simply from local heat flux at the surface.

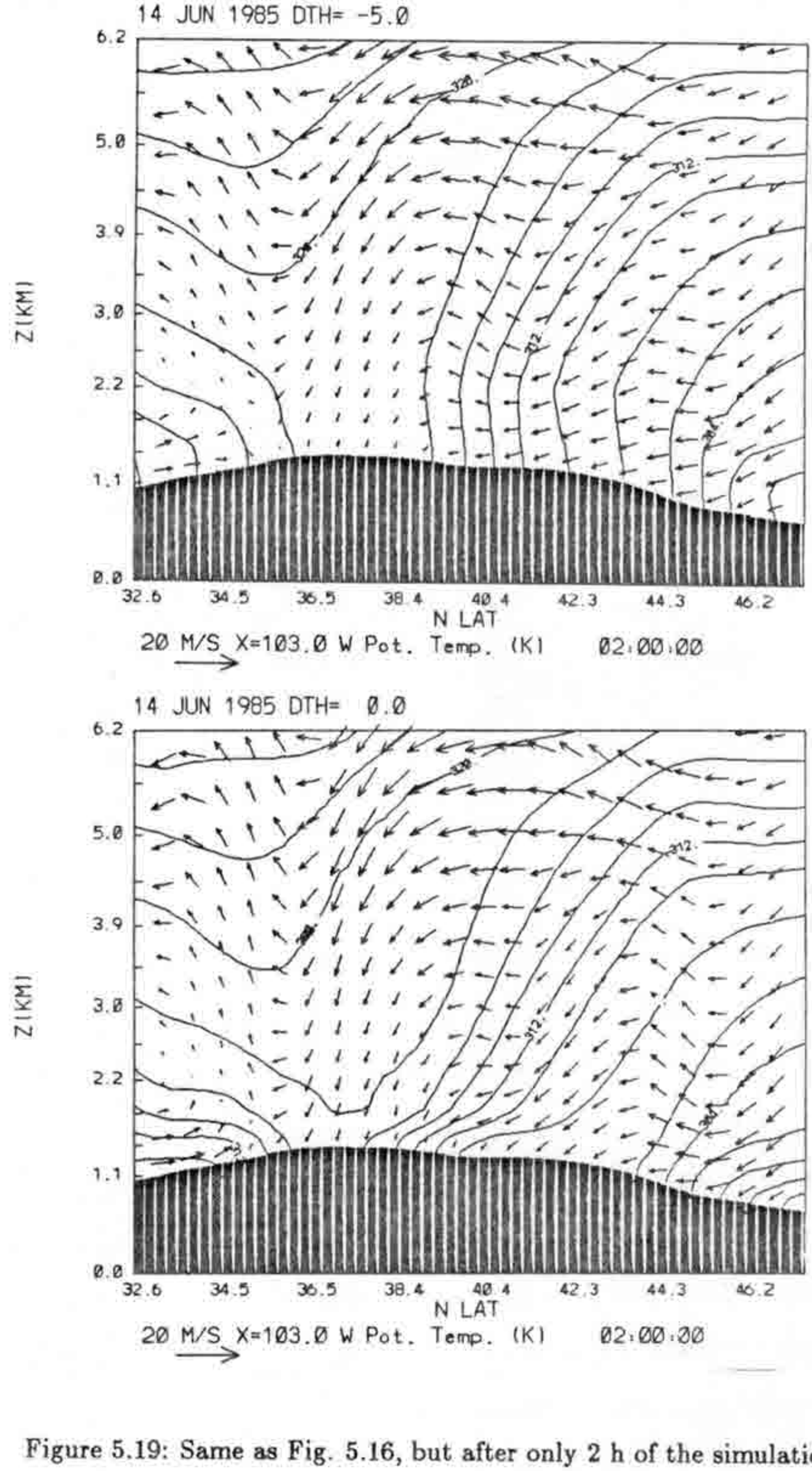

Figure 5.19: Same as Fig. 5.16, but after only 2 h of the simulation.

A possible explanation for this discrepancy is that adiabatic, mean-flow processes also acted to significantly decrease the vertical temperature gradient in this area for the day case. Analogous to the equation for the change in the y-component of the temperature gradient, the equation for the z-component is:

$$\frac{D}{Dt}\left(\frac{\partial\theta}{\partial z}\right) = \left(\frac{\partial}{\partial t} + u\frac{\partial}{\partial x} + v\frac{\partial}{\partial y} + w\frac{\partial}{\partial z}\right)\frac{\partial\theta}{\partial z} = \frac{\partial}{\partial z}\left(\frac{D\theta}{Dt}\right) - \frac{\partial u}{\partial z}\frac{\partial\theta}{\partial x} - \frac{\partial v}{\partial z}\frac{\partial\theta}{\partial y} - \frac{\partial w}{\partial z}\frac{\partial\theta}{\partial z}\,.$$

The three adiabatic terms are analyzed in Fig. 5.20. The dominant term, by two orders of magnitude, is vertical divergence. At this time, above the surface baroclinic zone, vertical divergence within the 2.0–3.0 km layer was reducing the stability there. An alternative description of this process is that, at mid-levels, rising motion on the warm side of the front and sinking motion on the cold side resulted in a propagation of the mid-level front beyond where it would move due to cold advection alone. A more rapid movement of the front at mid-levels than at the surface resulted in decreasing stability at the leading edge. The baroclinic zone in this layer did advance south through the day, as can be seen by comparing Fig. 5.17 with Fig. 5.15. This contributed to the development of a deep neutral layer by the end of the day. But it does not explain the additional warming near the surface during the first two hours.

The magnitude of the two tilting terms (bottom two panels of Fig. 5.18) is much smaller than the convergence term. There is partial cancellation between them at the leading edge of the baroclinic zone, and they are small in comparison to diabatic effects. The only possible explanation for the additional local warming appearing in the daytime cross-section is that there was advection of warm air heated over the higher terrain to the west. The horizontal advection terms contributing to the local change at the surface are

$$\frac{\partial}{\partial t}\left(\frac{\partial\theta}{\partial z}\right) = \frac{D}{Dt}\left(\frac{\partial\theta}{\partial z}\right) - u\frac{\partial}{\partial x}\left(\frac{\partial\theta}{\partial z}\right) - v\frac{\partial}{\partial y}\left(\frac{\partial\theta}{\partial z}\right)\,.$$

In fact near the surface, north-south advection was negligible, but eastward advection of warmer air (Fig. 5.21) was an important contributor to the erosion of the front by surface heating. Unlike the vertical divergence term, which becomes weaker with smaller temperature gradients and thus is maximized above the boundary layer, the advection

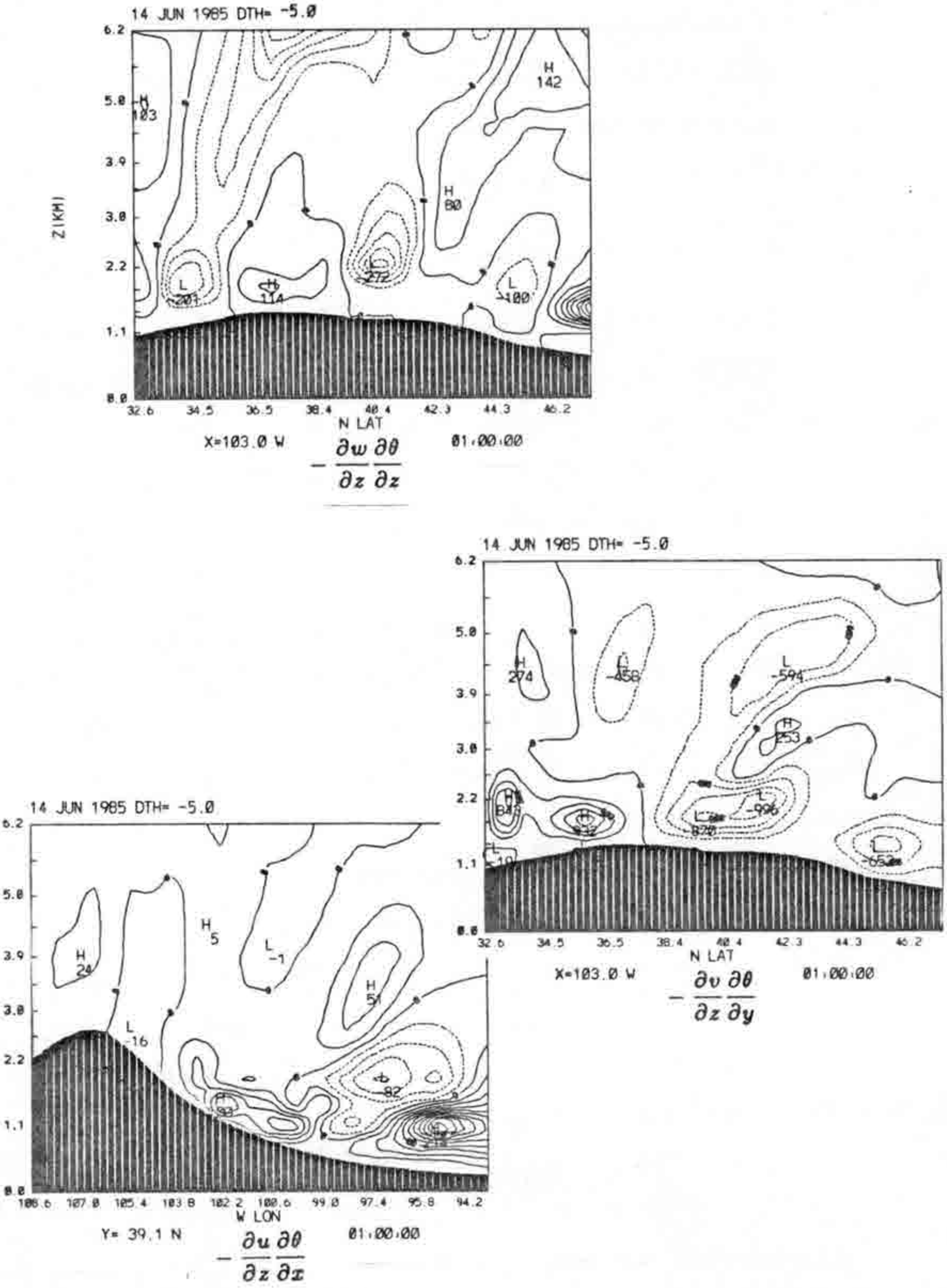

Figure 5.20: Adiabatic terms, near the surface baroclinic zone, after 2h, contributing to changes in the vertical component of the potential temperature gradient. The contour interval in the top panel (convergence term) is 0.02°C m^{-1} h^{-1}. The interval for the bottom two panels (tilting terms) is 7.2×10^{-5} °C m^{-1} h^{-1}.

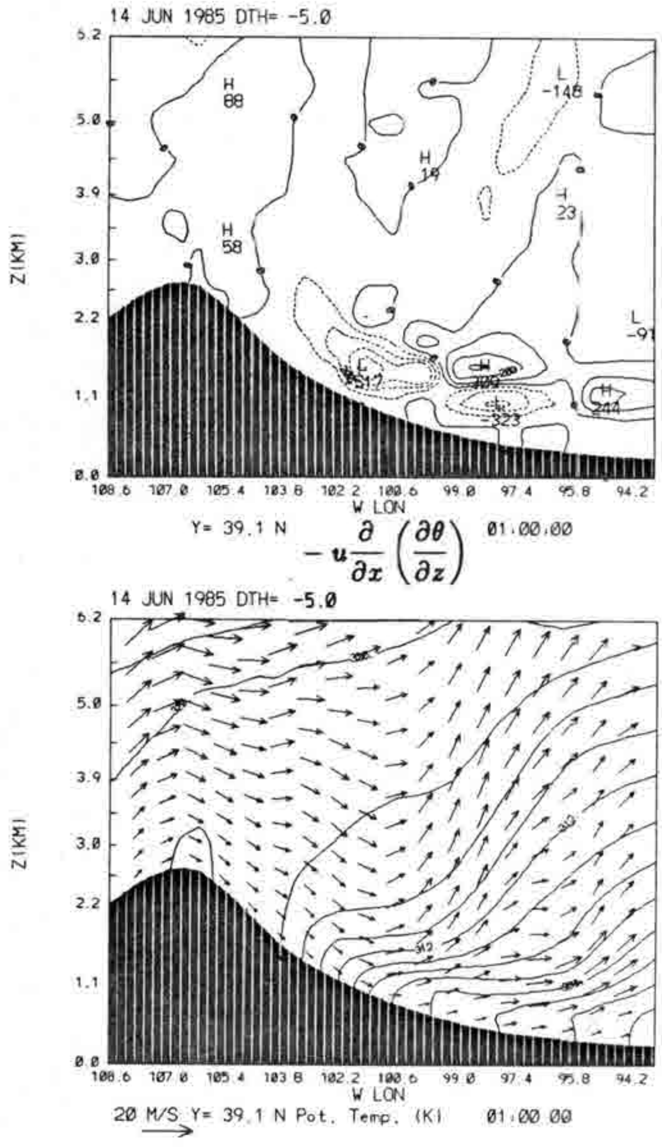

Figure 5.21: Eastward advection of vertical stability (top) corresponding to the westerly component of the flow in the cross-section at the bottom of the figure. The east-west cross-section is near the surface front. Contour interval for the advection term is 3.6×10^{-4} °C m^{-1} h^{-1}.

term was strongest at the sloping top of the boundary layer (Fig. 5.21, bottom panel). At its maximum, this term is equivalent to a decrease in stability of $2°C\ km^{-1}\ h^{-1}$. More simply, this term represents the fact that the boundary layer deepened partly because a portion of it was being advected from the higher terrain to the west.

As was the case for the processes contributing to the development of an intense baroclinic zone at night, the warming associated with this daytime advection pattern could be interpreted as a positive feedback process. A deep neutral layer is required in order for northwesterly flow heated diabatically over higher terrain to sink and warm adiabatically while flowing to the southeast, contributing to an erosion of the surface baroclinic zone. Warming at the surface reduces the stability, contributing to the development of a deep boundary layer and further warming.

5.4 Summary

Since the warm–surface simulation reproduced the observed 14 June 1985 baroclinic zone just as well as the simulation with radiation physics and a surface energy budget, the slowing of cold fronts east of the Continental Divide can be attributed simply to a uniform upward surface heat flux. But there are complex interactions since the surface flow over higher terrain may become coupled to the surface flow at lower elevations; the slowing is not due simply to a "burn–off" of the leading edge of the cold air. It appears that in some cases the propagation of a surface front might be very sensitive to small changes in the thermal and flow patterns aloft. The contributing processes are explored further in the next chapter using even more idealized situations.

Chapter 6

IDEALIZED MODEL SIMULATIONS

In this chapter, the basic physical mechanisms that affect the movement of shallow cold surges near a mountain range are investigated further using highly idealized situations. The mechanisms are discussed in the two broad categories of terrain heating and of terrain blocking. Terrain heating will be considered first separately, and then the development of blocking without heating will be contrasted with the heating effects. Although heating alone could be considered two-dimensionally, the blocking mechanisms are inherently three-dimensional. In order to compare the two effects, numerical experiments for both mechanisms remain three-dimensional. The topography is, however, simplified to two-dimensions and is illustrated in Fig. 6.1.

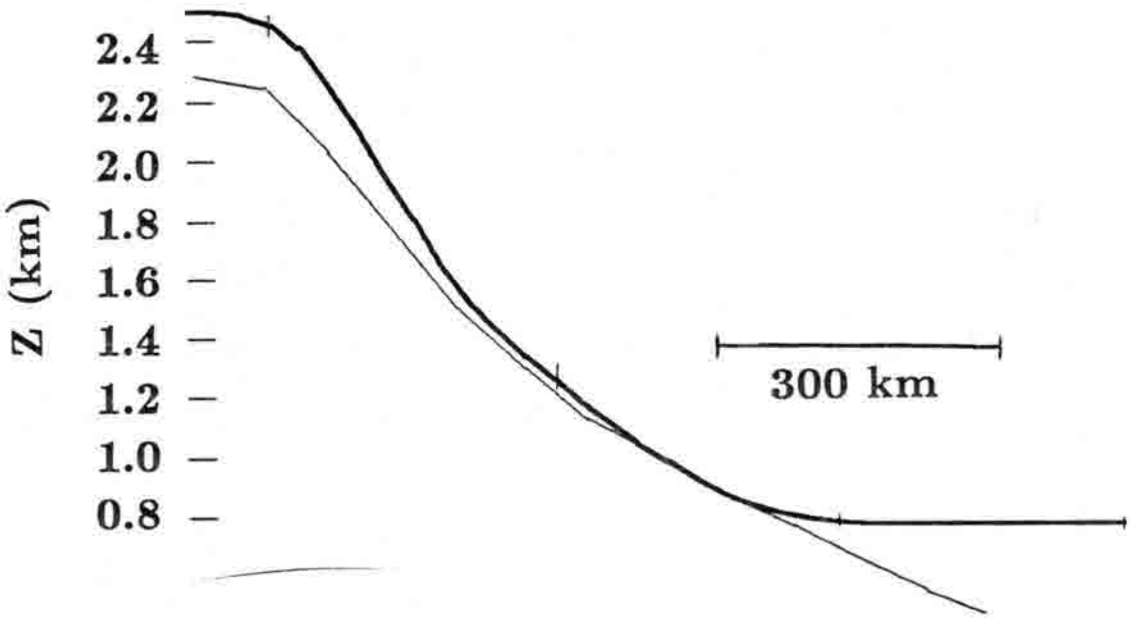

Figure 6.1: Idealized topography used for the simulations in this chapter (thick line) and smoothed topography for an actual cross-section through Colorado (thin line).

6.1 Role of surface heat flux

Initial conditions with horizontal isentropes shown in Fig. 6.2 were used to examine the model flow that develops solely in response to surface heating. The packing of the isentropes over the lower elevations was chosen to simulate the presence of a purely horizontal frontal inversion. Alternatively, this could be interpreted as the western edge of

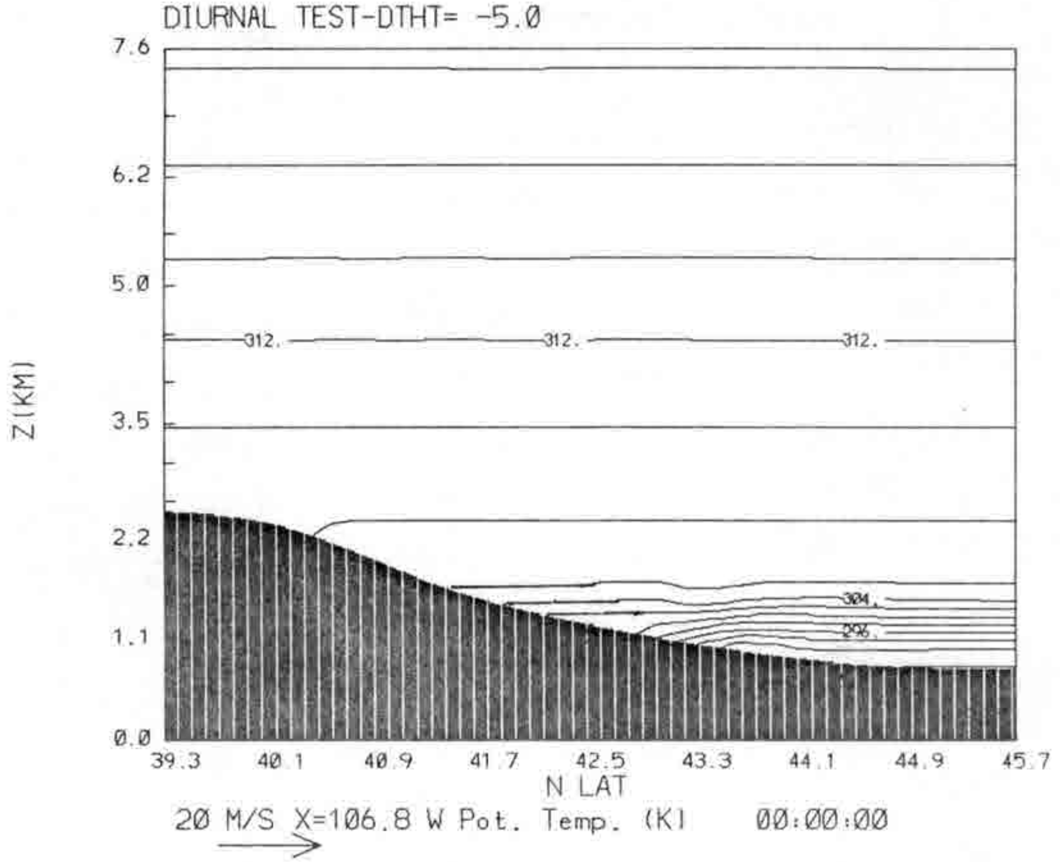

Figure 6.2: Initial temperature structure used for heating experiment. Isentropes are at 2 K intervals.

a capping inversion. Surface heat flux depended on a specified temperature difference of -5°C. This is identical to the idealized simulation of the 14 June 1985 case described in the previous chapter. For this simulation only, the mountain range was oriented east-west, with upslope to the south. Except for small variations in the Coriolis force, the results for a north-south mountain range would be identical. Other model specifics are listed in Table 2.

Table 2

Horizontal Domain	960×780 km; centered at 43°N latitude
Horizontal Grid Size; Spacing	33×27; 30 km
Timestep	Long 30 s, Short 10 s
Integration Time	12 h
Lateral Boundaries	Klemp–Lilly radiation
Top Boundary	Prognostic surface pressure; upward integration of hydrostatic equation

The surface flow after 12 h is shown in Fig. 6.3. Maximum wind speeds are 3 m s^{-1}. The winds rotated but, because of friction, never quite attained a geostrophic balance. An interesting feature is the left-right gradient of warming at the top-left corner of the figure. This is obviously a non-physical effect introduced by the boundary condition, and it is encouraging that this effect appears to be very minor.

The evolution of the isentropes is shown in Fig. 6.4. Total heating ($\sim$ 120 W m^{-2}) during the period resulted in a warming of 2°C over a depth of 2.5 km above the higher terrain. Over the lower terrain to the north, beneath the frontal inversion, the same amount of heating was distributed over a much shallower layer, and naturally resulted in much greater warming there. The result is a diffuse horizontal temperature gradient within the boundary layer, similar to the surface frontal zone late on the afternoon of 14 June 1985.

As the air expanded due to heating, pressure perturbations developed which were maximized at the top of the boundary layer (Fig. 6.5). After a circulation developed and mass was redistributed horizontally, a *surface* (vs. *horizontal*) perturbation pressure gradient developed. In Fig. 6.5, the surface gradient amounts to 100 Pa across the model domain. But it is the *horizontal* gradient which drives the circulation, and this

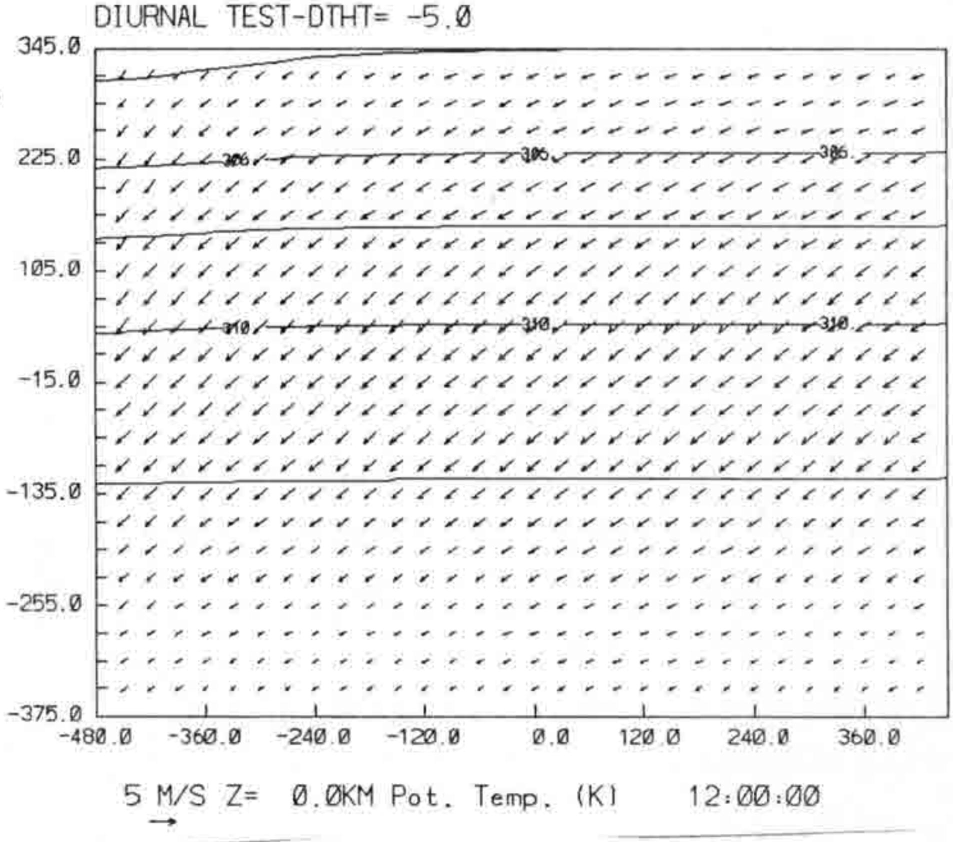

Figure 6.3: Surface flow after 12 h with surface heating alone. Isentrope interval 2 K.

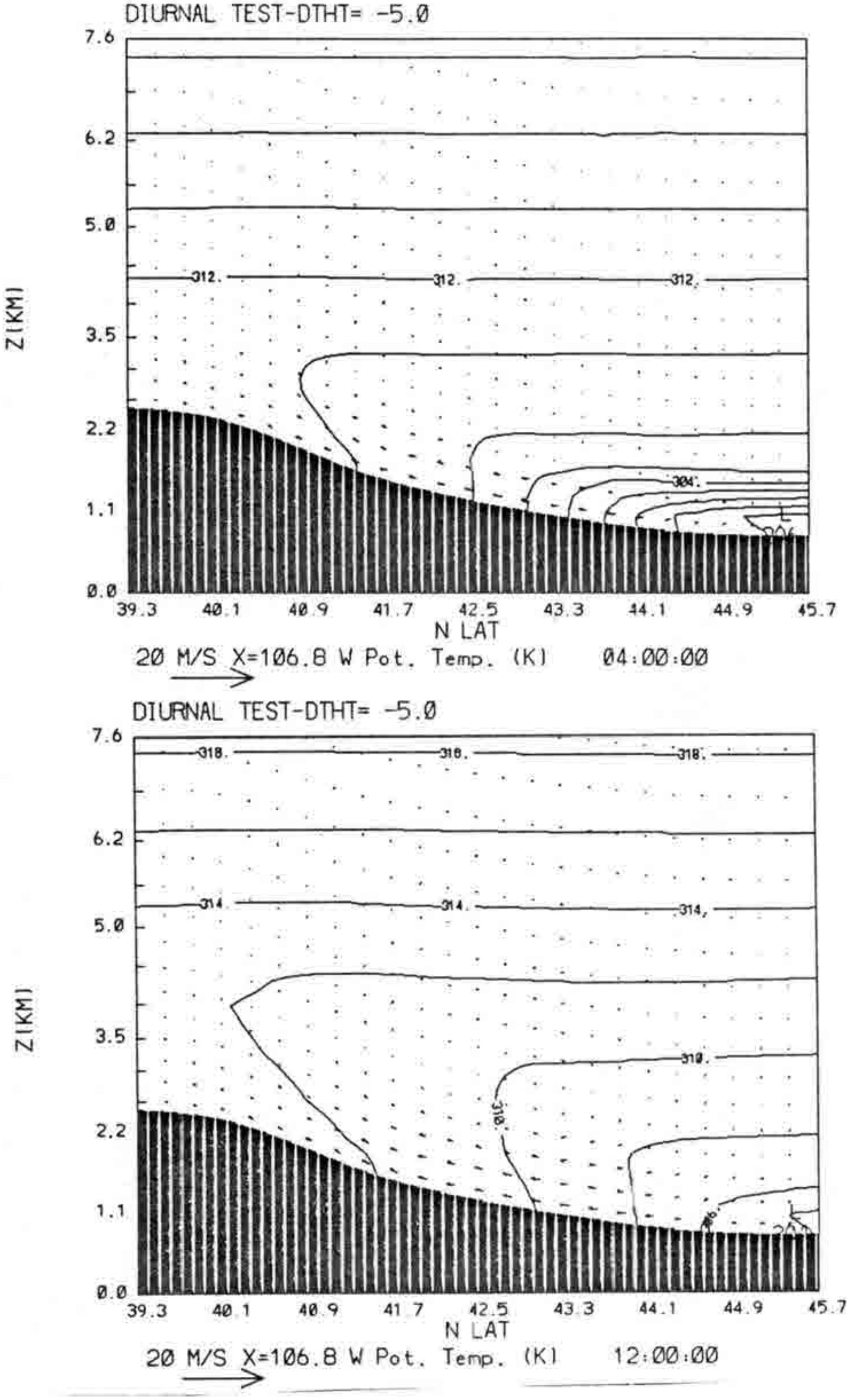

Figure 6.4: North-south isentropic cross-sections after 4 h (top panel) and after 12 h (bottom panel). Contour interval 2 K.

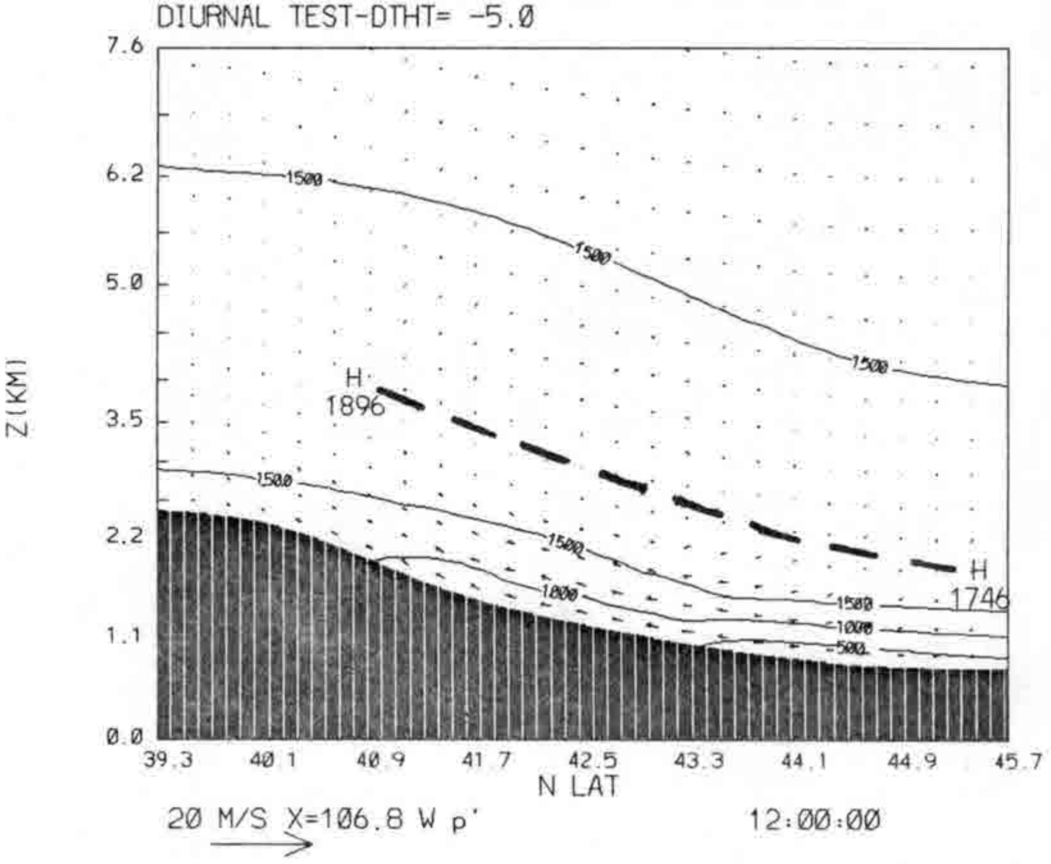

Figure 6.5: Contours (50 Pa interval) of pressure perturbation after 12 h. The thick dashed line indicates the axis of maximum perturbation.

exists because the isobars of perturbation pressure slope along with the terrain. In fact, if a circulation did not develop, the perturbation pressure along the top of the sloping boundary layer would be approximately constant. That this is true in spite of variable depth can be seen by considering the change in pressure at the top of the boundary layer due to hydrostatic expansion of the air below, $\Delta p = -\Delta \bar{\rho} g z_i$. Since the temperature change, and resulting density change, is inversely proportional to z_i, Δp is approximately constant. This provides a useful interpretation for the forcing of circulations by uniform heating around either sloping terrain or sloping frontal zones, or a combination of both. This point will be discussed more in the following section.

Finally, the evolution of the mountain-parallel component of the wind is shown in Fig. 6.6. After 12 h, the flow out of the page above the boundary layer is in approximate geostrophic balance with the pressure gradient there (Fig. 6.5). This was not the case at the surface. Near the middle of the figure close to the ground, the 2.2 m s^{-1} flow into the page is only two-thirds of its geostrophic value. Friction is important here, so the balance is not geostrophic. Even if the surface flow that developed in response to the heating of higher terrain were geostrophic, it alone could not account for the difference between the day and night model simulations presented in Chapter 5, and likely neither for the large observed diurnal variation in the mountain–parallel speed of cold fronts along the Colorado Front Range.

The above results are consistent with previous composite observational results and with other numerical studies. They show that this version of the model is capable of simulating the effects of surface heating in a physically realistic way. The blocking effects of the model topography will now be examined.

6.2 Impact of terrain blocking

Shallow cold surges may be generated, or at least enhanced, by the outflow from a mesoscale convective system, as was demonstrated in Chapter 4. To explore the role of terrain blocking, an idealized outflow propagating from the northeast quadrant of the model domain was generated. Points within a circle of 390 km radius centered at model

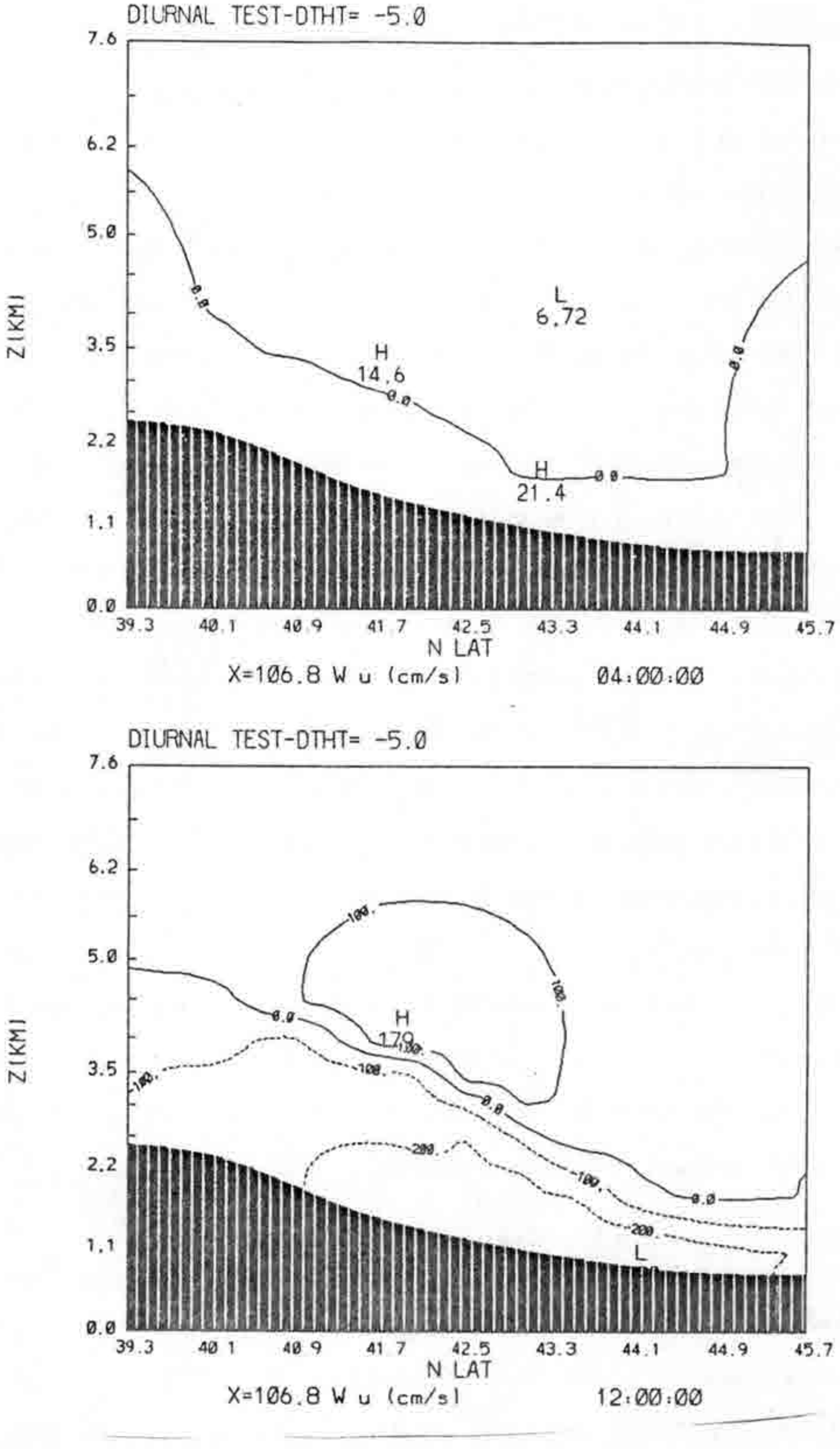

Figure 6.6: Mountain-parallel component of the wind (1 m s^{-1} interval) after 4 h (top panel) and after 12 h (bottom panel).

coordinates (75., 405.) km were cooled by 5.0°C through a depth of 3.0 km above the ground. Prior to the cooling, the model was initialized horizontally homogeneous using the 1200 UTC 1 August 1986 North Platte temperature sounding (Chap 4). In contrast to the simulation in the previous section, the terrain now slopes up to the west, the domain is square (33 × 33), and the Klemp-Durran (1983) radiation condition has been used for the top boundary.

The magnitude and depth of the cooling created an approximate 450 Pa surface pressure near-discontinuity at the quarter-circle edge of the cold air, resulting in strong outflow there (Fig. 6.7). Cold air flowed both upslope to the west and level to the south. At this early time, the outflow extended only over a 200 km zone near the leading edge of the cold air, but already a return flow with subsidence warming aloft had started (Fig. 6.8). The warming gradually destroyed the cold pool. For this reason, the simulations were ended at 9 h. The decay of the cold pool is realistic for a dissipating convective system, but not for a mature convective system nor for a synoptic-scale front. Nevertheless, the extent and duration of the hypothetical cold surge are sufficient to illustrate the large-scale interaction with terrain.

In the remainder of this section, later developments will be contrasted for an outflow without surface heating and for one with heating. Heating was generated by specifying a surface temperature difference of 5.0°C, the same as in the previous section. Since there is a slight dependence of heat flux on wind speed (Fig. 5.1), the heat flux initially approached 200 W m^{-2} near the leading edge of the cold surge. For other locations and times, the heat flux was approximately 120-150 W m^{-2}.

After 9 h, a tendency for cold air damming appeared in the no-heating case, but was absent for the heating case (Fig. 6.9). In addition to the overall warming and more diffuse baroclinic zone for the heating case in the bottom panel of Fig. 6.9, the southward ridging of the isentropes and northerly component of the flow did not develop. There is also a corresponding absence of a southward ridging of high pressure (Fig. 6.10). In both the heating and the no heating cases, the surface flow was approaching geostrophic balance by this time. But in the no heating case, a portion of the flow has a northerly component

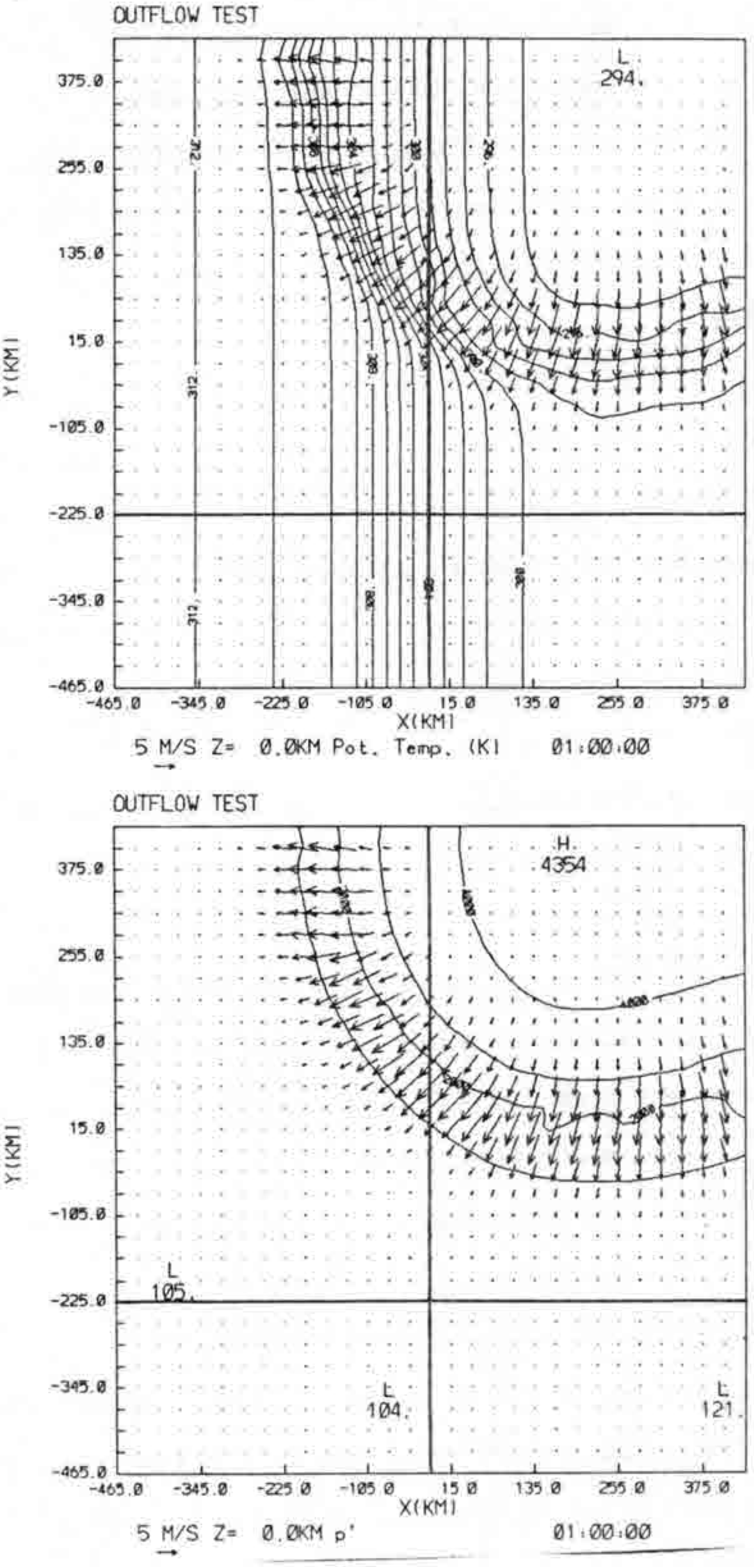

Figure 6.7: Surface outflow 1 h after the initial conditions described in the text. Surface potential temperature (1 K interval) is analyzed in the top panel, and surface pressure perturbation (100 Pa interval) in the bottom one. The no-heating case is shown. Vertical and horizontal lines indicate location of cross-sections shown later.

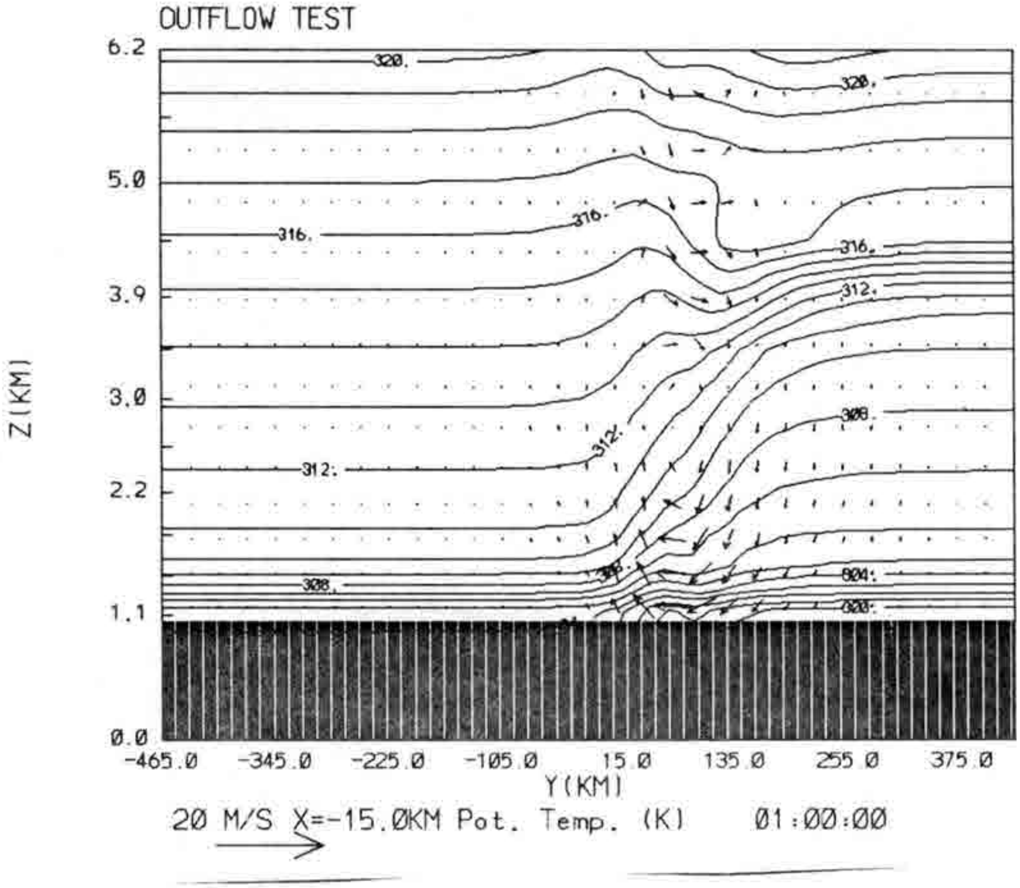

Figure 6.8: North south cross-section with isentropic analysis (2 K interval) after 1 h. Location of the section is shown in the previous Figure.

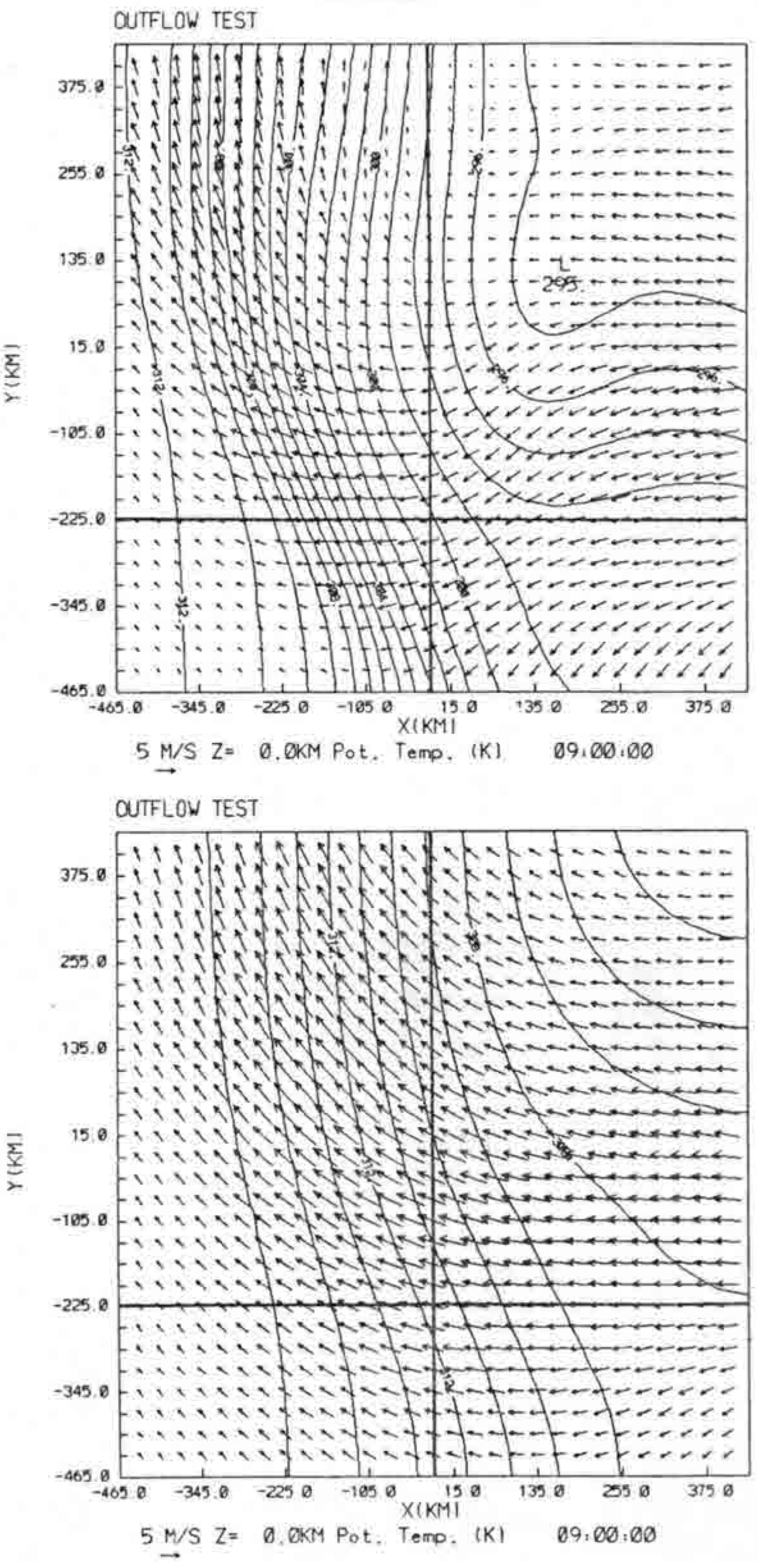

Figure 6.9: Surface isentropes, same as the top panel of Fig. 6.7, but after 9 h for the no-heating case (top) and heating case (bottom). Location of east-west cross section is indicated.

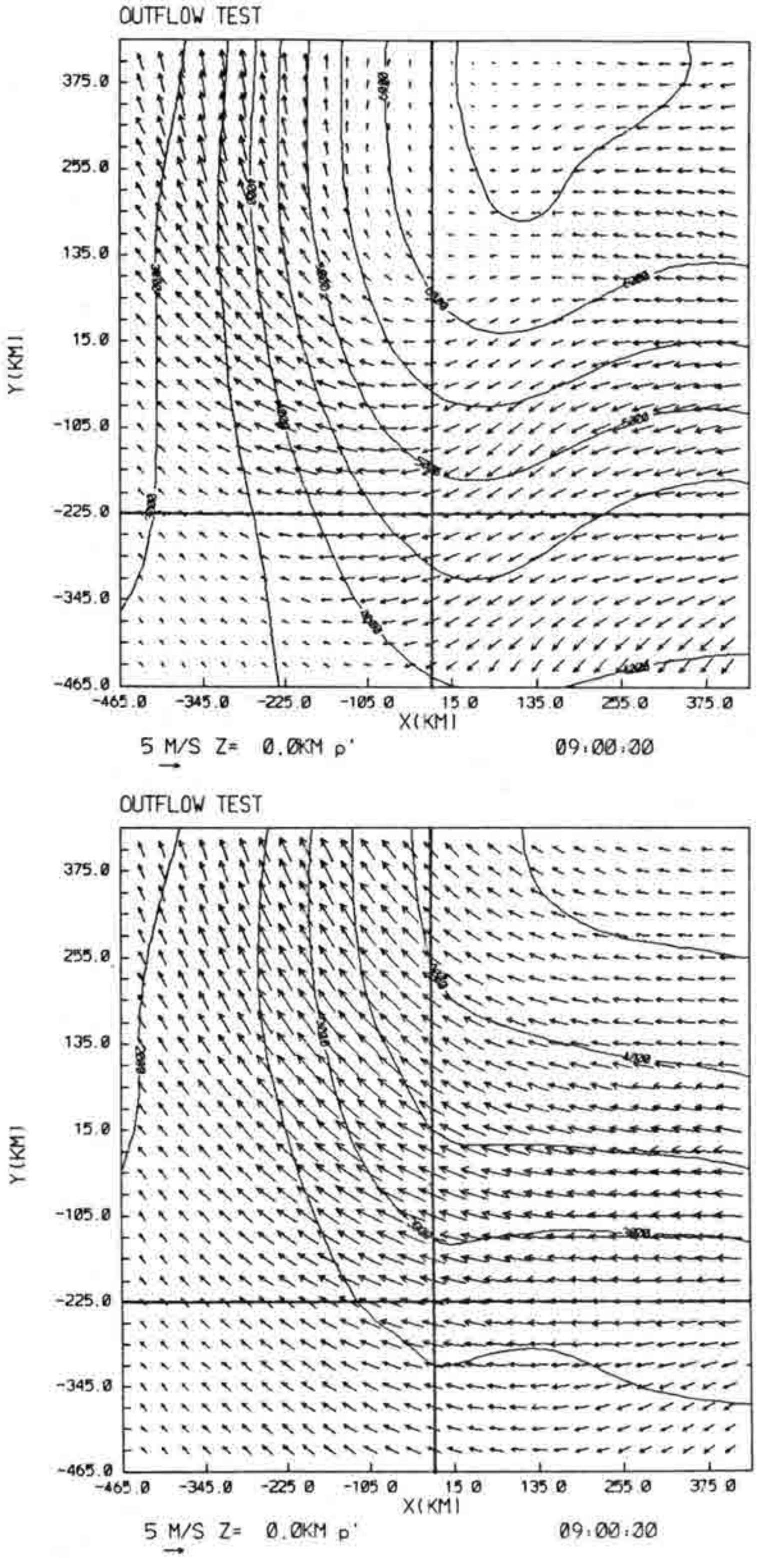

Figure 6.10: Same as 6.9, but for pressure perturbation (interval 50 Pa).

that is advecting cold air southward. The cold advection maintains the southward pressure ridging, and this in turn supports continued northerly flow.

This process is better seen in analyses for an east-west cross-section shown in Figs. 6.11-6.13. The section lies near the leading edge of the area of increasing northerly flow in the no heating case. An upslope advection of cold air exists for both the heating and the no heating cases as shown in Fig. 6.11. Without heating, the cold air begins to pile-up against the mountain, developing a slight but significant upslope tilt in the isentropes. This results in a maximum perturbation pressure at the surface near the middle of the cross section (top panel of Fig. 6.12). Thus the easterly component of surface flow approaching that area was being decelerated. In contrast, because of the strong warming at the leading edge of the cold air in the heating case, there is at the surface a westward pressure gradient force across the entire section (bottom panel of Fig. 6.12). The significance of this difference in pressure gradient is that a surface northerly flow was established in the no heating case that did not develop with heating (Fig. 6.13). The difference amounts to only 2 m s^{-1} at this point, but at a point 120 km farther north the difference is 6 m s^{-1} (Fig. 6.10).

This difference in cold air damming develops in an area where the model terrain slope is relatively small (1:300), yet this slope is representative of the plains east of the Colorado Front Range. It appears that the cold air need not reach the steep slope of the Continental Divide in order for damming effects to be important. But in many cases the cold air does strike the near-vertical wall of the Front Range, and there is a continued supply of cold air from the north. It is easy to see that the tendency for surface heating to inhibit the development of cold air damming during the day could account for a rapid acceleration of cold air to the south at night, especially when there is an existing northerly component of the geostrophic wind above the cold air.

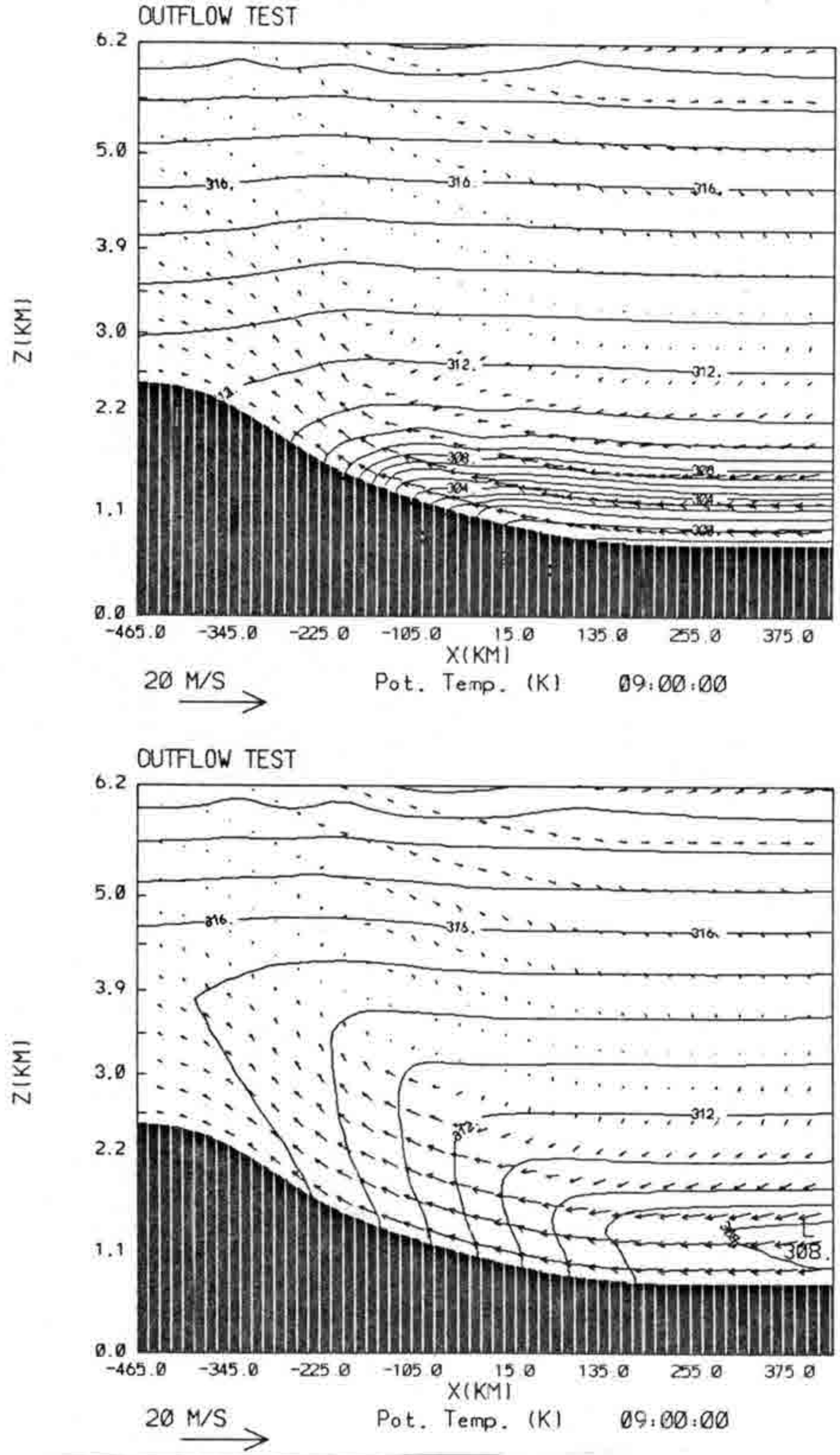

Figure 6.11: East-west cross section (location indicated in the previous two Figures) with isentropic analyses (1 K interval) for the no heating case (top panel) and for the heating case (bottom panel).

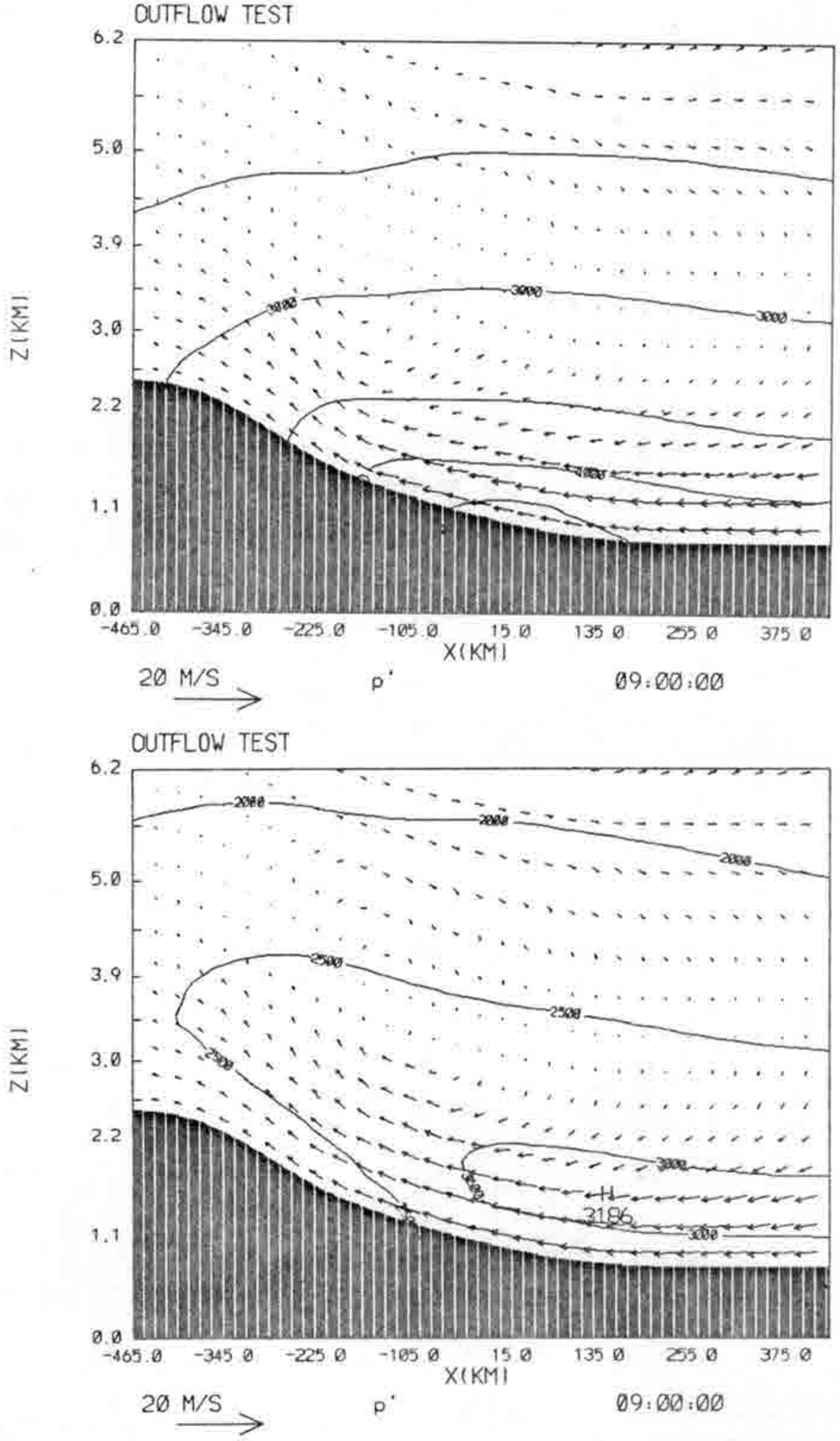

Figure 6.12: Same as Fig. 6.11, but with pressure perturbation analyzed (50 Pa interval).

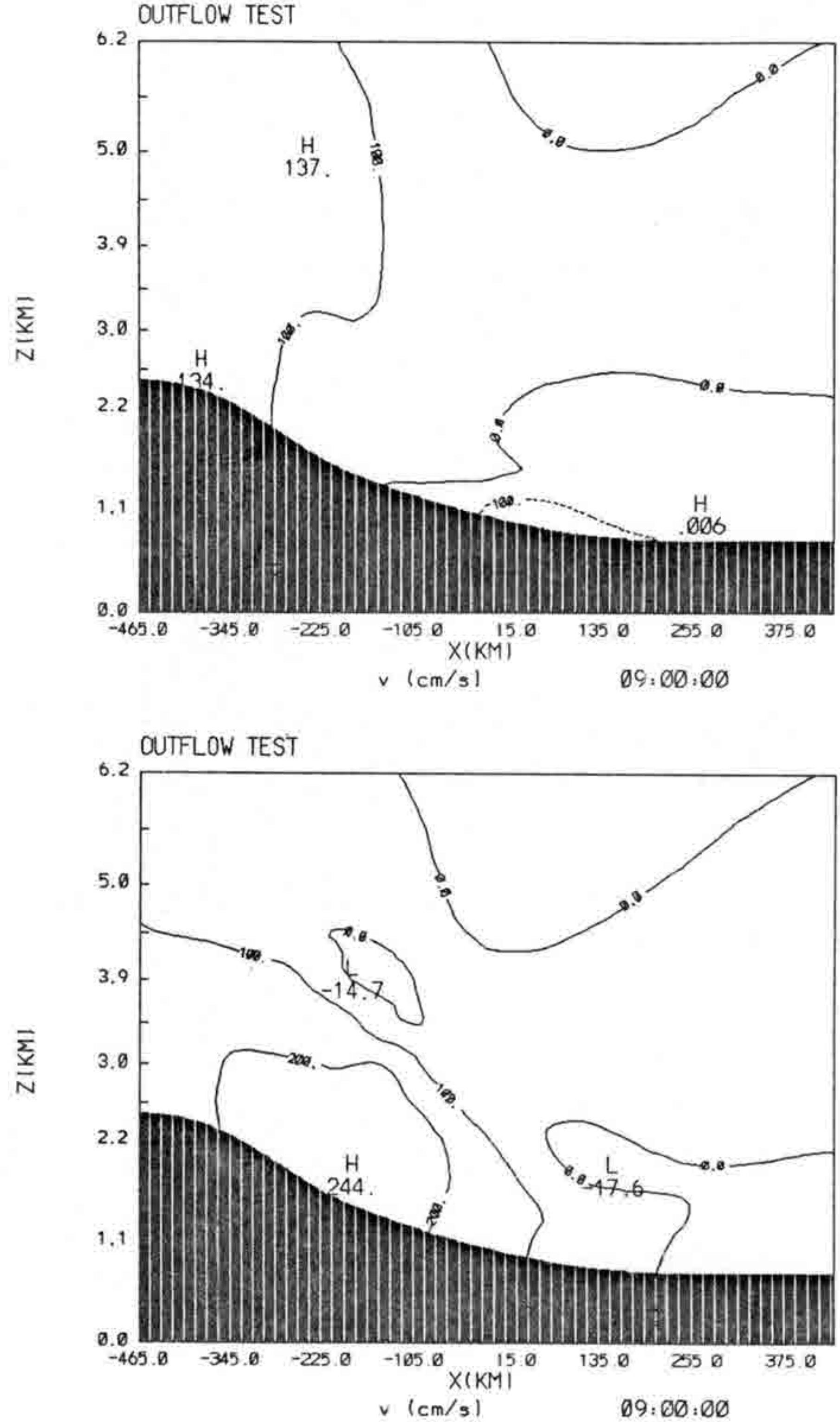

Figure 6.13: Same as Fig. 6.11, but with the wind component perpendicular to the cross section analyzed (1 m s^{-1} interval). Southerly flow is positive.

Chapter 7

CONCEPTUAL MODELS OF THE INTERACTION OF COLD SURGES WITH TOPOGRAPHY

With or without the impact of variable topography, the flow in a cold surge ultimately depends on the horizontal pressure gradients. Knowing the relationship of the pressure field to the flow for simple, idealized cases provides a starting point for understanding the accelerations and adjustments in more complex situations. The exact, steady-state, linear solution for the Gill model of flow in a channel (Chap. 2) can be easily extended to account for the effects of friction. Consider shallow, stably-stratified air flowing steadily and uniformly parallel to a mountain ridge, with the mountain to the right of the flow. Only one pressure field is consistent with that flow (Fig. 7.1a). Friction requires cross-isobar flow even over flat terrain, so as an addition to the geostrophic solution, there is a component of the pressure gradient force in the direction of the flow, balancing the frictional force in the boundary layer. The mountain ridge alone does not change either the frictional force (except for horizontal diffusion within, perhaps, 1 km of the side of the mountain) or the Coriolis force. Explanations for cold-air damming (Emanuel, 1984; Mass and Albright, 1987) often state that geostrophic balance cannot be maintained near a mountain. In some cases it is not made clear that this is true only for the mountain-perpendicular component of the flow. The mountain-parallel flow can be, as shown in Fig. 7.1a, close to geostrophic. To the extent that diversion of the cold air results in a front approximately parallel to the mountains, the steady mountain-parallel flow on the cold side of the front should be no more ageostrophic than the steady flow on the cold side of a front over flat terrain.

There are, of course, inertial effects due to variations in the direction or speed of the flow, as well as transient effects and variability in boundary layer friction, all of which can produce highly ageostrophic flow even over flat terrain. Obviously, diversion of the flow near a mountain range creates strong inertial effects, and these are likely important during the initiation of cold air damming. But a steady-state flow in gradient wind balance might still be established after several hours of mountain-parallel flow. Even transient effects should result in an adjustment over a period of several hours by a rearrangement of the cold air mass. For example, assume that the surface pressure gradient in Fig. 7.1a was due

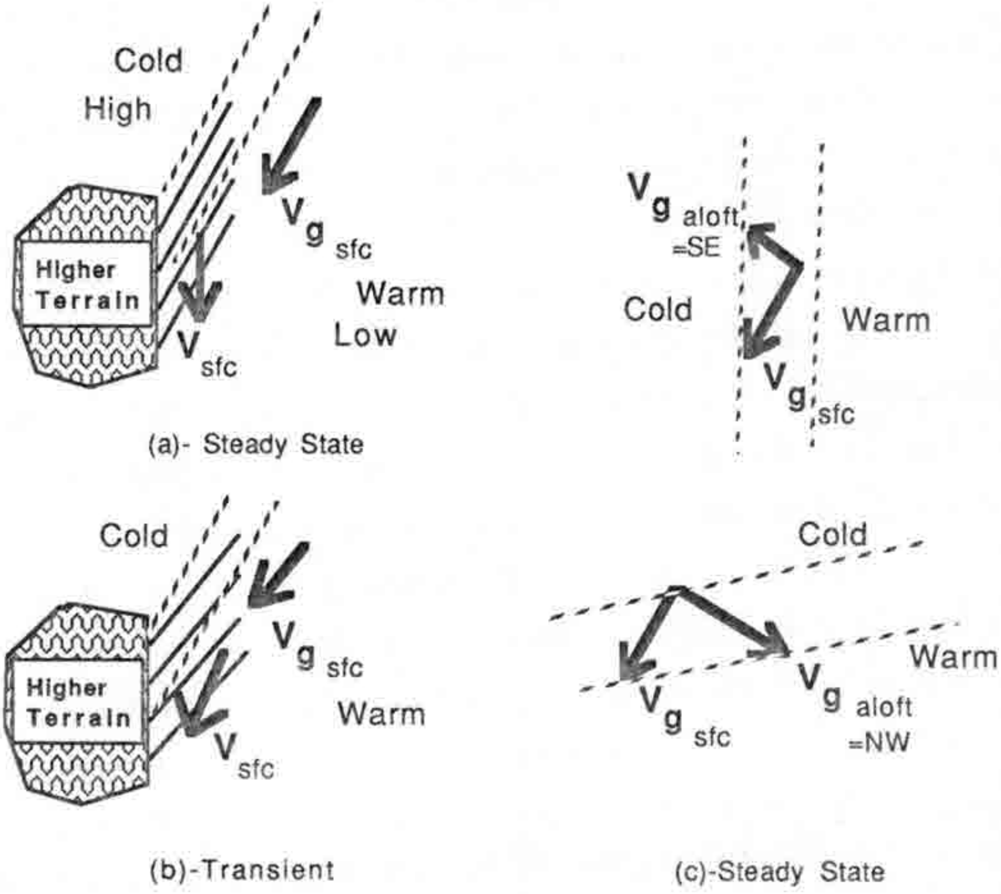

Figure 7.1: Idealized relationship of cold air, pressure gradient, and wind for damming situations. Solid lines indicate pressure contours, dashed lines indicate isotherms, and bold arrows indicate geostrophic and actual winds. (a) damming with no pressure gradient aloft (b) negative feedback when pressure gradient is disturbed (c) different orientation of cold air consistent with different geostrophic flow aloft.

primarily to the depth of the cold air (the isotherms indicate cold air depth). Suppose some process (upper air heights falling to the northwest) acted to destroy the steady–state flow decreasing the magnitude of the surface pressure gradient. Then the original mountain-parallel component of the surface flow would be slightly supergeostrophic, the Coriolis force would accelerate the surface flow towards the mountain (Fig. 7.1b), the cold air would "pile-up" against the mountain, the thermal wind would increase and, hydrostatically, the original pressure gradient would be restored. Alternatively, the actual wind might slow and adjust to the reduced pressure gradient. In either case, the mountain-parallel flow would remain in near geostrophic balance or, if the flow curved significantly, in gradient balance. Thus, if highly agradient flow is observed, with the wind crossing isobars at a 90° angle, as has been claimed for cold-air damming cases east of the Appalachians (Forbes *et al.*,1987), then the flow or pressure gradient there must be changing rapidly. In fact, such observations may be due mostly to poor estimates of the horizontal pressure gradient, such as the unadjusted altimeter setting analysis used by Forbes *et al.*

7.1 Impact of the geostrophic wind above the cold air

For archetypical cold air damming situations, there is warmer air at ridgetop level flowing towards the mountain. This is true for the Appalachian damming case described by Forbes *et al.* (1987) and for the northeast Colorado overrunning precipitation situation described by Schultz (1985). In these situations, cold air near the surface is strongly banked towards the mountain (Fig. 7.1c). But for the cases described in this study, and in fact for many shallow cold surges east of the Continental Divide, there is a westerly, downslope component of the flow aloft. This has an impact on the orientation of the cold air.

Assuming that the mountain-parallel flow evolves to a near steady–state, the hydrostatic implications of a southeast and northwest geostrophic wind above the cold air are illustrated in Fig. 7.1c. The surface pressure gradient must be the same for both cases. Only the impact of the thermal wind, not vertical momentum mixing, between the two layers is considered.

The illustration of northwesterly flow aloft corresponds to both the 14 June 1985 and the 1 August 1986 case. In both cases there was cold advection from the north at the surface and extending up to just above 70 kPa. In order to have a mountain-parallel flow at the surface, as occurred for the no-heating model simulation of the 14 June 1985 case and during the morning on 1 August 1986, the cold air need not be banked strongly against the mountain. In both of the cases described, the top of the cold air appeared to be relatively flat in the east-west direction.

The distribution of cold air for the two damming situations illustrated in Fig. 7.1c also has an impact on the temperature advection parallel to the mountain. In the Forbes *et al.* (1987) and the Schultz (1985) cases, with southeasterly flow aloft, horizontal cold advection may or may not (e.g., vertical advection may raise the cold air) be important for setting-up the damming situation at an earlier time. But, upon reaching a steady-state, although the cold air remains dammed, the actual cold advection may be weak or non-existent (Fig. 16a of Forbes *et al.*) since the flow is nearly parallel to the isotherms. By contrast, for the shallow cold surges documented in Chaps. 3, 4 and 5 of this study, there was northwesterly flow aloft. In these cases, without surface heating, the cold air sloped mainly towards the north, parallel to the mountain, and there was strong cold advection at the surface. This idealized structure was strongly modified by the effects of surface heating.

7.2 The impact of surface heating

With stably-stratified air, the actual depth of the cold air would have little effect on the structure and dynamics described in the previous section. It is only with surface heating that the distinction between a shallow and a deep cold surge becomes important. There are several, interrelated impacts of a strong (over land) upward surface heat flux.

After some time of imposed heat flux, the leading edge of the cold air is "burned–off". The surface position of the front retreats and at the same time becomes more diffuse, as suggested in Fig. 7.2b. The tendency to become more diffuse at the surface is essentially a result of the diabatic frontal processes operating around the front, as shown in Fig 7.2a. Even though the heating is the same on both sides of the front, it is confined to a shallower layer behind the front. Therefore, the warming is larger on the cold side–a

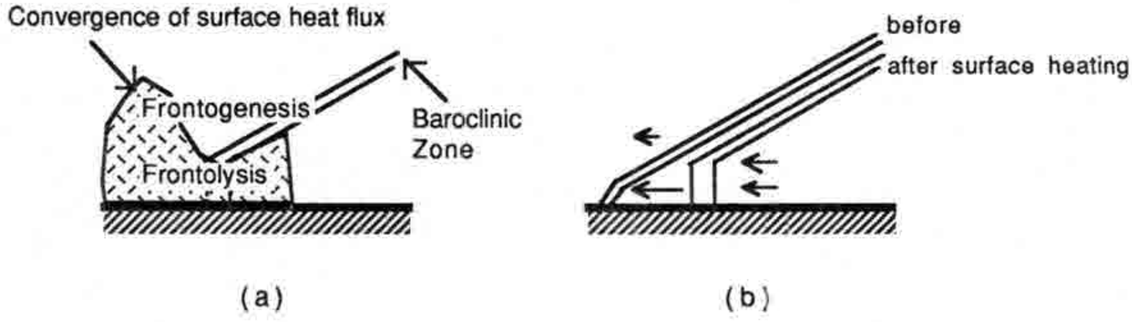

Figure 7.2: Effect of uniform surface heating on a sloping frontal zone (a) distribution of surface heat flux convergence (b) the initial surface temperature discontinuity becomes diffuse.

frontolytic process at the surface. This occurs at the leading edge of a front over even flat terrain. But when the underlying terrain is not flat, and is closer to the top of the cold air in some areas, then the burn-off process will also be effective in those areas. Specifically, over a sloping plain, there will be a tendency for the front to become aligned along a topographical contour, even though the cold air would be deep enough to penetrate well past that contour in the absence of surface heating. In Colorado, this process contributes to the tendency for shallow cold surges to become "hung-up" on the east-west ridges that jut into the plains. For a land-sea case, there will be a tendency for the front to become aligned along the coast. Furthermore, in the Colorado situation, when there is a westerly component of ridgetop flow, there is additional retardation of the front due to downslope air warmed diabatically over the higher terrain to the west.

If prior to surface heating the front had collapsed to a density current structure, then with heating it returns to a broad baroclinic zone, for which semigeostrophic theory (Hoskins, 1982) is appropriate. As the gradient of the cold air depth increases (Fig. 7.2a), there will initially be an isallobaric direct thermal circulation near the leading edge of the front, increasing cold advection there at the surface. This tends to oppose, but unsuccessfully, the retreat of the front. In the absence of friction, after several hours, a wind shear in balance with the thermal wind would develop in the deep, steep baroclinic zone at the leading edge. But in fact, there is strong vertical mixing of momentum through the deep, broad baroclinc zone. Due to friction, cross-isobar flow develops at the surface (Fig. 5.11). There is cold advection at the surface, but it is weaker than for the night, density current case.

On the other hand, when averaged over a deep layer of the troposphere, the cold advection is approximately the same for the day and night cases (Fig. 7.3). During the

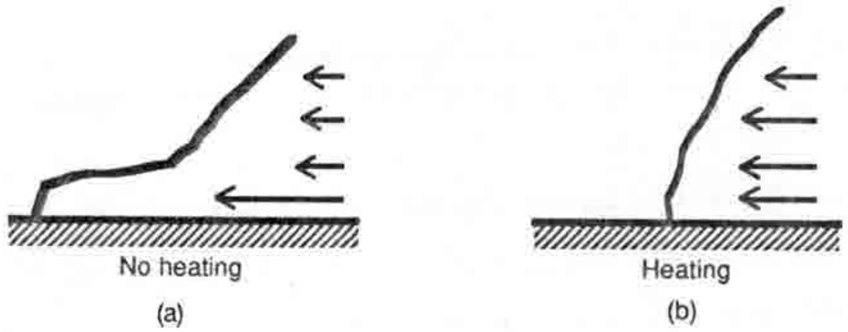

Figure 7.3: Cold advection, intensity proportional to the length of the arrows, without heating (left) and with surface heating (right).

day, there is intense vertical mixing of heat and momentum through a deep layer of the troposphere around the frontal zone. Cold advection at the surface is weak, as it is at upper levels. There is a tendency for convergence and upward motion of the cold air parcels. This all changes rapidly at night. Surface friction is confined to a very shallow boundary layer. Increased stability prevents cold air parcels from rising. The surface front takes on more of a density current structure. For these reasons, a nighttime acceleration of surface cold fronts should be expected even over flat terrain. But there is an additional contribution from the higher terrain (Fig. 7.1a and b) constraining the cold air not to flow west. The damming and diversion to the south of cold air becomes stronger as differential temperature advection between the plains flow and the ridgetop flow generates ever larger stability.

Finally, as cold air reaches the mountains and is diverted to the south at night, there is a real increase in the northerly geostrophic wind at the surface. But this does not result simply from cooling over higher terrain and a resulting downslope flow that gradually veers to a geostrophic balance, as suggested by Wiesmueller (1982). Instead, the advection of cold air towards the mountains generates a hydrostatic increase in pressure there much larger than would result from diurnal flow alone. Thus the front should not be thought of as a passive surface embedded in the diurnal flow of a homogeneous airmass. Instead, the front actively magnifies the impact of the oscillation of surface heating.

In summary, uniform surface heat flux over flat terrain (right–hand side of Fig. 7.4) modifies the leading edge of shallow cold surges and, to some extent, deep cold surges. Convergence of surface sensible heat flux is confined to a shallow layer beneath the frontal inversion, yet extends over a deep layer of the troposphere ahead of the front. Diabatic warming of surface air parcels on the cold side of the front is thus larger than for parcels on the warm side. The result is surface frontolysis and a decrease in vertical stability near the leading edge of the cold air. A deep, broad baroclinic zone develops and is quite different from a gravity current. There is strong mixing of momentum, and so the advance of the baroclinic zone at the surface closely coincides with the advance through a deep layer of the troposphere. This advance is in general much slower than for a shallow density current.

The addition of mountains (left–hand side of Fig. 7.4) further contributes to a daytime slowing of the cold surge. The cold air is "burned–off" at the point where it intersects the higher terrain. This thermal process is identical to that at the leading edge over the flat terrain, resulting in a broad, diffuse, deep baroclinic zone. Because of the near–neutral stability in this zone, warm air heated over higher terrain is able to mix down to the surface, further retarding the progression of the front. The damming effect of the mountains (i.e., the diversion of cold air to the south) is defeated since cold air parcels encounter little resistance to either upward or westward motion. In fact, the mountain–perpendicular pressure gradient is reversed by the effects of the surface heating. This pressure gradient actually supports an upslope advance of the cold air, although this advance is opposed by strong vertical mixing with warmer air.

This conceptual model (Fig. 7.4) is highly idealized and involves an interaction between several mechanisms. Ultimately these cooperative mechanisms all depend on the

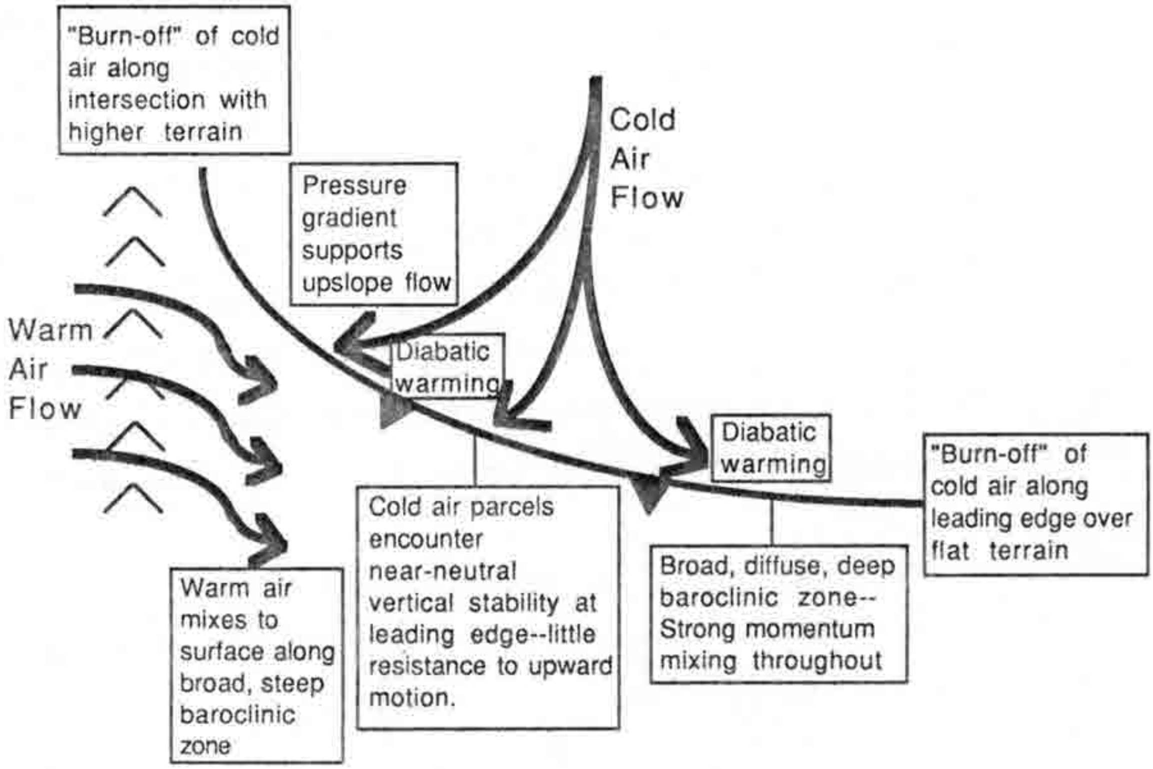

Figure 7.4: Interaction of mechanisms contributing to a daytime retardation of cold surges east of the Continental Divide.

evolution of the intensity and slope of the baroclinic zone and on the vertical stability within the zone. Uniform surface heating may, as indicated by the model results, strongly modify a shallow baroclinic zone. But in the atmosphere, the evolving baroclinic zone is in general accompanied by a development of non–uniform cloud cover. The impact of cloud cover requires further research.

Chapter 8

SUMMARY AND CONCLUSIONS

The purpose of this paper has been to examine the interaction of shallow cold surges with topography, particularly the impact that surface heating has on the diversion of cold air by a mountain range. Two case studies were described in detail, and several other events were cited. Since observations alone did not provide a complete description of this process, numerical model simulations provided additional insight into important mechanisms.

8.1 Conclusions

In the absence of heating, the diversion of a shallow cold surge east of the Continental Divide was inferred from the observations and could be seen in the model results. Although the resolution of the model was relatively coarse, the cold surge appeared to evolve in a way that resembled a density current propagating in the along-mountain direction. At the same time, the along-mountain flow developed so that it was in approximate geostrophic balance with the mountain-perpendicular pressure gradient–i.e., a rotating gravity current as described by Griffiths (1986). Surface heating typical of daytime conditions inhibited the development of this density current and thus slowed the daytime progression of the surface front. The change during the day was due to a combination and interaction of (1) the frontolytic effect of heating near the surface, (2) decreased stability resulting in little or no resistance to upward rather than southward displacement of the cold air, (3) increased momentum mixing through a deep layer of the troposphere, and (4) warm advection of air heated over higher terrain to the west. With surface heating removed, the cold surge rapidly (~3 h) evolved and returned to a state more closely resembling a gravity current.

Another cold surge event, although not modeled, was observed to evolve in a manner consistent with the above description. The impact of the cold surge on the development of moist convection could be clearly seen in the satellite imagery. The cold surge propagated rapidly ($\sim$15 m s^{-1}) into northeast Colorado during the early morning hours. There were pronounced wind shifts and pressure jumps at the leading edge. But by afternoon, after strong surface heating, the leading edge became very diffuse and nearly stationary.

8.2 Suggestions for future research

As noted in Chapter 5, future numerical simulations of shallow cold surges should incorporate a two-way nested grid model. Such a model would allow for finer resolution of the topography and for a more detailed study of the diversion of cold air (*e.g.*, the 1 August 1986 case). Realistic development of cloud cover should then be included for typical situations. The effects of cloud cover were not included in these model simulations, but the results suggested that the development of a thick cloud layer, extending uniformly ahead of and behind the leading edge of the cold front, could be almost as important as a setting sun and result in a rapid southward acceleration of the surface front. Differential surface heat flux generated by non–uniform cloud cover would cause additional changes. The impact of the cloud cover on the surface energy budget and on the overall movement of a cold surge should be investigated numerically. Furthermore, possible scale– interactions that develop due to the influence of topography on cold surges could be explored. These would include both smaller-scale systems, such as the Denver convergence-vorticity zone, and larger-scale systems, such as mesoscale convective systems and even synoptic-scale waves. The release of potential energy as the cold air accelerates southward might affect the larger-scale systems.

Surface heating alone potentially has a significant impact on shallow cold surges. Even without mountains, or without land–water contrast in coastal areas, strong surface sensible heat flux near the leading edge, combined with strong mixing through a deep layer of the troposphere, contributes to a daytime retardation of the progression of the cold surge. Thus, over a flat continental region, an acceleration of fronts should be expected at night, although perhaps not as pronounced as near a mountain range. Outflows from mesoscale convective systems over flat areas, e.g. over the Mississippi valley of the United States, can also be expected to behave differently at night. In fact, the ability of cold air to flow away in a shallow layer near the surface during the night may be an important factor contributing to the organization of large mesoscale convective systems. In some cases, the speed of a nocturnal outflow might match the speed of the opposing low–level inflow jet, generating a stationary area of convection that would not be possible during the daylight hours.

Continued development of the observational network will allow some of these topics to be explored without the use of a model. In particular, the anticipated network of wind profilers over the central United States is expected to furnish information from lower in the troposphere than has been possible with the Colorado profiler network. In addition to being able to resolve very shallow cold surges, the anticipated network will extend over a much larger area. When combined with conventional surface data, it should be possible to develop a climatology of not only surface frontal passage, but also mean-layer temperature difference, slope of the frontal inversion, etc. by season and by time-of-day. However, the spacing of the profiler network will still offer poor horizontal resolution ($\sim$ 200 km) when compared to model simulations.

Finally, as an aid in interpreting both numerical model and observational data, there is a need for further development of simple models describing rotating gravity currents over non–flat terrain. The analytic model of Baines (1980) considers only a flat surface intersecting a vertical wall. Griffiths (1986) considers a gravity current on a slope. But both the sloping plains and the near-vertical wall of the Continental Divide appear to be important in the evolution of rapidly accelerating cold surges. An idealized analytic model incorporating both effects would be useful in understanding the relative importance of each in contributing to the evolution of cold surges near a mountain range.

REFERENCES

Abbs, D. J., and R. A. Pielke, 1986: Thermally forced surface flow and convergence patterns over northeast Colorado. *Mon. Wea. Rev.*, **114**, 2281-2296.

Augustine, J. A., and E. J. Zipser, 1987: The use of wind profilers in a mesoscale experiment. *Bull. Amer. Meteor. Soc.*, **68**, 4-17.

Baines, P. G., 1980: The dynamics of the southerly buster. *Aust. Meteor. Mag.*, **28**, 175-198.

—, 1987: Upstream blocking and airflow over mountains. *Ann. Rev. Fluid Mech.*, **19**, 75-97.

Bannon, P. R., 1981: Synoptic-scale forcing of coastal lows: Forced double Kelvin waves in the atmosphere. *Quart. J. Roy. Meteor. Soc.*, **107**, 313-327.

—, 1984: Frontogenesis over topography. *Contrib. Atmos. Physics*, **57**, 393-408.

— , 1986: Deep and shallow quasi-geostrophic flow over mountsins. *Tellus*, **38A**, 162-169.

Banta, R. M., 1984: Daytime boundary-layer evolution over mountainous terrain. Part I: Observations of the dry circulations. *Mon. Wea. Rev.*, **112**, 340-356.

Bluestein, H. B., J. M. Brown and L. F. Bosart, 1984: A case study of intense convection in eastern Colorado on 1 June 1983. Preprints, 10th Conf. on Wea. Forecasting and Analysis, AMS, Boston, MA, 165-170.

Boatman, J. F. and R. F. Reinking, 1984: Synoptic and mesoscale circulations and precipitation mechanisms in shallow upslope storms over the western High Plains. *Mon. Wea. Rev.*, **112**, 1725-1744.

Bosart, L. F., V. Pagnotti and B. Lettau, 1973: Climatological aspects of eastern United States back-door cold frontal passages. *Mon. Wea. Rev.*, **101**, 627-635.

Brundidge, K. C., 1965: The wind and temperature structure of nocturnal cold fronts in the first 1,420 feet. *Mon. Wea. Rev.*, **93**, 587-603.

Carbone, R. E., 1982: A severe frontal rainband. Part I: Stormwide hydrodynamic structure. *J. Atmos. Sci.*, **39**, 258-279.

Chen, C., and W.R. Cotton, 1983: A one–dimensional simulation of the stratocumulus–capped mixed layer. *Bound. Layer Meteor.*, **25**, 289- -321.

Chen, Wen-Dar, 1984: Mesoscale lee cyclogenesis. Ph.D. dissertation, Princeton University, Princeton, NJ.

Chen, Shou-Jun, and L. Dell'Osso, 1986: The effect of Qinghai-Tibet Plateau forcing on the meso-scale rain-bearing systems over eastern China during presummer rainy season. *J. Meteor. Soc. Japan*, **64**, 53-63.

Christie, D. R., K. J. Muirhead and A. L. Hales, 1979: Intrusive density flows in the lower troposphere: A source of atmospheric solitons. *J. Geophys. Res.*, **84**, 4959-4970.

Clark, T.L., 1977: A small-scale dynamic model using a terrain-following coordinate transformation. *J. Comp. Phys.*, **24**, 186-215.

Cotton, W. R., R. L. George, P. J. Wetzel and R. L. McAnelly, 1983: A long-lived mesoscale convective complex. Part I: The mountain-generated component. *Mon. Wea. Rev.*, **111**, 1893-1918.

Coulman, C. E., J. R. Colquhoun, R. K. Smith and K. McInnes, 1985: Orographically forced cold fronts-mean structure and motion. *Bound. Layer Meteor.*, **32**, 57-83.

Crook, N.A., 1987: Trapping of low level internal gravity waves. *Extended Abstracts, Third Conference on Mesoscale Processes*, Amer. Meteor. Soc., Boston, MA, p. 56.

Cunning, J. B., 1986: The Oklahoma-Kansas Preliminary Regional Experiment for STORM-Central. *Bull. Amer. Meteor. Soc.*, **67**, 1478-1486.

Davies, H. C., 1984: On the orographic retardation of a cold front. *Contrib. Atmos. Physics*, **57**, 409-418.

Dorman, C. E., 1985: Evidence of Kelvin waves in California's marine layer and related eddy generation. *Mon. Wea. Rev.*, **113**, 827-839.

Doswell, C. A., 1980: Synoptic-scale environments associated with High Plains severe thunderstorms. *Bull. Am. Meteor. Soc.*, **61**, 1388-1400.

Doviak, R. J. and R. S. Ge, 1984: An atmospheric solitary gust observed with a Doppler radar, a tall tower and a surface network. *J. Atmos. Sci.*, **41**, 2559-2573.

Droegemeier, K. K., and R. B. Wilhelmson, 1985: Three dimensional numerical modeling of convection produced by interacting thunderstorm outflows. Part I: Control simulation and low-level moisture variations. *J. Atmos. Sci.*, **22**, 2381-2403.

Dunn, L., 1987: Cold air damming by the Front Range at the Colorado Rockies and its relationship to locally heavy snows. *Weather and Forecasting*, **2**, 177-189.

Emanuel, K., 1984: Lecture notes on fronts and frontogenesis. In *Dynamics of Mesoscale Weather Systems*, J. Klemp, Ed., National Center for Atmospheric Research, P.O. Box 3000, Boulder, CO 80307.

Forbes, G.S., R.A. Anthes and D.W. Thomson, 1987: Synoptic and mesoscale aspects of an Appalachian ice storm associated with cold-air damming. *Mon. Wea. Rev.*, **115**, 564-591.

Garratt, J. R., and W. L. Physick, 1987: Numerical study of atmospheric gravity currents. II: Evolution and external influences. *Contrib. Atmos. Physics*, **60**, 88-103.

Gill, A. E., 1976: Adjustment under gravity in a rotating channel. *J. Fluid Mech.*, **77**, 603-621.

Gill, A.E., 1977: Coastally trapped waves in the atmosphere. *Quart. J. Roy. Meteor. Soc.*, **103**, 431-440.

—, 1982: Atmosphere-Ocean Dynamics. Academic Press, 662 pp.

Griffiths, R. W., 1986: Gravity currents in rotating systems. *Ann. Rev. Fluid Mech.*, **18**, 59-89.

Haase, S. P. and R. K. Smith, 1984: Morning glory wave clouds in Oklahoma: A case study. *Mon. Wea. Rev.*, **112**, 2078-2089.

Hales, J. E. Jr., 1972: Surges of maritime tropical air northward over the Gulf of California. *Mon. Wea. Rev.*, **100**, 298-306.

Hoskins, B.J., 1982: the mathematical theory of frontogenesis. *Ann. Rev. fluid Mech.*, **14**, 131–151.

Hsu, H.-H., and J. M. Wallace, 1985: Vertical structure of wintertime teleconnection patterns. *J. Atmos. Sci.*, **42**, 1693-1710.

Johnson, R. H. and J. J. Toth, 1982: A climatology of the July 1981 surface flow over northeast Colorado. Atmos. Sci. Paper No. 342, Colorado State Univ., Fort Collins, CO, 80523, 52 pp.

Keyser, D. and R. A. Anthes, 1982: The influence of planetary boundary layer physics on frontal structure in the Hoskins-Bretherton horizontal shear model. *J. Atmos. Sci.*, **39**, 1783-1802.

Klemp, J. B., and D. R. Durran, 1983: An upper boundary condition permitting internal gravity wave radiation in numerical mesoscale models. *Mon. Wea. Rev.*, **111**, 430-444.

Kuettner, J.P., P.A. Hildebrand, and T.L. Clark, 1987: Convection waves: Observations of gravity wave systems over convectively active boundary layers. *Quart. J. roy. Meteor. Soc.*, **113**, 445–467.

Lilly, D. K., 1981: Doppler radar observations of upslope snowstorms. Preprints, 2nd Conf. on Mountain Meteor., AMS, Boston, MA, 346-353.

—, M. D. Albright and D. J. Brees, 1986: The onshore surge of marine air into the Pacific Northwest: A coastal region of complex terrain. *Mon. Wea. Rev.*, **114**, 2602-2627.

Louis, J.-F., 1979: A parametric model of vertical eddy fluxes in the atmosphere. *Bound. Layer Meteor.*, **17**, 187–202.

Mass, C.F., and M.D. Albright, 1987: Coastal southerlies and alongshore surges of the west coast of North America: Evidence of mesoscale topographically trapped response to synoptic forcing. *Mon. Wea. Rev.*, **115**, 1707–1738.

Maxworthy, T., 1983: Experiments on solitary internal Kelvin waves. *J. Fluid Mech.*, **129**, 365-383.

McPherson, R.D., 1986: Operational objective analysis techniques and potential applications for mesoscale meteorology. In *Mesoscale Meteorology and Forecasting*, P..S. Ray, Ed., American Meteorological Society, Boston, MA, 151–172.

Meitiń, J. G., and J. B. Cunning, 1985: The Oklahoma-Kansas Preliminary Regional Experiment for STORM-Central (O-K PRE-STORM): Volume I. Daily Operations Summary. NOAA Tech. Memo. ERL ESG-20, U. S. Dept. Commerce, Boulder, CO. 313 pp.

Murakami, T., and L. Y. C. Ho, 1981: Orographic influence of the Rocky mountains on the winter circulation over the contiguous United States. *J. Meteor. Soc. Japan*, **59**, 683-706.

—, and H. Nakamura, 1983: Orographic effects on cold surges and lee-cyclogenesis as revealed by numerical experiment. Part II: Transient aspects. *J. Meteor. Soc. Japan*, **61**, 547-567.

Nakamura, H., and T. Doutani, 1985: A numerical study on the coastal Kelvin wave features about the cold surges around the Tibetan Plateau. *J. Meteor. Soc. Japan*, **63**, 547-563.

Orlanski, I., 1986: Localized baroclinicity: A source for meso-a cyclones. *J. Atmos. Sci.*, **43**, 2857-2885.

Panofsky, H.A., and J.A. Dutton, 1984: *Atmospheric Turbulence*, John Wiley and Sons, Inc., 397 pp.

Phillips, N.A., 1979: The nested grid model, NOAA Tech. Rep. NWS-22, Silver Spring, MD, 80 pp.

Pinkerton, J. E., 1978: Numerical experiments on boundary layer effects on frontal structure. Ph. D. Thesis, Drexel University, 213 pp.

Reeder, M. J., and R. K. Smith, 1986: A comparison between frontogenesis in the two-dimensional Eady model of baroclinic instability and summertime cold fronts in the Australia region. *Quart. J. Roy. Meteor. Soc.*, **112**, 293-313.

Reiter, E.R., and M. Tang, 1984: Plateau effects on diurnal circulatin patterns. *Mon. Wea. Rev.*, **112**, 638–651.

Richwien, B. A., 1980: The damming effect of the southern Appalachians. *Nat. Wea, Digest*, **5**, 2-12.

Rossby, G. G., 1937: On the mutual adjustment of pressure and velocity distributions in certain simple surrent systems. I. *J. Mar. Res.*, **1**, 15-28.

Sanders, F., 1955: An investigation of the structure and dynamics of an intense surface frontal zone. *J. Meteor.*, **12**, 542-552.

Schlatter, T. W., 1984: Forecasting convection with the PROFS system: A detailed look at thunderstorms and interacting gust fronts on the afternoon of 12 August 1983. Preprints, 10th Conf. on Wea. Forecasting and Analysis, AMS, Boston, MA, 199-202.

Schlatter, T. W., D. V. Baker and J. F. Henz, 1983: Profiling Colorado's Christmas Eve blizzard. *Weatherwise*, **36**, 60-66.

Schultz, P., 1985: The first experiment in forecasting cool–season weather at PROFS. *Bull. Amer. Meteor. Soc.*, **66**, 1166–1167.

Shapiro, M. A., 1984: Meteorological tower measurements of a surface cold front. *Mon. Wea. Rev.*, **112**, 1634-1639.

—, T. Hample and D. W. van de Kamp, 1984: Radar wind profiler observations of fronts and jet streams. *Mon. Wea. Rev.*, **112**, 1263-1266.

—, T. Hample, D. Rotzoll and F. Mosher, 1985: The frontal hydraulic head: A micro-a scale (~1 km) triggering mechanism for mesoconvective systems. *Mon. Wea. Rev.*, **113**, 1166-1183.

Sinclair, P. C. and J. F. W. Purdom, 1983: Shuttle recovery requirements and the development of arc cloud lines from thunderstorm outflows. Preprints, 9th Conf. on Aerospace and Aeronautical Meteor., AMS, Boston, MA, 287-292.

Smith, J. K. and T. B. McKee, 1983: Undisturbed clear day diurnal wind and temperature pattern in northeastern Colorado. Atmos. Sci. Paper No. 365, Colorado State Univ., Fort Collins, CO, 80523, 103 pp.

Smith, R. B., 1982: Synoptic observations and theory of orographically disturbed wind and pressure. *J. Atmos. Sci.*, **39**, 60-70.

—, 1986: Mesoscale mountain meteorology in the Alps. In *Scientific Results of the Alpine Experiment* (ALPEX), GARP Pub. No. 27, 407-423.

Smith, R. K., N. Crook and G. Roff, 1982: The morning glory: An extraordinary atmospheric undular bore. *Quart. J. Roy. Meteor. Soc.*, **108**, 937-956.

—, M. J. Coughlan and J. Lopez, 1986: Southerly nocturnal wind surges and bores in northeastern Australia. *Mon. Wea. Rev.*, **114**, 1501-1518.

Stauffer, D.R., and T.T. Warner, 1987: A numerical study of Appalachian cold- -air damming and coastal frontogenesis. *Mon. Wea. Rev.*, **115**, 799- -821.

Sumi, A., 1985: A study on cold surges around the Tibetan Plateau by using numerical models. *J. Meteor. Soc. Japan*, **63**, 377-395.

Szoke, E. J., M. L. Weisman, T. W. Schlatter, F. Y. Caracena and J. M. Brown, 1984: A subsynoptic analysis of the Denver tornadoes of 3 June 1981. *Mon. Wea. Rev.*, **112**, 790-808.

Toth, J.J., and R. H. Johnson, 1985: Summer surface flow characteristics over northeast Colorado. *Mon. Wea. Rev.*, **113**, 1458-1469.

Tremback, C. J., and R. Kessler, 1985: A surface temperature and moisture parameterization for use in mesoscale numerical models. Preprints, 7th Conference on Numerical Weather Prediction, June 17-20, 1985, Montreal, Quebec, Canada, AMS.

Tremback, C. J., G. J. Tripoli and W. R. Cotton, 1985: A regional scale atmospheric numerical model including explicit moist physics and a hydrostatic time-split scheme. Preprints, 7th Conference on Numerical Weather Prediction, June 17-20, 1985, Montreal, Quebec, Canada, AMS.

—, J. Powell, W. R. Cotton and R. A. Pielke, 1987: The forward-in-time upstream advection scheme: Extension to higher orders. *Mon. Wea. Rev.*, **115**, 540-555.

Tripoli, G. J., and W. R. Cotton, 1982: The Colorado State University three-dimensional cloud/mesoscale model–1982. Part I: General theoretical framework and sensitivity experiments. *J. Rech. Atmos.*, **16**, 185-219.

Wakimoto, R.M., 1982: The life–cycle of thunderstormm gust fronts as viewed with Doppler radar and rawinsonde data. *Mon. Wea. Rev.*, **110**, 1060–1082.

Wiesmueller, J. L., 1982: The effect of diurnal heating on the movement of cold fronts through eastern Colorado. NOAA Tech. Memo. NWS-CR-66, U. S. Dept. Commerce, Rockville, MD, 14 pp.

Wilson, J., and W. E. Schreiber, 1986: Initiation of convective storms at radar-observed boundary-layer convergence lines. *Mon. Wea. Rev.*, **114**, 2516-2536.

Young, G. S., and R. H. Johnson, 1984: Meso- and microscale features of a Colorado cold front. *J. Climate Appl. Meteor.*, **23**, 1315-1325.

Zipser, E.J., 1977: Mesoscale and convective–scale downdrafts as distinct components of squall–line structure. *Mon. Wea. Rev.*, **105**, 1568– 1589.